

**Alma Mater Studiorum – Università di Bologna**

**DOTTORATO DI RICERCA**

---

**Ciclo XXII**

**Settore/i scientifico disciplinari di afferenza: ING-INF/03**

*“Wireless multimedia systems: equalization techniques, nonlinearities on OFDM signals and echo suppression”*

**Presentata da: FLAVIO ZABINI**

**Coordinatore Dottorato: Chiar.ma Prof.ssa Paola Mello**

**Relatore: Chiar.mo Prof. Oreste Andrisano  
Co-Relatore: Prof. Andrea Conti**

---

**Esame finale anno 2010**

# Wireless multimedia systems: equalization techniques, nonlinearities on OFDM signals and echo suppression

F. Zabini



*Wireless multimedia systems: equalization techniques, nonlinearities on OFDM signals and echo suppression*



Wireless multimedia systems: equalization techniques,  
nonlinearities on OFDM signals and echo suppression

F. Zabini

March 12, 2010





## CONTENTS

1. <i>Partial Equalization for MC-CDMA Systems in Non-Ideally Estimated Correlated Fading</i> . . . . .	5
1.1 Introduction . . . . .	6
1.2 System Model and Assumptions . . . . .	7
1.2.1 Transmitted Signal . . . . .	7
1.2.2 Channel Model . . . . .	8
1.2.3 Received Signal . . . . .	8
1.2.4 Imperfect Channel Estimation . . . . .	9
1.2.5 Assumptions . . . . .	9
1.3 Decision Variable . . . . .	9
1.3.1 Interference Term . . . . .	11
1.3.2 Noise Term . . . . .	12
1.3.3 Useful Term . . . . .	13
1.3.4 Independence of Interference, Noise and Useful Terms . . . . .	13
1.4 Performance Evaluation . . . . .	13
1.4.1 Bit Error Probability Evaluation . . . . .	13
1.4.2 Optimum PE Parameter . . . . .	15
1.4.3 Particular Case: Ideal Channel Estimation . . . . .	17
1.4.4 Fixed Bit Error Probability . . . . .	17
1.4.5 Bit Error Outage . . . . .	17
1.5 Numerical Results . . . . .	18
1.6 Conclusions . . . . .	28

---

2. <i>Echo Cancellers Based on Pseudo-Noise Training Sequences and Pulse Methods: Performance and Stability Analysis</i> . . . . .	35
2.1 Introduction . . . . .	35
2.2 System description . . . . .	37
2.3 Coupling channel estimation and echo cancellation . . . . .	39
2.3.1 Pseudo-noise Method . . . . .	40
2.3.2 Pulse Method . . . . .	43
2.4 Performance Evaluation . . . . .	45
2.4.1 Rejection Ratio . . . . .	45
2.4.2 Mean Rejection Ratio . . . . .	46
2.4.3 Echo Suppression . . . . .	49
2.4.4 Echo Suppression at Nominal Position . . . . .	50
2.5 Upper bound on the Probability of Instability . . . . .	52
2.5.1 Probability of Instability as a mark of real performance . . . . .	52
2.5.2 Transfer Function of the OCR . . . . .	54
2.5.3 Random Polynomial . . . . .	55
2.6 Numerical Results . . . . .	58
2.6.1 MRR . . . . .	58
2.6.2 ESNP vs ES . . . . .	59
2.6.3 ESNP: comparison between theory and experimental results . . . . .	60
2.6.4 Probability of instability . . . . .	60
2.7 Conclusions . . . . .	61
2.8 Appendix A . . . . .	62
2.9 Appendix B . . . . .	64

---

3. Out of Band Spectrum Reduction through Cancellation Carriers for OFDM with Nonlinearities . . . . .	69
3.1 Introduction . . . . .	69
3.2 System Model . . . . .	70
3.2.1 Key Idea . . . . .	70
3.2.2 OFDM Transmitter with nonlinearities . . . . .	71
3.2.3 Transmitted Signal . . . . .	73
3.2.4 Non-Linear Power Amplifier Model . . . . .	75
3.2.5 Cost Function . . . . .	75
3.3 Frequency Domain Method: Cancellation Carriers . . . . .	76
3.3.1 Cost Function . . . . .	76
3.3.2 Optimization . . . . .	77
3.4 Time Domain Method: Adaptive Symbol Transition . . . . .	80
3.4.1 Cost Function . . . . .	80
3.4.2 Optimization . . . . .	82
3.5 Numerical Results . . . . .	87
3.5.1 Notation . . . . .	87
3.5.2 Methodology . . . . .	87
3.5.3 Out of Band Spectrum . . . . .	88
3.5.4 Frequency Domain . . . . .	88
3.5.5 Time Domain . . . . .	88
3.6 Conclusions . . . . .	90



## LIST OF FIGURES

1.1	Transmitter and receiver block schemes. . . . .	21
1.2	Subcarrier spectrum in frequency BFC. . . . .	22
1.3	BEP as a function of $\beta$ for different values of $\varepsilon \triangleq \sigma_E^2/\sigma_H^2$ when $N_u = M = 1024$ , $L = M/16$ , and $\bar{\gamma} = 10\text{dB}$ . . . . .	23
1.4	Optimum value of $\beta$ as a function of $\xi$ in dB for different values of normalized estimation error $\varepsilon \triangleq \sigma_E^2/\sigma_H^2$ . . . . .	24
1.5	BEP vs. the mean SNR $\bar{\gamma}$ adopting the optimum $\beta$ in case of perfect CSI, varying the normalized estimation errors $\varepsilon \triangleq \sigma_E^2/\sigma_H^2$ : comparison between $N_U = M = 1024$ and $N_U = M/8 = 128$ , with $L = M/16$ . . . . .	25
1.6	BEP vs. the number of active users, varying the normalized estimation errors, $\varepsilon \triangleq \sigma_E^2/\sigma_H^2$ , when $\bar{\gamma} = 10\text{dB}$ . Comparison among different combining techniques (i.e., different values of $\beta$ ). . . . .	26
1.7	System load vs. $\beta$ giving the target BEP $P_b^* = 10^{-1}$ (red), $P_b^* = 10^{-2}$ (black), and $P_b^* = 10^{-3}$ (green), for different normalized estimation errors $\varepsilon \triangleq \sigma_E^2/\sigma_H^2$ . . . . .	26
1.8	Median SNR vs. $\beta$ giving $P_b^* = 10^{-2}$ and $P_o^* = 10^{-2}$ , for different estimation errors $\varepsilon \triangleq \sigma_E^2/\sigma_H^2$ and system loads. . . . .	27
1.9	BEO vs $\mu_{\text{dB}}$ , for different estimation errors $\varepsilon \triangleq \sigma_E^2/\sigma_H^2$ and $P_b^* = 10^{-2}$ . Comparison among different combining techniques. . . . .	28
2.1	Block architecture of the considered OCR. ■[■MM]Figura da sistemare . . . . .	39
2.2	Pseudonoise method. MRR as a function of the number of taps P when the coupling channel has only one tap: comparison between rectangular and raised cosine filtering for different values of the length of sequences $M$ . . . . .	48

2.3	Pulse method. MRR as a function of the number of taps $P$ when the coupling channel has only one tap: comparison between rectangular and raised cosine filtering for different values of the number of accumulations $N$ . . .	49
2.4	Pseudonoise method. MRR as a function of the coupling channel delay $\tau_0$ (only one tap channel is supposed): comparison between rectangular and raised cosine filtering for different values of the length of sequences $M$ . . .	50
2.5	Pulse method. MRR as a function of the coupling channel delay $\tau_0$ (only one tap channel is supposed): comparison between rectangular and raised cosine filtering for different values of the number of accumulations $N$ . . .	51
2.6	Pseudonoise method. MRR as a function of the number of taps $P$ when the coupling channel is modeled as TU12 and 1,6 and 12 echoes on 12 are considered respectively: comparison between different values of the length of sequences $M$ . . . . .	52
2.7	Pulse method. MRR as a function of the number of taps $P$ when the coupling channel is modeled as TU12 and 1,6 and 12 echoes on 12 are considered respectively: comparison between different values of the number of accumulations $N$ . . . . .	53
2.8	Pulse Method. Echo suppression as a function of the estimation SNR. Theoretical comparison between ES and ESNP . . . . .	61
2.9	Pulse Method. ESNP as a function of the number of accumulations: comparison between theoretical values and measurements. . . . .	62
2.10	The Upper Bound of the Probability of Instability as a function of the Estimation Signal-to-Noise Ratio for different number of considered echoes $L$ (modeled according to TU12-channel) . . . . .	63
3.1	OOB radiation as depending on the symbol sequence $S$ . A very simple example ( $N = 4$ , BPSK modulation): on the left the contributions of each symbols in the frequency domain are depicted and on the right the related spectrum is shown. It is evident as the OOB of the sequence with alternate sign is much more higher with respect the sequence with the same sign . .	71
3.2	Data symbols in the subcarrier vector in a classic OFDM scheme . . . . .	72
3.3	Data symbols in the subcarrier vector in with Cancellation Carriers . . . . .	72
3.4	Block Scheme of an OFDM transmitter with nonlinear HPA . . . . .	73

---

3.5	Block Scheme of an OFDM transmitter with nonlinear HPA and Cancellation Carriers . . . . .	73
3.6	Input-Output non-linear characteristic, Rapp Model with $A = 0.9$ , $x_{\text{sat}} = 0.53V$ and $p = 1.5$ . . . . .	89
3.7	OFDM Spectrum at the input of the nonlinearity ( $IBO = 15dB$ . Comparison between theory and measurements) . . . . .	89
3.8	OFDM Spectrum at the output of the nonlinearity ( $IBO = 15dB$ . Comparison between theory and measurements) . . . . .	90
3.9	ACLR vs IBO for Frequency Domain - 64 Subcarriers . . . . .	91
3.10	ACLR vs IBO for Time Domain - 64 Subcarriers . . . . .	92



## LIST OF TABLES



## ACKNOWLEDGEMENTS

I want to take the opportunity to thank my advisor, Prof. O.Andrisano, for his continuous encouragements and suggestions and for having given me the opportunity to have this PhD experience.

I warmly thank Andrea Conti, for his constant support, valuable guidance and unending patience in following the work and in giving precious suggestions in technical subjects and in social interaction: I am deeply indebted to him.

I thank also my advisor at DoCoMo Eurolabs, Ivan Cosovic, who help me, both at work and in social relationship, during my sixth mounths in Munich (Germany).

I sincerely would like to thank Gianni Pasolini, Barbara Masini, Matteo Mazzotti and Rudi Bandiera, for several discussions and precious suggestions that helped to improve the value of this work. I thank also all the people of WiLab, where it is fantastic to work.



## INTRODUCTION

This thesis addresses the main aspects of multicarrier wideband wireless communication systems, such as equalization, echo cancellation in digital video broadcasting, and spectrum shaping to reduce effects of non-linear devices. In the first part a partial equalization technique for equalization of downlink of MC-CDMA systems with correlated fading and non-ideal channel estimation is presented. The analytical results of the proposed solution are encouraging and they are in good agreement with simulations. In the second part an echo canceller technique is proposed and analyzed to solve the problem of the coupling channel between the transmitting antenna and the receiving one in a repeater (it is an issue not too much investigated in literature, but which will become critical with the diffusion of Single Frequency Network such as in the terrestrial digital video broadcasting, DVB-T, case). The analytical framework leads to performance results in the terms of echo cancelling capability that show a very good agreement with the measurements done on a FPGA board implemented prototype. In the third part, the out-of-band radiation in OFDM in the presence of non-linear high power amplifiers is analyzed. An algorithm to reduce the out-of-band emissions through the insertion of properly designed codes in some subcarriers is proposed and its performance evaluated both through analysis and simulations. This activity has been developed during my working period at DoCoMo Eurolabs, Munich, Germany. It has been extended for the case of insertion of properly designed codes in the time domain (an experimental campaign to verify the analysis is ongoing).



## 1. PARTIAL EQUALIZATION FOR MC-CDMA SYSTEMS IN NON-IDEALLY ESTIMATED CORRELATED FADING

Multi-carrier code division multiple access (MC-CDMA) is capable of supporting high data rates in next generation multiuser wireless communication systems. Partial equalization (PE) is a low complexity receiver technique combining the signals of subcarriers for improving the achievable performance of MC-CDMA systems in terms of their bit error probability (BEP) and bit error outage (BEO) in comparison to maximal ratio combining, orthogonality restoring combining and equal gain combining techniques. We analyze the performance of the multiuser MC-CDMA downlink and derive the optimal PE parameter expression, which minimizes the BEP. Realistic imperfect channel estimation and frequency-domain (FD) block fading channels are considered. More explicitly, the analytical expression of the optimum PE parameter is derived as a function of the number of subcarriers, the number of active users (i.e., the system load), the mean signal-to-noise ratio, the variance of the channel estimation errors for the above-mentioned FD block fading channel. The choice of the optimal PE technique significantly increases the achievable system load for given target BEP and BEO.

## 1.1 Introduction

Multi-carrier code division multiple access (MC-CDMA) systems harness the combination of orthogonal frequency division multiplexing (OFDM) and code division multiple access (CDMA) to efficiently combat frequency selective fading and interference in high-rate multiuser communication [44–50]. Hence, they constitute promising candidates for next generation mobile communications [51]. Multipath fading destroys the orthogonality of the users' spreading sequences and thus multiple-access interference (MAI) occurs. In the downlink (DL) of classical MC-CDMA systems, MAI mitigation can be accomplished at the receiver using low-complexity linear combining techniques. Following the estimation of the channel state information (CSI), the signals of different subcarriers are appropriately weighted and summed using equal gain combining (EGC) [45], maximum ratio combining (MRC) [45, 52], orthogonality restoring combining (ORC) (also known as zero forcing) [45, 52], or threshold-based ORC (TORC) [44, 45, 54]. The MRC technique represents the optimal choice, when the system is noise-limited; by contrast, when the system is interference-limited, ORC may be employed to mitigate the MAI at the cost of enhancing the noise.<sup>1</sup> The minimum mean square error (MMSE) criterion may also be used for deriving the equalizer coefficients, while an even more powerful optimization criterion is the minimum bit error ratio (MBER) criterion [53]. However, while MRC, EGC, and ORC only require the CSI, the MMSE and MBER equalizers are more complex, since they exploit additional knowledge, such as the number of active users and the mean SNR. As an alternative, the partial equalization (PE) technique of [55, 56] weights the signal of the  $m^{\text{th}}$  subcarrier by the complex gain of

$$G_m = \frac{H_m^*}{|H_m|^{1+\beta}}, \quad (1.1)$$

where  $H_m$  is the  $m^{\text{th}}$  subcarriers gain and  $\beta$  is a parameter having values in the range of  $[-1, 1]$ . It may be observed that (1.1) reduces to EGC, MRC and ORC for  $\beta = 0, -1$ , and  $1$ , respectively. Again, MRC and ORC are optimum in the extreme cases of noise-limited and interference-limited systems, respectively, and for each intermediate situation an optimum value of the PE parameter  $\beta$  can be found to optimize the performance [56]. Note that, the PE scheme has the same complexity as the EGC, MRC, and ORC, but it is more robust to channel impairments and to MAI-fluctuations. In [56], the bit error probability (BEP) of the MC-CDMA DL employing PE has been analyzed in perfectly estimated

<sup>1</sup> ORC is often improved with the aid of threshold ORC (TORC), in which a threshold is introduced to cancel the contributions of the subcarriers gravely corrupted by the noise, hence facilitating good performance at low complexity.

uncorrelated Rayleigh fading channels. It was also shown that despite its lower complexity, the PE is capable of approximating the optimum MMSE scheme's performance. In practical situations the signals of adjacent subcarriers may experience correlated fading. A channel model, which enables us to account for both the frequency-domain (FD) fading correlation and for FD interleaving is the FD block fading channel (FDBFC) of [57, 58].

In this paper, we analyze MC-CDMA systems using PE in FD correlated fading modelled by the FDBFC, and using realistic imperfect channel estimation. The mean BEP and bit error outage (BEO) [59, 60] are characterized as a function of the system parameters, such as the mean SNR, the number of users, the number of subcarriers, the channel estimation errors, and the particular FDBFC model employed.

The paper is organized as follows. In Sec. 1.2 the system model and our assumptions are presented, while the decision variable is derived in Sec. 1.3. In Sec. 1.4 the BEP and BEO performance is characterized and the optimum PE parameter is determined. In Sec. 1.5 our analytical results are provided and compared to our simulations, while in Sec. 1.6 our conclusions are presented.

## 1.2 System Model and Assumptions

In this section we present our system model and assumptions, followed by the characterization of the signals at the various processing stages.

### 1.2.1 Transmitted Signal

We consider the MC-CDMA architecture presented in [45], where FD spreading is performed using orthogonal Walsh-Hadamard (W-H) codes, having a spreading factor (SF), which is equal to the number of subcarriers. Hence, each data-symbol is spread across all subcarriers, and multiplied by the chip assigned to each particular subcarrier, as shown in Fig. 1.1(a). For binary phase shift keying (BPSK) modulation, the signal transmitted in the DL is given by

$$s(t) = \sqrt{\frac{2E_b}{M}} \sum_{k=0}^{N_u-1} \sum_{i=-\infty}^{+\infty} \sum_{m=0}^{M-1} c_m^{(k)} a^{(k)}[i] g(t - iT_b) \cos(2\pi f_m t + \phi_m) \quad (1.2)$$

where  $E_b$  is the energy per bit,  $M$  is the number of subcarriers, the indices  $k$ ,  $i$ , and  $m$  represent the user, data and subcarrier indices, respectively,  $N_u$  is the number of active users,  $c_m$  is the  $m^{\text{th}}$  spreading chip (taking values of  $\pm 1$ ),  $a^{(k)}[i]$  is the symbol transmitted during the  $i^{\text{th}}$  interval,  $g(t)$  is a rectangular signalling pulse waveform with duration  $[0, T]$

and a unity energy,  $T_b$  is the bit duration of user  $k$ ,  $f_m$  is the  $m^{\text{th}}$  subcarrier frequency, and  $\phi_m$  is the  $m^{\text{th}}$  subcarrier phase. Furthermore,  $T_b = T + T_g$  is the total MC-CDMA symbol duration, where the time-guard  $T_g$  is inserted between consecutive multi-carrier symbols to eliminate the inter-symbol interference (ISI) due to the channel's delay spread.

### 1.2.2 Channel Model

In the DL, the signal of different users undergoes the same fading. We assume that the channel's impulse response (CIR)  $h(t)$  is time-invariant for several MC-CDMA symbols and we employ a FD channel transfer function (FDCHTF),  $H(f)$ , characterized by

$$H(f) \simeq H(f_m) \quad \text{for } |f - f_m| < \frac{W_s}{2}, \forall m \quad (1.3)$$

where  $H_m$  has real and imaginary parts of  $X_m$  and  $Y_m$ , respectively, while  $W_s$  is the bandwidth of each subcarrier. Since a non-dispersive Dirac-shaped CIR represents a frequency-flat fading FDCHTF, this FDBFC assumption may be loosely interpreted in practical terms as having a low-dispersion CIR. We assume that for each FD sub-channel, the channel-induced spreading of the rectangular signalling pulse is such that the response to  $g(t)$ , namely  $g'(t)$ , still remains rectangular with a unity energy and duration of  $T' \triangleq T + T_d$ , with  $T_d$  being the time-dispersion, which is lower than the guard time  $T_g$  [46] (this will not limit the scope of our framework, but simplifies the analysis).

Again, we consider a FDBFC [57, 58, 61, 62] across  $M$  subcarriers, implying that the total number of subcarriers can be divided into  $L$  independent groups of  $B = M/L$  subcarriers, as represented in Fig. 1.2, for which we have

$$H_{lB+1} = \tilde{H}_l \quad l = 0, 1, \dots, L-1 \quad \text{and} \quad i = 0, 1, \dots, B-1. \quad (1.4)$$

Hence, it is possible to describe the FDCTF using  $L$  rather than  $M$  coefficients  $\tilde{H}_l$ . We assume having  $\tilde{H}_l = \alpha_l e^{j\vartheta_l}$  independent identical distributed (IID) random variables (RVs) with  $\tilde{H}_l = X_l + jY_l$  and  $X_l, Y_l \sim \mathcal{N}(0, \sigma_{\tilde{H}}^2)$ .

### 1.2.3 Received Signal

The received signal may be expressed as

$$r(t) = \frac{2E_b}{M} \sum_{k=0}^{N_u-1} \sum_{i=-\infty}^{+\infty} \sum_{l=0}^{L-1} \sum_{b=0}^{B-1} \alpha_l c_{lB+b}^{(k)} a^{(k)}[i] g'(t - iT_b) \cos(2\pi f_{lB+b}t + \vartheta_l) + n(t) \quad (1.5)$$

where  $n(t)$  represents the additive white Gaussian noise (AWGN) with a double-sided power spectral density (PSD) of  $N_0/2$ .

### 1.2.4 Imperfect Channel Estimation

We analyze the performance with imperfect CSI by assuming a channel estimation error of  $E_l$  for each subcarriers block, which is complex Gaussian distributed with zero-mean and a variance of  $2\sigma_e^2$ , thus  $E_l \sim \mathcal{CN}(0, 2\sigma_e^2)$ .<sup>2</sup> Hence, the  $l^{\text{th}}$  estimated complex FDCHTF coefficient is

$$\widehat{H}_l = H_l + E_l \quad (1.6)$$

where we have  $\widehat{H}_l = \widehat{\alpha}_l e^{j\widehat{\vartheta}_l}$ , and  $E_l = X_{E_l} + jY_{E_l}$  so that  $X_{E_l}, Y_{E_l} \sim \mathcal{N}(0, \sigma_e^2)$ . Note that  $X_{E_l}$  and  $Y_{E_l}$  are IID.

### 1.2.5 Assumptions

We also stipulate the following common assumptions for the DL of a MC-CDMA system:

- the system is synchronous (different users and subcarriers experience the same delay, because their differences were perfectly compensated);
- the number of subcarriers is equal to the FD SF;
- the number of subcarriers is sufficiently high to enable the assessment of the BEP by exploiting the central limit theorem (CLT) and the law of large numbers (LLN).

The approximations that will be derived from the CLT and the LLN will all be verified by simulations. However, note that in standardized systems, such as WiMAX [67, 68] and DVB-T [69] the number of subcarriers is sufficiently high (e.g., 2K or 8K) to justify these assumptions.

## 1.3 Decision Variable

The performance evaluation and the PE parameter optimization require the following analytical flow: *(i)* decomposition of the decision variable in useful, interfering and noise terms; *(ii)* statistical characterization of terms in *(i)*; *(iii)* performance evaluation of conditioned and unconditioned BEP; *(iv)* derivation of the optimum PE parameter; *(v)* BEO evaluation.

---

<sup>2</sup> This is the case of pilot assisted channel estimation, where the  $\sigma_e^2$  depends on the number and energy of pilot symbols [63–66].

The signal of the  $q^{\text{th}}$  subcarrier for the  $n^{\text{th}}$  user at symbol instant  $j$  after the correlation receiver (see Fig. 1.1(b)) is given by

$$z_q^{(n)}[j] = \int_{jT_b}^{jT_b+T} \frac{r(t)}{\sqrt{T}} c_q^{(n)} \sqrt{2} \cos(2\pi f_q t + \hat{\vartheta}_{\lfloor \frac{q}{B} \rfloor}) dt. \quad (1.7)$$

By substituting (1.5) in (1.7) we obtain

$$\begin{aligned} z_q^{(n)}[j] = & \sqrt{\frac{E_b}{M} \frac{T}{T'}} \sum_{k=0}^{N_u-1} \sum_{l=0, \frac{q+1}{B}-1 < l < \frac{q}{B}}^{L-1} \alpha_l c_q^{(k)} c_q^{(n)} a^{(k)}[j] u_{l, q-lB, q}[j] + \\ & + \sqrt{\frac{E_b}{M} \frac{T}{T'}} \sum_{k=0}^{N_u-1} \sum_{l=0}^{L-1} \sum_{b=0, b \neq q-lB}^{B-1} \alpha_l c_{lB+b}^{(k)} c_q^{(n)} a^{(k)}[j] u_{l, b, q}[j] + n_q[j], \end{aligned} \quad (1.8)$$

where  $n_q[j] \triangleq \int_{jT_b}^{jT_b+T} \sqrt{2} \frac{c_q^{(n)}}{\sqrt{T}} n(t) \cos(2\pi f_q t + \hat{\vartheta}_{\lfloor \frac{q}{B} \rfloor}) dt$  and  $u_{l, b, q}[j] \triangleq \frac{1}{T} \int_{jT_b}^{jT_b+T} 2 \cos(2\pi f_{lB+b} t + \vartheta_l) \cos(2\pi f_q t + \hat{\vartheta}_{\lfloor \frac{q}{B} \rfloor}) dt$ . It can be shown that  $n_q[j]$  is zero-mean Gaussian RV (GRV) with a variance of  $N_0/2$  and that  $u_{lB+b, q}[j]$  is independent of index  $j$ , and is given by

$$u_{lB+b, q}[j] = u_{l, b, q} = \begin{cases} \cos(\vartheta_l - \hat{\vartheta}_{\lfloor \frac{q}{B} \rfloor}) & \text{for } lB + b = q \\ 0 & \text{otherwise.} \end{cases} \quad (1.9)$$

Hence, (1.8) becomes

$$z_q^{(n)}[j] = \sqrt{\frac{E_b}{M}} \delta_d \alpha_{\lfloor \frac{q}{B} \rfloor} \cos(\vartheta_{\lfloor \frac{q}{B} \rfloor} - \hat{\vartheta}_{\lfloor \frac{q}{B} \rfloor}) + \sqrt{\frac{E_b}{M}} \delta_d \sum_{k=0, k \neq n}^{N_u-1} \alpha_{\lfloor \frac{q}{B} \rfloor} c_q^{(k)} c_q^{(n)} \cos(\vartheta_{\lfloor \frac{q}{B} \rfloor} - \hat{\vartheta}_{\lfloor \frac{q}{B} \rfloor}) + n_q[j],$$

where  $\delta_d \triangleq 1/(1 + T_d/T)$  represents the loss of energy caused by the channel-induced spreading of the rectangular signalling pulse. For the sake of simplicity, since the ISI is avoided by using a guard-time, we will neglect the time-index  $j$  in the following. The decision variable  $v^{(n)}$  is obtained by a linear combination of the PE-based weighting of the signals gleaned from each subcarrier as

$$v^{(n)} = \sum_{q=0}^{M-1} |G_q| z_q^{(n)}, \quad (1.10)$$

where  $G_q$  is the  $q^{\text{th}}$  PE gain given by (1.1). More particularly, for imperfect FDCHTF estimation and FDBFCs we have

$$G_q = \frac{\hat{H}_{\lfloor \frac{q}{B} \rfloor}^*}{|\hat{H}_{\lfloor \frac{q}{B} \rfloor}|^{1+\beta}}, \quad (1.11)$$

with  $|G_q| = |\widehat{H}_{\lfloor \frac{q}{B} \rfloor}|^{-\beta} = \widehat{\alpha}_{\lfloor \frac{q}{B} \rfloor}^{-\beta}$ , and  $\angle G_q = -\angle \widehat{H}_{\lfloor \frac{q}{B} \rfloor} = -\widehat{\vartheta}_{\lfloor \frac{q}{B} \rfloor}$ . Note that for  $\beta = -1, 0$ , and  $1$ , the coefficient in (1.11) leads to the cases of MRC, EGC, and ORC, respectively. Therefore, substituting (1.11) in (1.10) the decision variable becomes

$$v^{(n)} = \underbrace{\sqrt{\frac{E_b \delta_d}{M}} \sum_{q=0}^{M-1} \alpha_{\lfloor \frac{q}{B} \rfloor} \widehat{\alpha}_{\lfloor \frac{q}{B} \rfloor}^{-\beta} \cos(\vartheta_{\lfloor \frac{q}{B} \rfloor} - \widehat{\vartheta}_{\lfloor \frac{q}{B} \rfloor}) a^{(n)}}_{U^{(n)}} \quad (1.12)$$

$$+ \underbrace{\sqrt{\frac{E_b \delta_d}{M}} \sum_{q=0}^{M-1} \sum_{k=0, k \neq n}^{N_u-1} \alpha_{\lfloor \frac{q}{B} \rfloor} \widehat{\alpha}_{\lfloor \frac{q}{B} \rfloor}^{-\beta} \cos(\vartheta_{\lfloor \frac{q}{B} \rfloor} - \widehat{\vartheta}_{\lfloor \frac{q}{B} \rfloor}) c_q^{(n)} c_q^{(k)} a^{(k)}}_{I^{(n)}} + \underbrace{\sum_{q=0}^{M-1} \widehat{\alpha}_{\lfloor \frac{q}{B} \rfloor}^{-\beta} n_q}_{N^{(n)}},$$

where  $U^{(n)}$ ,  $I^{(n)}$ , and  $N^{(n)}$  represent the useful, interfering, and noise terms, respectively, of user  $n$ . By defining

$$\Theta_q(\beta) \triangleq \alpha_{\lfloor \frac{q}{B} \rfloor} \widehat{\alpha}_{\lfloor \frac{q}{B} \rfloor}^{-\beta} \cos(\vartheta_{\lfloor \frac{q}{B} \rfloor} - \widehat{\vartheta}_{\lfloor \frac{q}{B} \rfloor}) \quad (1.13)$$

and observing that  $\alpha_l$ ,  $\widehat{\alpha}_l$ ,  $\vartheta_l$ , and  $\widehat{\vartheta}_l$  are IID for different subscripts  $l$ , the different  $\Theta_{lB+b}$  values are also IID for different subscripts  $l$ , whereas we have  $\Theta_{lB+b} = \Theta_{lB+b'}$  for the same  $l$ . Thus, we can rewrite (1.12) as

$$v^{(n)} = \underbrace{\sqrt{\frac{E_b \delta_d}{M}} \sum_{q=0}^{M-1} \Theta_q(\beta) a^{(n)}}_{U^{(n)}} + \underbrace{\sqrt{\frac{E_b \delta_d}{M}} \sum_{q=0}^{M-1} \sum_{k=0, k \neq n}^{N_u-1} \Theta_q(\beta) c_q^{(n)} c_q^{(k)} a^{(k)}}_{I^{(n)}} + \underbrace{\sum_{q=0}^{M-1} \widehat{\alpha}_{\lfloor \frac{q}{B} \rfloor}^{-\beta} n_q}_{N^{(n)}} \quad (1.14)$$

To derive the BEP, we derive the distribution of  $v^{(n)}$  from those of  $U^{(n)}$ ,  $I^{(n)}$ , and  $N^{(n)}$ .<sup>3</sup>

### 1.3.1 Interference Term

The interference term of (1.14) may be easily rewritten as

$$I = \sqrt{\frac{E_b \delta_d}{M}} \sum_{k=0, k \neq n}^{N_u-1} a^{(k)} \sum_{l=0}^{L-1} \Theta_{lB}(\beta) \sum_{b=0}^{B-1} c_{lB+b}^{(n)} c_{lB+b}^{(k)}. \quad (1.15)$$

By exploiting the properties of the W-H spreading matrices, it can be shown that for all  $i$  integers and non-zero with values of  $i$  satisfying  $-n/B \leq i \leq -n/B + N_u - 1$ , we have

$$\sum_{b=0}^{B-1} c_{lB+b}^{(n)} c_{lB+b}^{(k)} = \begin{cases} 0 & k \neq n + iB \\ B & k = n + iB, l \in \mathcal{L}_+ \\ -B & k = n + iB, l \in \mathcal{L}_- \end{cases} \quad (1.16)$$

<sup>3</sup> To simplify the notation, we will neglect the index  $n$  in the following without loss of generality.

where  $\mathcal{L}_+$  and  $\mathcal{L}_-$  are specifically set to ensure cardinalities  $\#\mathcal{L}_+ = \#\mathcal{L}_- = L/2$  and  $\mathcal{L}_+ \cup \mathcal{L}_- = 0, 1, \dots, L-1$ . Thus the interference term of (1.15) becomes

$$I = \sqrt{\frac{E_b \delta_d}{M}} \sum_{i=-\lfloor \frac{n}{B} \rfloor, i \neq 0}^{\lfloor \frac{-n+N_u-1}{B} \rfloor} a^{(n+iB)} B \left( \overbrace{\sum_{l \in \mathcal{L}_+} \Theta_{lB}(\beta)}^{A_1^{(i)}} - \overbrace{\sum_{l \in \mathcal{L}_-} \Theta_{lB}(\beta)}^{A_2^{(i)}} \right). \quad (1.17)$$

For large values of  $L$ , we may apply the CLT to each of the internal sums in (1.17), obtaining  $A_1^{(i)}$  and  $A_2^{(i)} \sim \mathcal{N}(\mathbb{E}\{\Theta_{lB}(\beta)\} L/2, \zeta_\beta L/2)$ , where  $\zeta_\beta$  is the variance of  $\Theta_{lB}^{1-\beta}$  defined as<sup>4</sup>

$$\zeta_\beta \triangleq \mathbb{E}\{\Theta_{lB}^2(\beta)\} - \mathbb{E}\{\Theta_{lB}(\beta)\}^2, \quad (1.18)$$

whose expression is evaluated in the Appendix. Therefore,  $A^{(i)} \triangleq A_1^{(i)} - A_2^{(i)}$  is distributed as  $\mathcal{N}(0, L \zeta_\beta)$ . By exploiting the symmetry of the Gaussian probability density function (pdf) (i.e.,  $a^{(n+iB)} A^{(i)} \sim \mathcal{N}(0, L \zeta_\beta)$ ), and capitalizing on the independence of the terms  $a^{(n+iB)}$  in (1.17) (which ensure that  $\mathbb{E}\{(a^{(n+iB)} A^{(i)})(a^{(n+i'B)} A^{(i')})\} = 0, \forall i \neq i'$ ), and on the sum of uncorrelated, thus independent, GRVs, we infer that the interference term of (1.17) obeys the distribution  $I \sim \mathcal{N}(0, \sigma_I^2)$ , where we have

$$\sigma_I^2 = E_b \delta_d B \left\lfloor \frac{N_u - 1}{B} \right\rfloor \zeta_\beta. \quad (1.19)$$

### 1.3.2 Noise Term

The noise term of (1.14) is given by

$$N = \sum_{q=0}^{M-1} \hat{\alpha}_{\lfloor \frac{q}{B} \rfloor}^{-\beta} n_q = \sum_{l=0}^{L-1} \sum_{b=0}^{B-1} \hat{\alpha}_l^{-\beta} n_{lB+b} = \sum_{l=0}^{L-1} \hat{\alpha}_l^\beta \overbrace{\sum_{b=0}^{B-1} n_{lB+b}}^{N_l}. \quad (1.20)$$

Since  $n_{lB+b}$  of (1.20) represents IID GRVs,  $N_l \sim \mathcal{N}(0, \frac{N_0}{2} B)$  and  $N_l$  are also IID GRVs, where

$$N = \sum_{l=0}^{L-1} \hat{\alpha}_l^\beta N_l \quad (1.21)$$

consists of the sum of i.i.d zero mean RVs with a variance of  $\frac{N_0}{2} B \mathbb{E}\{\hat{\alpha}_l^{-2\beta}\}$ . From the CLT, we can approximate the unconditioned noise term  $N$  as a zero mean GRV with a

<sup>4</sup> Note that  $\zeta_\beta$  does not depend on index  $l$  and it is an IID RVs.

variance of

$$\sigma_N^2 = M \frac{N_0}{2} \mathbb{E} \left\{ \hat{\alpha}_l^{-2\beta} \right\}. \quad (1.22)$$

### 1.3.3 Useful Term

The useful term of (1.14) can be written as

$$U = \sqrt{\frac{E_b \delta_d}{M}} \sum_{q=0}^{M-1} \Theta_q(\beta) = \sqrt{\frac{E_b \delta_d}{M}} \sum_{l=0}^{L-1} \sum_{b=0}^{B-1} \Theta_{lB+b}(\beta) = \sqrt{\frac{E_b \delta_d}{M}} B \sum_{l=0}^{L-1} \Theta_{lB}(\beta) \quad (1.23)$$

By applying the CLT  $U$  is assumed to be GRV with a mean and a variance respectively of

$$\mu_U = \sqrt{M E_b \delta_d} \mathbb{E} \{ \Theta_{lB}(\beta) \} \quad (1.24)$$

$$\sigma_U^2 = E_b \delta_d B \zeta_\beta. \quad (1.25)$$

### 1.3.4 Independence of Interference, Noise and Useful Terms

We now discuss the independence of the terms of Sections 1.3.1, 1.3.2, 1.3.3 in (1.14). The independence of the data  $a^{(k)}$  and the other variables (i.e.,  $\alpha_l$ ,  $A$ , and  $n_l$ ) guarantees that the interference term  $I$  is uncorrelated with the noise term  $N$  and with the useful term  $U$ . Additionally, the independence between  $n_l$  and  $\alpha_l$  guarantees that  $N$  is uncorrelated with  $U$ , so that  $\mathbb{E}\{NU\} = 0$ . Similarly  $I$ ,  $N$ , and  $U$  are uncorrelated GRVs, hence they are also independent.

## 1.4 Performance Evaluation

We now evaluate the BEP and derive the optimum  $\beta$  parameter.

### 1.4.1 Bit Error Probability Evaluation

#### BEP

Given the decision variable (1.14) as  $z = Ua + I + N$  and considering that  $I + N$  is a zero mean RV with a variance of  $\sigma_I^2 + \sigma_N^2$ , the BEP conditioned on the variable  $U$  becomes

$$P_b|U = Q \left( \frac{U}{\sqrt{\sigma_I^2 + \sigma_N^2}} \right), \quad (1.26)$$

where  $Q(x)$  is the Gaussian Q-Function.

*Unconditioned BEP*

By applying the LLN (hence,  $U$  is substituted by its mean value  $\mu_U$ ), we obtain the following approximation for the unconditioned BEP as

$$P_b \simeq Q \left( \frac{\mu_U}{\sqrt{\sigma_I^2 + \sigma_N^2}} \right). \quad (1.27)$$

By substituting (1.24), (1.19), and (1.22) into (1.27) we obtain

$$P_b \simeq Q \left( \sqrt{\frac{E_b \delta_d (\mathbb{E} \{ \Theta_l(\beta) \})^2}{E_b \delta_d \frac{B}{M} \lfloor \frac{N_u-1}{B} \rfloor \zeta_\beta + \mathbb{E} \{ \hat{\alpha}_l^{-2\beta} \} \frac{N_0}{2}}} \right), \quad (1.28)$$

where we have (see Appendix)

$$\mathbb{E} \{ \hat{\alpha}_l^{-2\beta} \} = (2\sigma_H^2)^{-\beta} \left( 1 + \frac{\sigma_E^2}{\sigma_H^2} \right)^{-\beta} \Gamma(1-\beta) \quad (1.29)$$

$$\mathbb{E} \{ \Theta_l(\beta) \} = (2\sigma_H^2)^{\frac{1-\beta}{2}} \left( 1 + \frac{\sigma_E^2}{\sigma_H^2} \right)^{\frac{1-\beta}{2}} \Pi \left( \frac{\sigma_E^2}{\sigma_H^2} \right) \Gamma \left( \frac{3-\beta}{2} \right) \quad (1.30)$$

and

$$\zeta_\beta(\alpha) = (2\sigma_H^2)^{1-\beta} \left( 1 + \frac{\sigma_E^2}{\sigma_H^2} \right)^{1-\beta} \left[ \Sigma \left( \frac{\sigma_E^2}{\sigma_H^2}, \beta \right) \Gamma(2-\beta) - \Pi^2 \left( \frac{\sigma_E^2}{\sigma_H^2} \right) \Gamma^2 \left( \frac{3-\beta}{2} \right) \right], \quad (1.31)$$

with  $\Gamma(\cdot)$  being the Euler Gamma function [71]. Furthermore, in (1.31) we have

$$\Pi \left( \frac{\sigma_E^2}{\sigma_H^2} \right) \triangleq 1 - \frac{\frac{\sigma_E^2}{\sigma_H^2}}{\left( 1 - \frac{\sigma_E^4}{\sigma_H^4} \right)} \quad (1.32)$$

and

$$\Sigma \left( \frac{\sigma_E^2}{\sigma_H^2}, \beta \right) \triangleq 1 - \frac{\frac{\sigma_E^2}{\sigma_H^2}}{\left( 1 - \frac{\sigma_E^4}{\sigma_H^4} \right)} \left[ 1 + \frac{\left( \frac{\frac{1}{2}-\beta}{1-\beta} \right)}{\left( 1 + \frac{\sigma_E^2}{\sigma_H^2} \right)} \right]. \quad (1.33)$$

By substituting (1.29), (1.30), and (1.31) into (1.28) and by defining the mean SNR at the receiver as:

$$\bar{\gamma} \triangleq \frac{2\sigma_H^2 E_b \delta_d}{N_0}, \quad (1.34)$$

we arrive at the following BEP expression

$$P_b \simeq Q \left( \sqrt{\frac{\bar{\gamma} \Pi^2 \left( \frac{\sigma_E^2}{\sigma_H^2} \right) \Gamma^2 \left( \frac{3-\beta}{2} \right)}{\frac{1}{L} \lfloor \frac{N_u-1}{B} \rfloor \bar{\gamma} \left[ \Sigma \left( \frac{\sigma_E^2}{\sigma_H^2}, \beta \right) \Gamma(2-\beta) - \Pi^2 \left( \frac{\sigma_E^2}{\sigma_H^2} \right) \Gamma^2 \left( \frac{3-\beta}{2} \right) \right] + \frac{1}{2} \left( 1 + \frac{\sigma_E^2}{\sigma_H^2} \right)^{-1} \Gamma(1-\beta)}}} \right). \quad (1.35)$$

The BEP approximation provided by (1.35) derives from the applying the LLN to the unconditioned BEP expression given by (1.26). An exact evaluation of the BEP would require the averaging of (1.26) over the useful term. However, since we are not interested in the BEP exact expression and since (1.35) is a monotonic decreasing function with respect to its argument, the value of  $\beta$  which minimizes (1.35), represents the minimum also for the exact BEP given by (1.26), as will be verified in Sec. 1.5 through our simulations.

A further remark may be added: (1.35) represents the BEP of an uncoded system; remembering that we are not interested in the value of the BEP itself, but in the value of the PE parameter  $\beta$  minimizing the BEP, we may assert that for coded system where the codeword error probability is a monotonic function of the BEP, the derivation of the optimum value of  $\beta$  minimizing the uncoded BEP is equivalent of finding the value of  $\beta$  which minimizes the codeword error probability. Hence, in this work we can consider uncoded systems for simplicity, given that the framework is general and valid also for coded systems.

#### 1.4.2 Optimum PE Parameter

We aim at finding the optimum value of the PE parameter,  $\beta^{(\text{opt})}$ , defined as that particular value of  $\beta$  within the range  $[-1, 1]$  which minimizes the BEP. Since the BEP is monotonically decreasing as a function of  $\beta$ , we obtain

$$\begin{aligned} \beta^{(\text{opt})} &\triangleq \arg \min_{\beta} \left\{ P_b \left( \beta, \bar{\gamma}, \frac{\sigma_E^2}{\sigma_H^2} \right) \right\} \\ &= \arg \max_{\beta} \left\{ \frac{\bar{\gamma} \Pi^2 \left( \frac{\sigma_E^2}{\sigma_H^2} \right) \Gamma^2 \left( \frac{3-\beta}{2} \right)}{\frac{1}{L} \lfloor \frac{N_u-1}{B} \rfloor \bar{\gamma} \left[ \Sigma \left( \frac{\sigma_E^2}{\sigma_H^2}, \beta \right) \Gamma(2-\beta) - \Pi^2 \left( \frac{\sigma_E^2}{\sigma_H^2} \right) \Gamma^2 \left( \frac{3-\beta}{2} \right) \right] + \frac{1}{2} \left( 1 + \frac{\sigma_E^2}{\sigma_H^2} \right)^{-1} \Gamma(1-\beta)} \right\}. \end{aligned} \quad (1.36)$$

It will be shown in Sec. 1.5 that although the adoption of the CLT and the LLN may lead to a less accurate BEP expression for a low number of subcarriers and users, it still results in an accurate value for the optimum  $\beta$ .

Setting the derivative of the argument in (1.36) with respect to  $\beta$  to zero and, by defining

$\Gamma'(x) \triangleq d\Gamma(x)/dx$ , as well as remembering that  $\Gamma\left(\frac{3-\beta}{2}\right) \neq 0$  for  $-1 \leq \beta \leq 1$ , we obtain

$$\begin{aligned} & -\Gamma'\left(\frac{3-\beta}{2}\right) \Gamma\left(\frac{3-\beta}{2}\right) \left\{ \frac{1}{L} \left[ \frac{N_U - 1}{B} \right] \bar{\gamma} \left[ \Sigma\left(\frac{\sigma_E^2}{\sigma_H^2}, \beta\right) \Gamma(2-\beta) - \Pi^2\left(\frac{\sigma_E^2}{\sigma_H^2}\right) \Gamma^2\left(\frac{3-\beta}{2}\right) \right] \right. \\ & \left. + \frac{1}{2} \left(1 + \frac{\sigma_E^2}{\sigma_H^2}\right)^{-1} \Gamma(1-\beta) \right\} = \Gamma^2\left(\frac{3-\beta}{2}\right) \left\{ \frac{1}{L} \left[ \frac{N_U - 1}{B} \right] \bar{\gamma} \left[ \Sigma'\left(\frac{\sigma_E^2}{\sigma_H^2}, \beta\right) \Gamma(2-\beta) \right. \right. \\ & \left. \left. - \Sigma\left(\frac{\sigma_E^2}{\sigma_H^2}, \beta\right) \Gamma'(2-\beta) + \Pi^2\left(\frac{\sigma_E^2}{\sigma_H^2}\right) \Gamma\left(\frac{3-\beta}{2}\right) \Gamma'\left(\frac{3-\beta}{2}\right) \right] - \frac{1}{2} \left(1 + \frac{\sigma_E^2}{\sigma_H^2}\right)^{-1} \Gamma'(1-\beta) \right\} \end{aligned} \quad (1.37)$$

where

$$\Sigma'\left(\frac{\sigma_E^2}{\sigma_H^2}, \beta\right) \triangleq \frac{\partial}{\partial \beta} \Sigma\left(\frac{\sigma_E^2}{\sigma_H^2}, \beta\right) = \frac{\frac{\sigma_E^2}{\sigma_H^2}}{\left(1 - \frac{\sigma_E^4}{\sigma_H^4}\right) \left(1 + \frac{\sigma_E^2}{\sigma_H^2}\right) 2(1-\beta)^2}. \quad (1.38)$$

Since  $\Gamma'(x) = \Psi(x)\Gamma(x)$ , where  $\Psi(x)$  is the logarithmic derivative of the Gamma function (the so-called Digamma-function) defined as  $\Psi(x) \triangleq d\ln(\Gamma(x))/dx$  [71] and after some further mathematical manipulations we obtain

$$\begin{aligned} & \left(1 + \frac{\sigma_E^2}{\sigma_H^2}\right)^{-1} \Gamma(1-\beta) \left[ -\Psi\left(\frac{3-\beta}{2}\right) + \Psi(1-\beta) \right] = \\ & \bar{\gamma} \frac{2}{L} \left[ \frac{N_U - 1}{B} \right] \left\{ \Sigma'\left(\frac{\sigma_E^2}{\sigma_H^2}, \beta\right) \Gamma(2-\beta) + \Sigma\left(\frac{\sigma_E^2}{\sigma_H^2}, \beta\right) \Gamma(2-\beta) \left[ \Psi\left(\frac{3-\beta}{2}\right) - \Psi(2-\beta) \right] \right\}. \end{aligned} \quad (1.39)$$

By exploiting that  $\Gamma(x+1) = x\Gamma(x)$  and  $\Psi(x+1) = \Psi(x) + 1/x$  [71] and by considering that  $\Gamma(1-\beta) \neq 0$  for  $-1 \leq \beta \leq 1$  and  $1-\beta \neq 0, \beta < 1$ , we obtain

$$\begin{aligned} & \left[ \Psi\left(\frac{3-\beta}{2}\right) - \Psi(1-\beta) \right] = \bar{\gamma} \frac{2}{L} \left[ \frac{N_U - 1}{B} \right] \left(1 + \frac{\sigma_E^2}{\sigma_H^2}\right) \\ & \times (\beta-1) \left\{ \Sigma'\left(\frac{\sigma_E^2}{\sigma_H^2}, \beta\right) + \Sigma\left(\frac{\sigma_E^2}{\sigma_H^2}, \beta\right) \left[ \Psi\left(\frac{3-\beta}{2}\right) - \Psi(1-\beta) - \frac{1}{1-\beta} \right] \right\}. \end{aligned} \quad (1.40)$$

By defining

$$\chi\left(\frac{\sigma_E^2}{\sigma_H^2}\right) \triangleq \frac{1}{2} \frac{\frac{\sigma_E^2}{\sigma_H^2}}{\left(1 - \frac{\sigma_E^4}{\sigma_H^4}\right) \left(1 + \frac{\sigma_E^2}{\sigma_H^2}\right)} \quad (1.41)$$

and exploiting (1.38) as well as (1.33), (1.40) becomes

$$\begin{aligned} & \left[ \Psi\left(\frac{3-\beta}{2}\right) - \Psi(1-\beta) \right] = \bar{\gamma} \frac{2}{L} \left[ \frac{N_U - 1}{B} \right] \left(1 + \frac{\sigma_E^2}{\sigma_H^2}\right) \\ & \left\{ \frac{\chi\left(\frac{\sigma_E^2}{\sigma_H^2}\right)}{\beta-1} + \left[ \Pi\left(\frac{\sigma_E^2}{\sigma_H^2}\right) (\beta-1) - \frac{\chi\left(\frac{\sigma_E^2}{\sigma_H^2}\right)}{\left(1 + \frac{\sigma_E^2}{\sigma_H^2}\right)} (2\beta-1) \right] \left[ \Psi\left(\frac{3-\beta}{2}\right) - \Psi(1-\beta) + \frac{1}{\beta-1} \right] \right\}. \end{aligned} \quad (1.42)$$

We now define the parameter  $\xi$ , which quantifies to what degree the system is noise-limited (low values) or interference-limited (high values) as follows:

$$\xi \triangleq \bar{\gamma} \frac{2}{L} \left[ \frac{N_u - 1}{B} \right], \quad (1.43)$$

and we can derive the optimum value of  $\beta$  as the implicit solution of the following equation

$$\xi = \frac{\left[ \frac{\Pi(\sigma_{\text{E}}^2/\sigma_{\text{H}}^2) + \frac{\chi(\sigma_{\text{E}}^2/\sigma_{\text{H}}^2)}{\beta-1} \left( 1 - \frac{2\beta-1}{1+\sigma_{\text{E}}^2/\sigma_{\text{H}}^2} \right)}{\Psi\left(\frac{3-\beta}{2}\right) - \Psi(1-\beta)} + \Pi(\sigma_{\text{E}}^2/\sigma_{\text{H}}^2)(\beta-1) - \frac{\chi(\sigma_{\text{E}}^2/\sigma_{\text{H}}^2)}{(1+\sigma_{\text{E}}^2/\sigma_{\text{H}}^2)}(2\beta-1) \right]^{-1}}{(1 + \sigma_{\text{E}}^2/\sigma_{\text{H}}^2)} \quad (1.44)$$

#### 1.4.3 Particular Case: Ideal Channel Estimation

In the case of ideal CSI (i.e.,  $\sigma_{\text{E}}^2/\sigma_{\text{H}}^2$  approaching zero) and for channel having uncorrelated FDCHTFs over the subcarriers, it is easy to verify that,  $\Pi(0) = 1$ ,  $\chi(0) = 0$ , and then (1.44) becomes

$$\xi = \left( \frac{1}{\Psi\left(\frac{3-\beta}{2}\right) - \Psi(1-\beta)} + \beta - 1 \right)^{-1}, \quad (1.45)$$

confirming the results obtained in [56] for the ideal conditions, which are used as a benchmark.

#### 1.4.4 Fixed Bit Error Probability

By fixing the BEP to a target value  $P_b^*$  we now derive the system load,  $s_{\text{L}} \triangleq (1/L)[(N_u - 1/B)]$  from (1.35) as a function of the other systems parameters, which is given by

$$s_{\text{L}} = \frac{\frac{\Pi^2\left(\frac{\sigma_{\text{E}}^2}{\sigma_{\text{H}}^2}\right)}{[Q^{-1}(P_b^*)]^2} \Gamma^2\left(\frac{3-\beta}{2}\right) - \frac{\left(1 + \frac{\sigma_{\text{E}}^2}{\sigma_{\text{H}}^2}\right)^{-1}}{2\bar{\gamma}} \Gamma(1-\beta)}{\Sigma\left(\frac{\sigma_{\text{E}}^2}{\sigma_{\text{H}}^2}, \beta\right) \Gamma(2-\beta) - \Pi^2\left(\frac{\sigma_{\text{E}}^2}{\sigma_{\text{H}}^2}\right) \Gamma^2\left(\frac{3-\beta}{2}\right)}. \quad (1.46)$$

#### 1.4.5 Bit Error Outage

In wireless communications, where small-scale fading is superimposed on large-scale fading (i.e., shadowing), another important performance metric is given by (BEO) [59, 60, 72], defined as the probability that the BEP exceeds the maximum tolerable level (i.e., the target BEP  $P_b^*$ ), which is given by

$$P_o \triangleq \mathbb{P}\{P_b > P_b^*\} = \mathbb{P}\{\bar{\gamma}_{\text{dB}} < \bar{\gamma}_{\text{dB}}^*\}, \quad (1.47)$$

where  $\bar{\gamma}_{\text{dB}} = 10 \log_{10} \bar{\gamma}$  and  $\bar{\gamma}_{\text{dB}}^*$  is the SNR (in dB), which ensures that  $P_b(\bar{\gamma}^*) = P_b^*$ . We consider the case of a shadowing environment in which  $\bar{\gamma}$  is log-normal distributed with parameters of  $\mu_{\text{dB}}$  and  $\sigma_{\text{dB}}^2$  (i.e.,  $\bar{\gamma}_{\text{dB}}$  is a GRV with a mean of  $\mu_{\text{dB}}$  and variance of  $\sigma_{\text{dB}}^2$ ) [74]. Hence, the BEO is given by

$$P_o = Q \left( \frac{\mu_{\text{dB}} - \bar{\gamma}_{\text{dB}}^*}{\sigma_{\text{dB}}} \right). \quad (1.48)$$

By inverting (1.35) we can derive the required SNR,  $\bar{\gamma}^*$ , enabling the derivation of the optimal  $\beta$  for a target BEP and a given system load as

$$\bar{\gamma}^* = \frac{\Gamma(1 - \beta) \left( 1 + \frac{\sigma_{\text{E}}^2}{\sigma_{\text{H}}^2} \right)^{-1}}{\left\{ \frac{2}{[Q^{-1}(P_b^*)]^2} - 2s_L \left[ \frac{\Sigma \left( \frac{\sigma_{\text{E}}^2}{\sigma_{\text{H}}^2}, \beta \right) \Gamma(2 - \beta)}{\Pi^2 \left( \frac{\sigma_{\text{E}}^2}{\sigma_{\text{H}}^2} \right) \Gamma^2 \left( \frac{3 - \beta}{2} \right)} - 1 \right] \right\} \Pi^2 \left( \frac{\sigma_{\text{E}}^2}{\sigma_{\text{H}}^2} \right) \Gamma^2 \left( \frac{3 - \beta}{2} \right)}. \quad (1.49)$$

Given the target BEP and BEO, we obtain the required value of  $\mu_{\text{dB}}$  from (1.49) and (1.48) (i.e., the median value of the SNR) that can be used for wireless system design, since it is strictly related to the link budget, when the path-loss law is known.

### 1.5 Numerical Results

In this section, we report numerical results on the BEP and the BEO for the DL of a MC-CDMA system employing PE. Our results are also compared to those of other combining techniques. Both ideal and non-ideal channel estimation are considered in FDBFCs. The FDBFC estimation errors are taken into account in terms of the normalized estimation error  $\varepsilon \triangleq \sigma_{\text{E}}^2 / \sigma_{\text{H}}^2$ . The value of  $\sigma_{\text{H}}^2$  is considered equal to  $1/2$ .<sup>5</sup> We set the number of subcarrier to  $M = 1024$  and  $L = 64$  is for the FDBFC.<sup>6</sup>

In Fig. 1.3, the BEP given by (1.35) is shown as a function of the PE parameter  $\beta$  for different values of the normalized estimation error  $\varepsilon$  when the system is fully loaded ( $N_u = M = 1024$ ) and  $\bar{\gamma} = 10\text{dB}$ . The impact of channel estimation errors on the optimum value of  $\beta$  minimizing the BEP can be observed. In particular, we note that, as the estimation error increases, the optimum value of  $\beta$  shifts to the left (i.e., toward a less interference-limited situation). In fact, to be effective, ORC (i.e.,  $\beta = 1$ ) requires accurate CSI; when this is not guaranteed, the ORC does not perform close to the optimal solution. The analytical results are also compared to our Monte Carlo simulations in Fig. 1.3: it is

<sup>5</sup> Thus, the mean channel gain is normalized to 1 for each subcarrier.

<sup>6</sup> It means that each group consists in  $B = 16$  totally correlated subcarriers.

evident that, although the BEP approximation becomes less accurate for  $\beta < 0$  (due to the adoption of the LLN), a good agreement can be observed for the optimum values of  $\beta$ , confirming that the method adopted is valid for deriving the PE parameter  $\beta^{(\text{opt})}$ . In Fig. 1.4, the optimum value of  $\beta$  is plotted as a function of  $\xi$  in dB as defined in (1.43) (i.e., as a function of different combinations of  $\bar{\gamma}$ ,  $N_u$ ,  $B$ , and  $L$ ). It can be observed that, for high values of  $\xi$ , increasing the estimation errors shift down the curves, hence requiring a reduction of  $\beta$ ; this means that, in interference-limited situations (high  $\xi$ ), as the estimation error increases, having  $\beta \simeq 1$ , i.e., using the ORC is no longer optimal. In fact, the accuracy of CSI has a substantial impact on the ORC ( $\beta = 1$ ) rather than on the EGC ( $\beta = 0$ ) and MRC ( $\beta = -1$ ). Monte Carlo simulation results are also provided in Fig. 1.4, showing a good agreement concerning the choice of the optimum  $\beta$ .

Fig. 1.5 shows the BEP as a function of the mean SNR  $\bar{\gamma}$ , for different levels of estimation errors, and system loads ( $N_u = M$  and  $N_u = M/8$ ). The results were plotted for the optimum value of  $\beta$  in conjunction with perfect CSI (i.e., for each SNR, the value of  $\beta$  is derived from (1.44)). The analytical results evaluated from (1.35) are compared to our simulation results, showing again an agreement in the region of interest for uncoded systems (i.e.,  $P_b \in [10^{-2}, 10^{-1}]$ ).<sup>7</sup> However, we remark that the goal of this paper is not the exact derivation of an analytical formula for the BEP itself, but rather the specific value of  $\beta$  for which the BEP is minimum. In Fig. 1.6, the BEP is shown as a function of the number of active users  $N_u$ , for different values of  $\beta$ , while varying the normalized channel estimation error and considering  $\bar{\gamma} = 10\text{dB}$ . Note that the choice of  $\beta = 0.5$  results in a better performance for almost any system load, except for very low system loads, for which the optimum combiner is the EGC ( $\beta = 0$ ).

In Fig. 1.7, the maximum achievable system load resulting in a specific target BEP is plotted for different normalized estimation errors as a function of  $\beta$  according to (1.46). It can be observed that, the closer  $\beta$  is to the optimum according to (1.44), the higher the attainable system load. The presence of the estimation error decreases the maximum achievable system load and, as observed before, shifts the optimal value of  $\beta$  slightly to the left towards  $-1$  (MRC).

In Fig. 1.8 the median SNR  $\mu_{\text{dB}}$ , maintaining the target BEO of  $P_o = 10^{-2}$ ,<sup>8</sup> is shown as a function of  $\beta$  for different system loads  $s_L$ . It can be noted that the higher the system load, the narrower the range of  $\beta$  values satisfying the target BEO. Finally, in Fig. 1.9, the

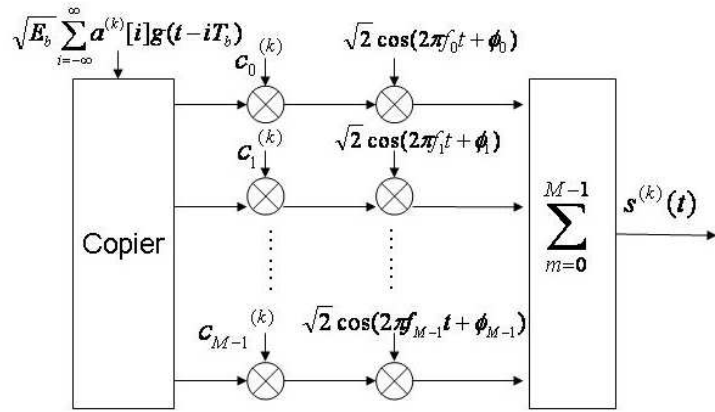
<sup>7</sup> Note, in fact, that while the noise term,  $N$ , in (1.20) is a weighted sum of GRVs, the term  $I$  in (1.15) is constituted by a weighted sum of non-GRVs, thus the adoption of the CLT to assert their independence because Gaussian and uncorrelated leads to an approximation.

<sup>8</sup> The target BEO is defined with respect to a target BEP equal to  $10^{-2}$  according to (1.49).

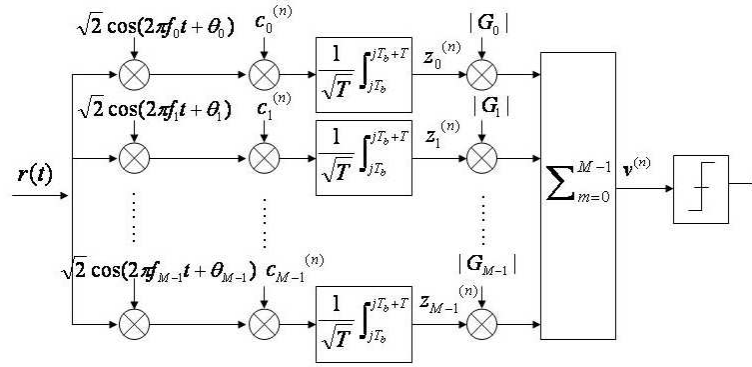
BEO is presented as a function of  $\mu_{\text{dB}}$  for  $P_{\text{b}}^* = 10^{-2}$  and for a half-loaded system, when the EGC, ORC, and PE using  $\beta = 0.5$  are adopted.<sup>9</sup> Note that the PE associated  $\beta = 0.5$  outperforms both the ORC and EGC. Moreover, the BEO is less affected by the presence of estimation errors in comparison to the classic estimation techniques, confirming that a suitable choice of the PE parameter facilitates a performance improvement with respect to classical combining techniques, while maintaining the same complexity.

---

<sup>9</sup> Note that  $\beta = 0.5$  is close to the optimum value in terms of BEO when half loaded systems are considered.



(a) Transmitter



(b) Receiver

Fig. 1.1: Transmitter and receiver block schemes.

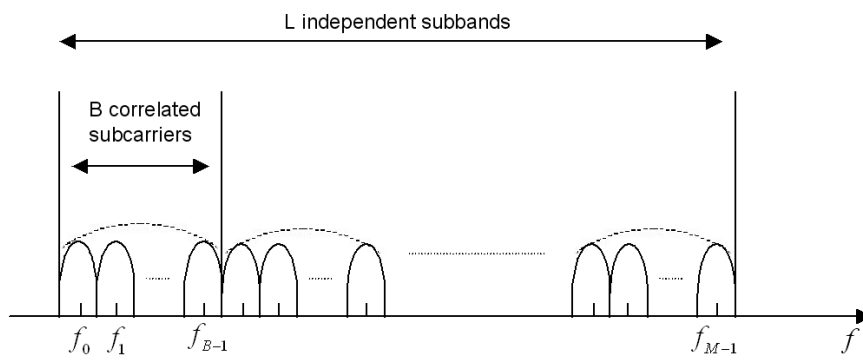


Fig. 1.2: Subcarrier spectrum in frequency BFC.

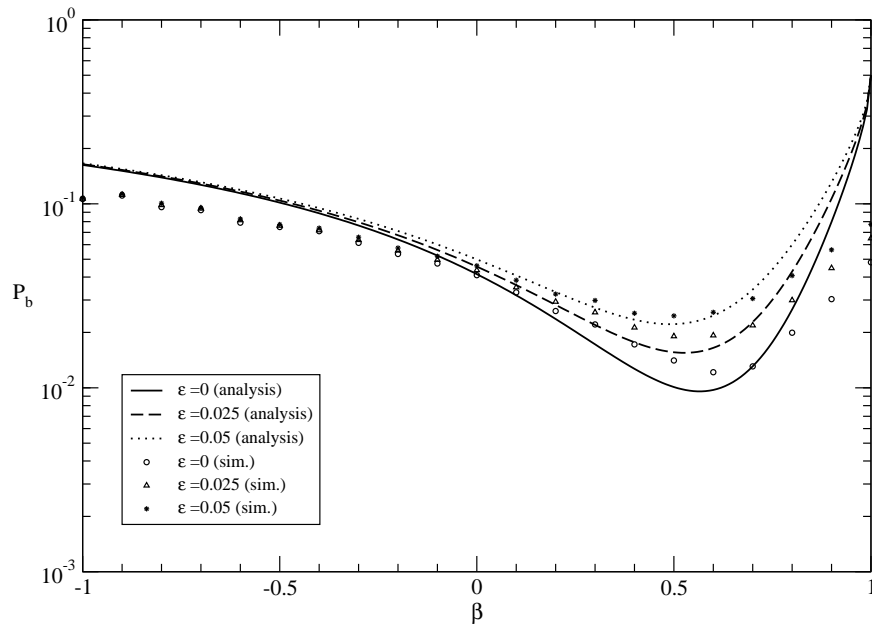


Fig. 1.3: BEP as a function of  $\beta$  for different values of  $\epsilon \triangleq \sigma_E^2/\sigma_H^2$  when  $N_u = M = 1024$ ,  $L = M/16$ , and  $\bar{\gamma} = 10\text{dB}$ .

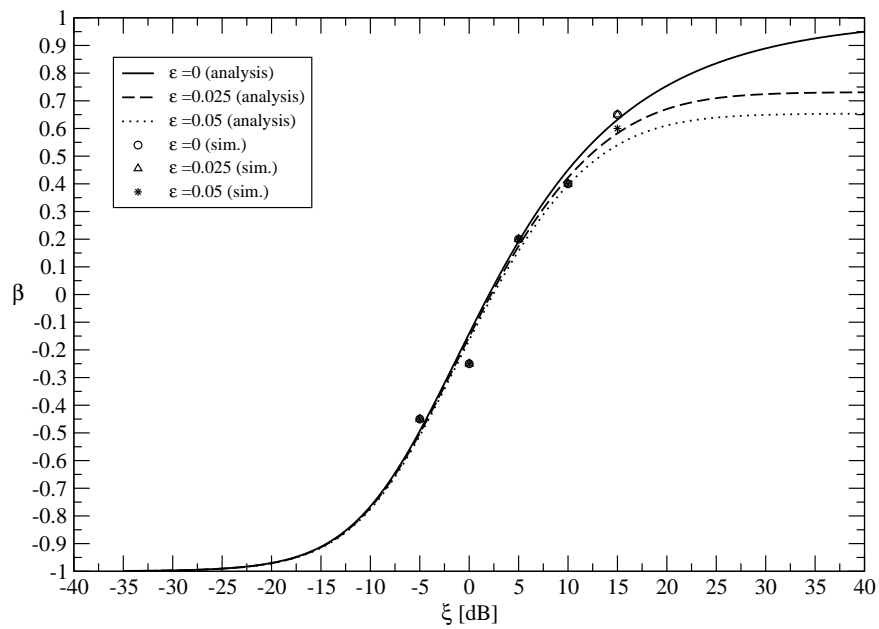


Fig. 1.4: Optimum value of  $\beta$  as a function of  $\xi$  in dB for different values of normalized estimation error  $\epsilon \triangleq \sigma_E^2/\sigma_H^2$ .

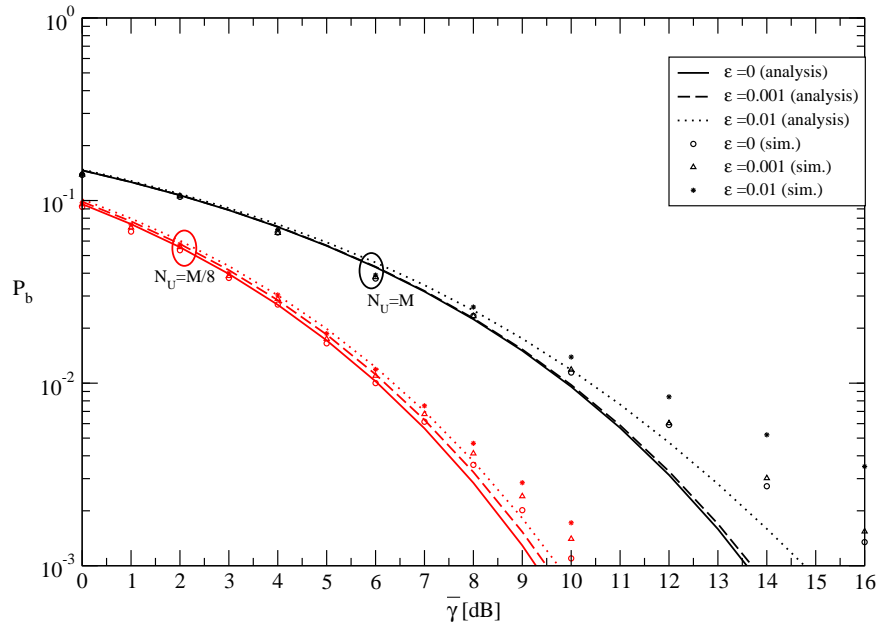


Fig. 1.5: BEP vs. the mean SNR  $\bar{\gamma}$  adopting the optimum  $\beta$  in case of perfect CSI, varying the normalized estimation errors  $\epsilon \triangleq \sigma_E^2/\sigma_H^2$ : comparison between  $N_U = M = 1024$  and  $N_U = M/8 = 128$ , with  $L = M/16$ .

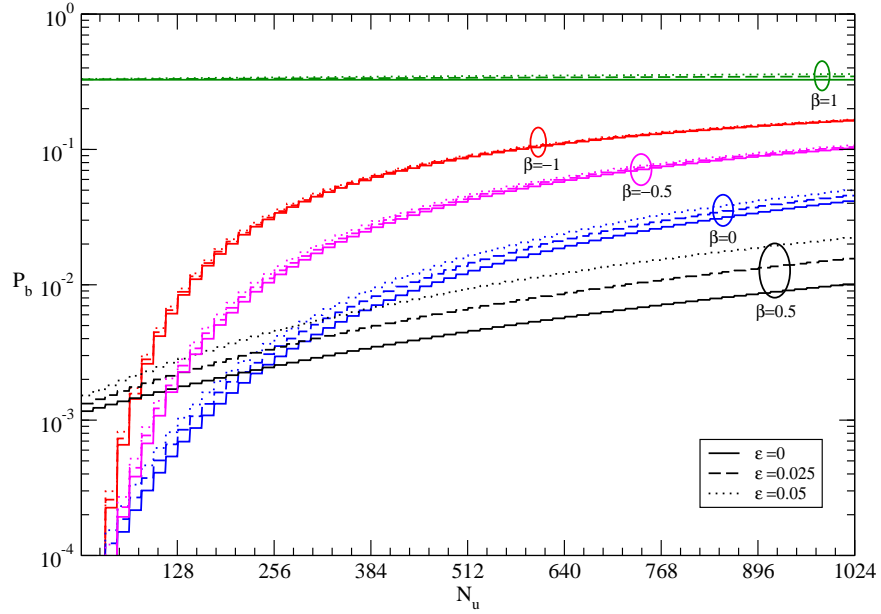


Fig. 1.6: BEP vs. the number of active users, varying the normalized estimation errors,  $\varepsilon \triangleq$

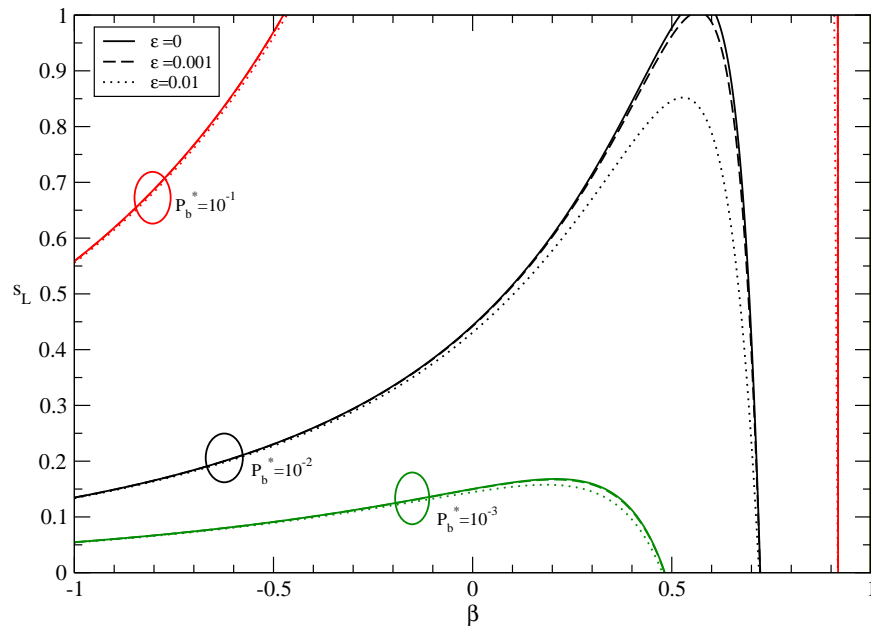


Fig. 1.7: System load vs.  $\beta$  giving the target BEP  $P_b^* = 10^{-1}$  (red),  $P_b^* = 10^{-2}$  (black), and  $P_b^* = 10^{-3}$  (green), for different normalized estimation errors  $\varepsilon \triangleq \sigma_E^2/\sigma_H^2$ .

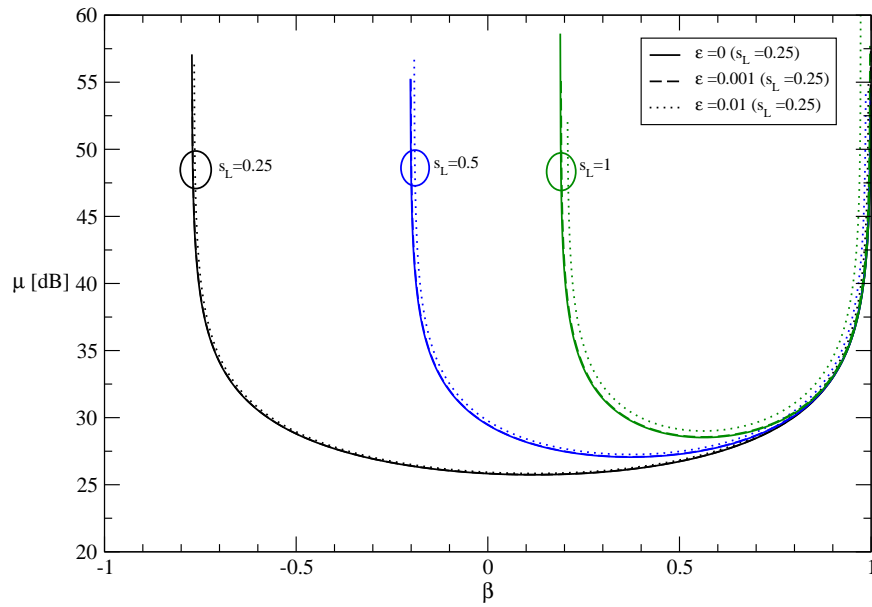


Fig. 1.8: Median SNR vs.  $\beta$  giving  $P_b^* = 10^{-2}$  and  $P_o^* = 10^{-2}$ , for different estimation errors  $\varepsilon \triangleq \sigma_E^2/\sigma_H^2$  and system loads.

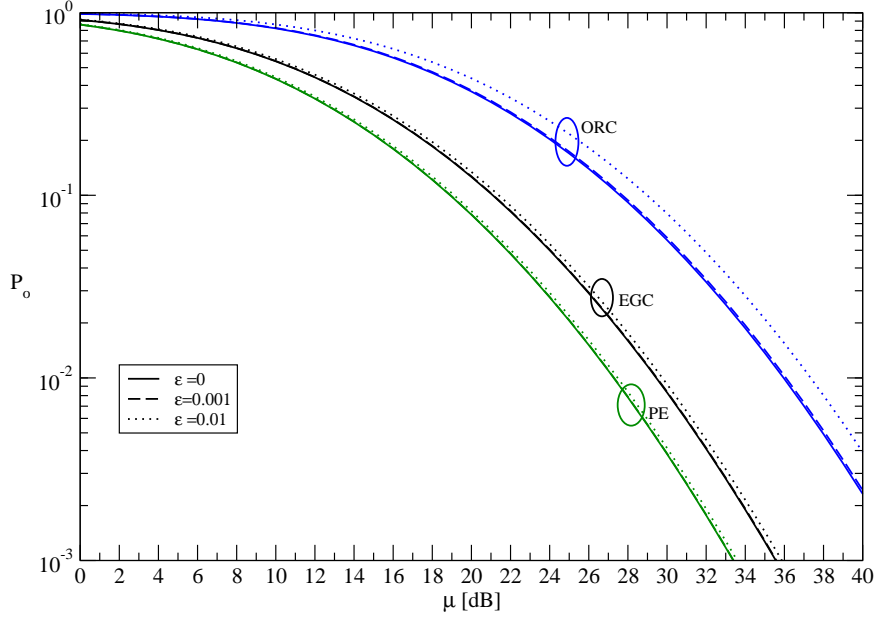


Fig. 1.9: BEO vs  $\mu_{\text{dB}}$ , for different estimation errors  $\varepsilon \triangleq \sigma_{\text{E}}^2/\sigma_{\text{H}}^2$  and  $P_{\text{b}}^* = 10^{-2}$ . Comparison among different combining techniques.

## 1.6 Conclusions

In this chapter we analyzed the DL performance of a MC-CDMA system adopting PE at the receiver with non-ideal channel estimation conditions and correlated FDBFC. We derived the optimum value of the PE parameter that minimizes the BEP, showing a beneficial performance improvement over the traditional linear combining techniques such as EGC, MRC, and ORC. We demonstrated that the optimum value of the PE parameter does not significantly change in the presence of less accurate CSI, implying that a system designer may adopt the optimum value of the PE parameter determined for perfect CSI conditions, despite having channel estimation errors. The analytical results are also compared to our simulation results, in order to confirm the validity of the analytical framework.

### Appendix

In this Appendix we evaluate the expression of: (i)  $\mathbb{E}\{\hat{\alpha}_l^{-2\beta}\}$ , (ii)  $\mathbb{E}\{\Theta_l(\beta)\}$ , (iii)  $\mathbb{E}\{\Theta_l^2(\beta)\}$ , and (iv)  $\zeta_\beta(\alpha) = \mathbb{E}\{\Theta_l^2(\beta)\} - (\mathbb{E}\{\Theta_l(\beta)\})^2$ , where,  $\hat{\alpha}_l$  are Rayleigh distributed with a pdf of  $p_{\hat{\alpha}_l}(x) = \frac{x}{\sigma_H^2 + \sigma_E^2} \exp\left[-\frac{x^2}{2(\sigma_H^2 + \sigma_E^2)}\right]$ . It is known [71] that

$$\int_0^{+\infty} x^{a-1} \exp[-px^2] dx = \frac{1}{2} p^{-\frac{a}{2}} \Gamma\left(\frac{a}{2}\right), \quad a > 0, \quad (1.50)$$

where  $\Gamma(z)$  represents the Euler Gamma function [71]. Hence we have

$$\mathbb{E}\{\hat{\alpha}_l^{-2\beta}\} = \int_0^{+\infty} x^{-2\beta} \frac{x}{\sigma_H^2 + \sigma_E^2} e^{-\frac{x^2}{2(\sigma_H^2 + \sigma_E^2)}} dx = (2\sigma_H^2)^{-\beta} \left(1 + \frac{\sigma_E^2}{\sigma_H^2}\right)^{-\beta} \Gamma(1 - \beta). \quad (1.51)$$

From (1.13) and by neglecting the index  $l$  (since we are studying IID RVs) we arrive at

$$\begin{aligned} \mathbb{E}\{\Theta_l(\beta)\} &= \mathbb{E}\left\{\alpha_l \hat{\alpha}_l^{-\beta} \cos(\vartheta_l - \hat{\vartheta}_l)\right\} = \mathbb{E}\left\{\alpha_l \hat{\alpha}_l^{-\beta} (\cos \vartheta_l \cos \hat{\vartheta}_l + \sin \vartheta_l \sin \hat{\vartheta}_l)\right\} \\ &= \mathbb{E}\left\{\sqrt{(X + X_E)^2 + (Y + Y_E)^2}^{-(\beta+1)} [X(X + X_E) + Y(Y + Y_E)]\right\}. \end{aligned}$$

We define the auxiliary variables  $\hat{X} = X + X_E$ ,  $\hat{X} \sim \mathcal{N}(0, \sigma_H^2 + \sigma_E^2)$  and  $\hat{Y} \sim \mathcal{N}(0, \sigma_H^2 + \sigma_E^2)$ . By exploiting the independence and zero mean of  $X$ ,  $Y$ ,  $X_E$ ,  $Y_E$ , we can write  $\mathbb{E}\{\hat{X}\hat{Y}\} = 0$ ,  $\mathbb{E}\{\hat{X}X_E\} = \sigma_E^2$ , and  $\mathbb{E}\{\hat{Y}Y_E\} = \sigma_E^2$ . Hence,

$$\begin{aligned} \mathbb{E}\{\Theta_l(\beta)\} &= \mathbb{E}\left\{\sqrt{\hat{X}^2 + \hat{Y}^2}^{-(\beta+1)} [(\hat{X} - X_E)\hat{X} + (\hat{Y} - Y_E)\hat{Y}]\right\} \\ &= \underbrace{\mathbb{E}\left\{\sqrt{\hat{X}^2 + \hat{Y}^2}^{1-\beta}\right\}}_{L_1} - \underbrace{\mathbb{E}\left\{\sqrt{\hat{X}^2 + \hat{Y}^2}^{-(1+\beta)} (\hat{X}X_E + \hat{Y}Y_E)\right\}}_{L_2}. \quad (1.52) \end{aligned}$$

Since  $\hat{X}$  and  $\hat{Y}$  are uncorrelated and thus independent GRVs, by defining  $r \triangleq \sqrt{\hat{X}^2 + \hat{Y}^2}$  and  $r_E \triangleq \sqrt{X_E^2 + Y_E^2}$ , they are Rayleigh distributed and  $\phi \triangleq \angle \hat{X} + j\hat{Y}$  as well as  $\phi_E \triangleq \angle X_E + jY_E$  are uniformly distributed in  $[0, 2\pi[$ . Thus,  $L_1$  becomes

$$L_1 = \mathbb{E}\{r^{1-\beta}\} = \int_0^{+\infty} r^{1-\beta} \frac{r}{\sigma_H^2 + \sigma_E^2} e^{-\frac{r^2}{2(\sigma_H^2 + \sigma_E^2)}} dr = (2\sigma_H^2)^{\frac{1-\beta}{2}} \left(1 + \frac{\sigma_E^2}{\sigma_H^2}\right)^{\frac{1-\beta}{2}} \Gamma\left(\frac{3-\beta}{2}\right). \quad (1.53)$$

and for the joint pdf of GRVs in polar coordinates (i.e., for  $\hat{X} = r \cos \phi$ ,  $\hat{Y} = r \sin \phi$ ,  $X_E = r_E \cos \phi_E$ ,  $Y_E = r_E \sin \phi_E$ ),  $L_2$  becomes

$$\begin{aligned}
 L_2 &= \int_{-\infty}^{\infty} \int_{-\infty}^{\infty} \int_{-\infty}^{\infty} \int_{-\infty}^{\infty} \sqrt{\hat{X}^2 + \hat{Y}^2}^{-(1+\beta)} (\hat{X}X_E + \hat{Y}Y_E) \\
 &\quad \times \frac{\exp \left\{ -\frac{1}{2} \left[ \frac{1}{\sigma_H^2} (\hat{X}^2 + \hat{Y}^2) - \frac{2}{\sigma_H^2} (\hat{X}Y_E + \hat{Y}X_E) + \left( \frac{1}{\sigma_H^2} + \frac{1}{\sigma_E^2} \right) (X_E^2 + Y_E^2) \right] \right\}}{4\pi^2 \sigma_E^2 (\sigma_H^2 - \sigma_E^2)} d\hat{X} dX_E d\hat{Y} dY_E \\
 &= \int_0^{\infty} \int_0^{\infty} \int_0^{2\pi} \int_0^{2\pi} r^{-(1+\beta)} r r_E \cos(\phi - \phi_E) \frac{\exp \left\{ - \left[ \frac{r^2}{2\sigma_H^2} + \left( \frac{1}{2\sigma_H^2} + \frac{1}{2\sigma_E^2} \right) r_E^2 \right] \right\}}{4\pi^2 \sigma_E^2 (\sigma_H^2 - \sigma_E^2)} \\
 &\quad \times \exp \left[ \frac{2r r_E \cos(\phi - \phi_E)}{2\sigma_H^2} \right] |r r_E| d\phi d\phi_E dr dr_E \\
 &= \int_0^{\infty} \int_0^{\infty} \int_0^{2\pi} r^{1-\beta} r_E^2 \frac{\exp \left\{ - \left[ \frac{r^2}{2\sigma_H^2} + \left( \frac{1}{2\sigma_H^2} + \frac{1}{2\sigma_E^2} \right) r_E^2 \right] \right\}}{2\pi \sigma_E^2 (\sigma_H^2 - \sigma_E^2)} \\
 &\quad \times \left( \frac{1}{2\pi} \int_0^{2\pi} \cos(\phi - \phi_E) \exp \left[ \frac{r r_E}{\sigma_H^2} \cos(\phi - \phi_E) \right] d\phi \right) d\phi_E dr dr_E. \tag{1.54}
 \end{aligned}$$

By exploiting the properties of periodic functions, it may be showed that

$$\frac{1}{2\pi} \int_0^{2\pi} \cos(\phi - \phi_E) \exp \left[ \frac{r r_E}{\sigma_H^2} \cos(\phi - \phi_E) \right] d\phi = I_1 \left( \frac{r r_E}{\sigma_H^2} \right) \tag{1.55}$$

where  $I_1(z)$  is the modified Bessel Function of the first order.<sup>10</sup> Then (1.54) becomes

$$L_2 = \int_0^{\infty} \frac{r^{1-\beta}}{\sigma_E^2 (\sigma_H^2 - \sigma_E^2)} e^{-\frac{r^2}{2\sigma_H^2}} \left( \int_0^{\infty} r_E^2 I_1 \left( \frac{r r_E}{\sigma_H^2} \right) \exp \left[ - \left( \frac{1}{2\sigma_H^2} + \frac{1}{2\sigma_E^2} \right) r_E^2 \right] dr_E \right) \tag{1.56}$$

For  $a, b > 0$ ,  $\int_0^{\infty} t^2 I_1(bt) \exp[-at^2] dt = \frac{b}{4a^2} e^{\frac{b^2}{4a}}$  [71] and (1.56) we obtain

$$\begin{aligned}
 L_2 &= \int_0^{\infty} \frac{r^{1-\beta}}{\sigma_E^2 (\sigma_H^2 - \sigma_E^2)} \exp \left[ -\frac{r^2}{2\sigma_H^2} \right] \left( \frac{r \exp \left[ \frac{r^2}{4\sigma_H^4 \left( \frac{1}{2\sigma_H^2} + \frac{1}{2\sigma_E^2} \right)} \right]}{4\sigma_H^2 \left( \frac{1}{2\sigma_H^2} + \frac{1}{2\sigma_E^2} \right)^2} \right) dr \\
 &= \frac{\frac{\sigma_E^2}{\sigma_H^2}}{\left( 1 - \frac{\sigma_E^4}{\sigma_H^4} \right)} (2\sigma_H^2)^{\frac{1-\beta}{2}} \left( 1 + \frac{\sigma_E^2}{\sigma_H^2} \right)^{\frac{1-\beta}{2}} \Gamma \left( \frac{3-\beta}{2} \right) \tag{1.57}
 \end{aligned}$$

<sup>10</sup> The modified Bessel Function of the  $n$ -th order is defined as  $I_n(z) = \frac{1}{\pi} \int_0^{\pi} \cos n\theta e^{z \cos \theta} d\theta$ .

Consequently, (1.52) becomes

$$\mathbb{E}\{\Theta_l(\beta)\} = (2\sigma_H^2)^{\frac{1-\beta}{2}} \left(1 + \frac{\sigma_E^2}{\sigma_H^2}\right)^{\frac{1-\beta}{2}} \left[1 - \frac{\frac{\sigma_E^2}{\sigma_H^2}}{\left(1 - \frac{\sigma_E^4}{\sigma_H^4}\right)}\right] \Gamma\left(\frac{3-\beta}{2}\right). \quad (1.58)$$

Following the same methodology, we derive:

$$\begin{aligned} \mathbb{E}\{\Theta_l^2(\beta)\} &= \mathbb{E}\left\{\alpha_l^2 \hat{\alpha}_l^{-2\beta} \cos^2(\vartheta_l - \hat{\vartheta}_l)\right\} = \mathbb{E}\left\{\overbrace{(\hat{X}^2 + \hat{Y}^2)^{1-\beta}}^{L_3}\right\} \\ &\quad - \underbrace{2\mathbb{E}\left\{(\hat{X}^2 + \hat{Y}^2)^{-\beta} (\hat{X}X_E + \hat{Y}Y_E)\right\}}_{L_4} + \mathbb{E}\left\{\underbrace{(\hat{X}^2 + \hat{Y}^2)^{-(\beta+1)} (\hat{X}X_E + \hat{Y}Y_E)^2}_{L_5}\right\} \end{aligned}$$

where

$$L_3 = \int_0^{+\infty} r^{2-2\beta} \frac{r}{(\sigma_H^2 + \sigma_E^2)} \exp\left[-\frac{r^2}{2(\sigma_H^2 + \sigma_E^2)}\right] dr = (2\sigma_H^2)^{1-\beta} \left(1 + \frac{\sigma_E^2}{\sigma_H^2}\right)^{1-\beta} \Gamma(2-\beta) \quad (1.59)$$

$$L_4 = (2\sigma_H)^{1-\beta} \left(1 + \frac{\sigma_E^2}{\sigma_H^2}\right)^{1-\beta} \frac{\frac{\sigma_E^2}{\sigma_H^2}}{\left(1 - \frac{\sigma_E^4}{\sigma_H^4}\right)} \Gamma(2-\beta) \quad (1.60)$$

and

$$L_5 = \int_0^\infty \int_0^\infty r^{1-2\beta} r_E^3 \frac{\exp\left\{-\left[\frac{r^2}{2\sigma_H^2} + \left(\frac{1}{2\sigma_H^2} + \frac{1}{2\sigma_E^2}\right)r_E^2\right]\right\}}{\sigma_E^2(\sigma_H^2 - \sigma_E^2)} \left(\frac{R_1(r, r_E) + R_2(r, r_E)}{2}\right) dr dr_E \quad (1.61)$$

In (1.61) we have

$$\begin{aligned} R_1(r, r_E) &\triangleq \frac{1}{4\pi^2} \int_0^{2\pi} \int_0^{2\pi} \exp\left[\frac{rr_E}{\sigma_H^2} \cos(\phi - \phi_E)\right] d\phi d\phi_E \\ &= I_0\left(\frac{rr_E}{\sigma_H^2}\right) \frac{1}{2\pi} \int_0^{2\pi} d\phi_E = I_0\left(\frac{rr_E}{\sigma_H^2}\right) \end{aligned} \quad (1.62)$$

and

$$\begin{aligned} R_2(r, r_E) &\triangleq \frac{1}{4\pi^2} \int_0^{2\pi} \int_0^{2\pi} \cos[2(\phi - \phi_E)] \exp\left[\frac{rr_E}{\sigma_H^2} \cos(\phi - \phi_E)\right] d\phi d\phi_E \\ &= I_2\left(\frac{rr_E}{\sigma_H^2}\right) \frac{1}{2\pi} \int_0^{2\pi} d\phi_E = I_2\left(\frac{rr_E}{\sigma_H^2}\right) \end{aligned} \quad (1.63)$$

with  $I_0(z)$  and  $I_2(z)$  being the modified Bessel Functions of order 0 and 2, respectively. By substituting (1.62) and (1.63) in (1.61) we obtain

$$L_5 = \int_0^\infty r^{1-2\beta} \frac{\exp\left[-\frac{r^2}{2\sigma_H^2}\right]}{\sigma_E^2(\sigma_H^2 - \sigma_E^2)} \left\{ \int_0^\infty \frac{1}{2} \left[ I_0\left(\frac{rr_E}{\sigma_H^2}\right) + I_2\left(\frac{rr_E}{\sigma_H^2}\right) \right] r_E^3 \exp\left[-\left(\frac{1}{2\sigma_H^2} + \frac{1}{2\sigma_E^2}\right)r_E^2\right] dr_E \right\} dr. \quad (1.64)$$

Since from [71] we have  $\int_0^{+\infty} \frac{1}{2}[I_0(bt) + I_2(bt)]t^3 \exp[-at^2] = \frac{(2a+b^2)}{8a^3} \exp\left[\frac{b^2}{4a}\right]$ , for  $a, b > 0$ , (1.64) becomes

$$\begin{aligned} L_5 &= \int_0^\infty r^{1-2\beta} \frac{\exp\left[-\frac{r^2}{2\sigma_H^2}\right]}{\sigma_E^2(\sigma_H^2 - \sigma_E^2)} \left\{ \frac{2\left(\frac{1}{2\sigma_H^2} + \frac{1}{2\sigma_E^2}\right) + \left(\frac{r}{\sigma_H^2}\right)^2}{8\left(\frac{1}{2\sigma_H^2} + \frac{1}{2\sigma_E^2}\right)^3} \exp\left[\frac{\left(\frac{r}{\sigma_H^2}\right)^2}{4\left(\frac{1}{2\sigma_H^2} + \frac{1}{2\sigma_E^2}\right)}\right] \right\} dr \\ &= \frac{\frac{\sigma_E^2}{\sigma_H^2} \left(Q_1 + \frac{\sigma_E^2}{\sigma_H^2} Q_2\right)}{\left(1 - \frac{\sigma_E^4}{\sigma_H^4}\right) \left(1 + \frac{\sigma_E^2}{\sigma_H^2}\right)} \end{aligned} \quad (1.65)$$

with

$$Q_1 \triangleq \int_0^{+\infty} r^{1-2\beta} \exp\left[-\frac{1}{2\sigma_H^2} \left(\frac{1}{1 + \frac{\sigma_E^2}{\sigma_H^2}}\right) r^2\right] dr = \frac{1}{2} (2\sigma_H^2)^{1-\beta} \left(1 + \frac{\sigma_E^2}{\sigma_H^2}\right)^{1-\beta} \Gamma(1-\beta) \quad (1.66)$$

and

$$Q_2 \triangleq \frac{1}{\sigma_H^2 \left(1 + \frac{\sigma_E^2}{\sigma_H^2}\right)} \int_0^{+\infty} r^{3-2\beta} \exp\left[-\frac{1}{2\sigma_H^2} \left(\frac{1}{1 + \frac{\sigma_E^2}{\sigma_H^2}}\right) r^2\right] dr = (2\sigma_H^2)^{1-\beta} \left(1 + \frac{\sigma_E^2}{\sigma_H^2}\right)^{1-\beta} \Gamma(2-\beta). \quad (1.67)$$

By substituting (1.66) and (1.67) in (1.65) we obtain

$$L_5 = (2\sigma_H^2)^{1-\beta} \left(1 + \frac{\sigma_E^2}{\sigma_H^2}\right)^{1-\beta} \frac{\frac{\sigma_E^2}{\sigma_H^2}}{\left(1 - \frac{\sigma_E^4}{\sigma_H^4}\right)} \left[1 - \frac{\left(\frac{1-\beta}{1-\beta}\right)}{\left(1 + \frac{\sigma_E^2}{\sigma_H^2}\right)}\right] \Gamma(2-\beta). \quad (1.68)$$

Now, by substituting (1.59), (1.60) and (1.68) in (1.59) we find that

$$\mathbb{E}\{\Theta_i^2(\beta)\} = (2\sigma_H^2)^{1-\beta} \left(1 + \frac{\sigma_E^2}{\sigma_H^2}\right)^{1-\beta} \Sigma\left(\frac{\sigma_E^2}{\sigma_H^2}, \beta\right) \Gamma(2-\beta) \quad (1.69)$$

where

$$\Sigma\left(\frac{\sigma_E^2}{\sigma_H^2}, \beta\right) \triangleq 1 - \frac{\frac{\sigma_E^2}{\sigma_H^2}}{\left(1 - \frac{\sigma_E^4}{\sigma_H^4}\right)} \left[1 + \frac{\left(\frac{1-\beta}{1-\beta}\right)}{\left(1 + \frac{\sigma_E^2}{\sigma_H^2}\right)}\right]. \quad (1.70)$$

By exploiting (1.58) and (1.69), we finally arrive at

$$\begin{aligned}
\zeta_\beta(\alpha) &= \mathbb{E}\{\Theta_l^2(\beta)\} - (\mathbb{E}\{\Theta_l(\beta)\})^2 = (2\sigma_H^2)^{1-\beta} \left(1 + \frac{\sigma_E^2}{\sigma_H^2}\right)^{1-\beta} \Sigma\left(\frac{\sigma_E^2}{\sigma_H^2}, \beta\right) \Gamma(2-\beta) \\
&\quad - (2\sigma_H^2)^{1-\beta} \left(1 + \frac{\sigma_E^2}{\sigma_H^2}\right)^{1-\beta} \left[1 - \frac{\frac{\sigma_E^2}{\sigma_H^2}}{\left(1 - \frac{\sigma_E^4}{\sigma_H^4}\right)}\right]^2 \Gamma^2\left(\frac{3-\beta}{2}\right) \\
&= (2\sigma_H^2)^{1-\beta} \left(1 + \frac{\sigma_E^2}{\sigma_H^2}\right)^{1-\beta} \left[\Sigma\left(\frac{\sigma_E^2}{\sigma_H^2}, \beta\right) \Gamma(2-\beta) - \Pi^2\left(\frac{\sigma_E^2}{\sigma_H^2}\right) \Gamma^2\left(\frac{3-\beta}{2}\right)\right] \quad (1.71)
\end{aligned}$$

where

$$\Pi\left(\frac{\sigma_E^2}{\sigma_H^2}\right) \triangleq 1 - \frac{\frac{\sigma_E^2}{\sigma_H^2}}{\left(1 - \frac{\sigma_E^4}{\sigma_H^4}\right)}. \quad (1.72)$$



## 2. ECHO CANCELLERS BASED ON PSEUDO-NOISE TRAINING SEQUENCES AND PULSE METHODS: PERFORMANCE AND STABILITY ANALYSIS

### 2.1 *Introduction*

An advantage of the recent Digital Video Broadcasting - Terrestrial/Handheld (DVB-T/H) standards [75] [76] is the possibility to realize a Single Frequency Network (SFN) to broadcast the video signal. As a consequence, the delicate task of planning the service coverage for a given geographical area is greatly simplified with respect to more traditional Multi Frequency Networks (MFNs), both because the frequency distribution on the territory stop being a critical issue and also because proper On-Channel Repeaters (OCRs) can be easily introduced as gap-fillers to extend or enhance the coverage [77]. Because of the Orthogonal Frequency Division Multiplexing (OFDM) modulation adopted by the standard, these devices should be characterized by very low processing delays and hence direct relay schemes are to be preferred to more complex regenerative solutions. Moreover, the possible presence of strong adjacent channels leads to the introduction of filters with good selectivity within the OCR.

Another phenomenon to consider when designing and installing an OCR is the coupling between the transmitting and the receiving antennas, which inevitably causes detrimental echoes in the received signal. In practice these echoes degrade the signal and limit the amplifier gain of the repeater, in order to avoid dangerous oscillations with potential system instability. To address this critical problem, several architectures for digital echo cancellers have been proposed, which mainly differ on the basis of the technique adopted to estimate the coupling channel. In [78] a strategy is proposed based on the pilot carriers of the DVB-T/H signal, while the solution in [79] has a lower complexity and is basically independent of the characteristics of the signal to repeat. In this paper we focus on the latter technique, which is based on the continuous transmission of a low-power training sequence performed by the OCR itself. At its receiver side, the OCR exploits the good au-

to correlation properties of this known signal to estimate the coupling channel and, then, compensates the echoes with an adaptive filter. The initial estimation of the coupling channel may be performed without re-transmitting the received signal, i.e. referring to an open-loop scheme, avoiding the risk of instability and reducing the duration of the first channel estimation.

While the idea of a local training signal based on PN or CAZAC sequences appears certainly appealing, some important aspects have not been sufficiently investigated yet. In particular, in [79] the effects of the filtering stage at the OCR receiving side have been neglected, while it has a remarkable impact on the performance of the echo canceller, since it contributes in determining the global channel impulse response. In [80] the effects of the filtering stages within the OCR have been considered and their impact on the performance of the echo canceller has been investigated. Moreover, the work in [80] has highlighted the need to address the electromagnetic compatibility issues imposed for the DVB-T/H power spectrum when designing echo cancelling units based on local training signals.

In this paper not only the PN technique presented in [79, 80] is more deeply investigated but an alternative method to perform the coupling channel estimation is also proposed and analyzed. In particular, proper pulse trains are locally generated to periodically estimate the echoes and correspondingly set the cancelling unit. After an initial theoretical analysis of the system, which allowed us to obtain the analytical expression of several important performance figures, we worked on the real implementation of our solution, based on FPGA (FPGA) technology. Our theoretical approach provided important insights into the behavior of the echo canceller and useful guidelines for the following design and implementation steps. Finally, the developed prototype has been tested through a campaign of measurements which validated our theoretical analysis, highlighting the good performance achievable by the proposed solution. The organization of the rest of the paper mimics the main stages followed in our work: in section II we present the system model, in section III we describe the estimation technique. In section IV we develop the analytical model of the echo canceller. In section V the performance of the echo canceller are analytically evaluated and compared with the results of the measurement campaign performed on the prototype presented in [81]. Finally, in section VI the problem of the repeater stability is discussed and an upper bound of the probability of instability is analytically found.

## 2.2 System description

The principles of an OCR are the following. The signal transmitted by the base station is received by the receiving antenna of the OCR, is properly filtered and it is retransmitted by the transmitting antennas towards the final user. Since there is a coupling channel between the two antennas, the filtering process of the OCR, in the case of SFN (where the receiving and the transmitting filters have to be centered on the same frequency), has to realize an echo cancellation.

Let us consider the general scheme depicted in Fig.2.1, where the equivalent low-pass representation of signals and processing blocks is adopted.

The basic

In the following we consider both the A/D and the D/A converters as ideal, with an infinite bit-precision such that, being  $x(t)$  its continuous-time input, its discrete-time output results in  $x[k] = x(kT_s)$ , where  $T_s$  is the time sample, and, being  $x[n]$  the discrete-time input of the D/A converter, its continuous-time output can be expressed as

$$x(t) = \sum_{n=-\infty}^{+\infty} x[n] \operatorname{sinc}\left(\frac{t - nT_s}{T_s}\right), \quad (2.1)$$

where:

$$\operatorname{sinc}(t) \doteq \begin{cases} \frac{\sin(\pi t)}{\pi t} & \text{if } t \neq 0 \\ 1 & \text{if } t = 0. \end{cases}$$

The received DVB-T/H signal  $d'(t)$  is sampled by an ideal A/D converter with sampling frequency  $f_s = 1/T_s$ , chosen high enough to avoid aliasing. Then it is passed through a digital filter aimed at reducing the amount of noise and interference from adjacent channels and characterized by the periodical transfer function

$$H_R(f) \triangleq \sum_{k=0}^{N_R-1} h_{R,k} e^{j2\pi f k T_s}, \quad (2.2)$$

where  $N_R$  is the number of taps and  $\{h_{R,k}\}_{k=0}^{N_R-1}$  are the corresponding coefficients. Dually, at the output, the D/A conversion is preceded by a digital transmission filter whose main goal is to make the transmitted signal compliant with the electromagnetic compatibility mask, with transfer function:

$$H_T(f) \triangleq \sum_{k=0}^{N_T-1} h_{T,k} e^{j2\pi f k T_s}, \quad (2.3)$$

where  $N_T$  is the number of taps and  $\{h_{T,k}\}_{k=0}^{N_T-1}$  are the corresponding coefficients. We remark that the operations of decimation at the receiver and of interpolation at the transmitter, which are necessary to reduce the complexity in practical implementations, as described in [82], can be here considered included in OCR filtering by an opportune choice of  $H_T(f)$  and  $H_T(f)$  coefficients. After the D/A conversion, the signal to be transmitted is amplified by a high power amplifier (HPA) with gain  $G$ . In this preliminary analysis we assume the amplifier as ideal, i.e. not affected by non-linear effects and not frequency-selective within the considered bandwidth. Due to coupling effects between the transmitter and receiver antennas, a part of the (re)transmitted signal returns at the OCR receiver side through the physical channel with transfer function  $H_p(f)$ . The correspondent continuous-time pulse response can be modeled as

$$h_p(t) = \sum_{l=0}^{L-1} h_l \delta(t - \tau_l), \quad (2.4)$$

where  $L$  is the total number of paths, and  $\tau_l$  and  $h_l$  are the delay and the complex gain of the  $l$ -th path, respectively.

If we denote the discrete-time coupling channel  $H_c(f)$  as the D/A followed by  $H_p(f)$ <sup>1</sup> and by A/D, it is<sup>2</sup>:

$$H_c(f) = \sum_{n=-\infty}^{+\infty} H_p \left( f - \frac{n}{T_s} \right) \text{rect}(fT_s - n), \quad (2.6)$$

and

$$\text{rect}(x) = \begin{cases} 1 & \text{if } |x| < 1/2 \\ 0 & \text{otherwise.} \end{cases}$$

Now we indicate with

$$H_{\text{eq}}(f) \triangleq \sqrt{G} H_T(f) H_c(f) H_R(f) \quad (2.7)$$

the (periodical) frequency response of the discrete-time equivalent coupling channel. In the frequency domain it is:

$$H_{\text{eq}}(f) = \sqrt{G} H_R(f) H_T(f) \sum_{n=-\infty}^{+\infty} \sum_{l=0}^{L-1} h_l e^{-j2\pi(f - \frac{n}{T_s})\tau_l} \text{rect}(fT_s - n), \quad (2.8)$$

<sup>1</sup>  $H_p(f) = \mathcal{F}\{h_p(t)\}$

<sup>2</sup> In general, it can be easily shown that a time continuous block with transferring function  $H(f)$ , preceded by an ideal D/A converter and followed by an A/D converter, is equivalent to a discrete-time block with transferring function:

$$H_d(f) = \sum_{n=-\infty}^{+\infty} H(f - \frac{n}{T}) \text{rect}(fT - n). \quad (2.5)$$

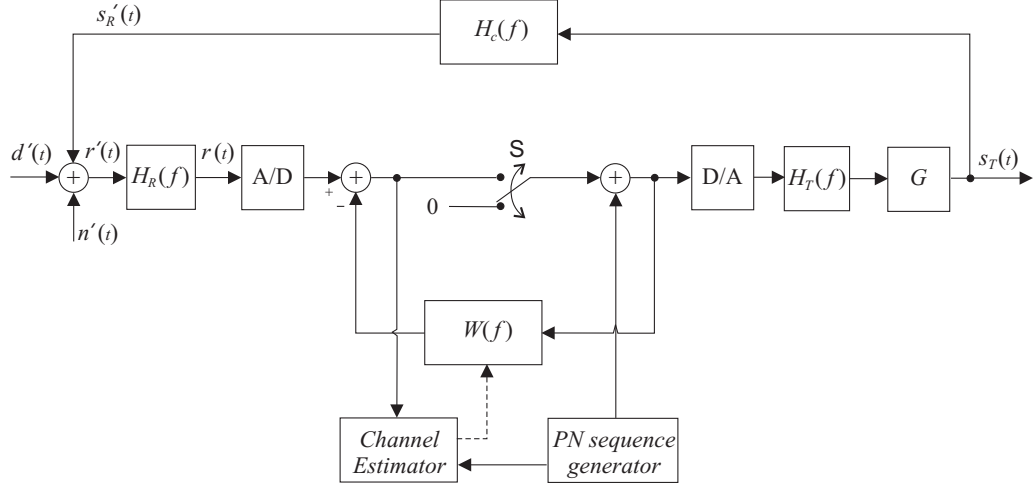


Fig. 2.1: Block architecture of the considered OCR. ■[■MM]Figura da sistemare

corresponding to the samples:

$$h_{\text{eq}}[n] = \sqrt{G} \sum_{l=0}^{L-1} h_l h(nT_s - \tau_l) \quad (2.9)$$

where  $h(t) = \mathcal{F}^{-1} \{T_s H_R(f) H_T(f) \text{rect}(fT_s)\}$ . Finally, in Fig.2.1 we have represented with  $W(f)$  the transfer function of the digital echo cancelling filter, which introduces the negative feedback capable to counterbalance the positive feedback due to coupling.

### 2.3 Coupling channel estimation and echo cancellation

The OCR operates in two different modes: in the first one (referred to as *start-up mode*), the switch S (see Fig.2.1) is open and the repeater estimates the coupling channel without retransmitting the received signal. This process is based on the open-loop transmission of estimation pulses. Once the channel has been estimated, the echo canceller block is properly initialized, the switch S is closed and the OCR starts repeating the received DVB-T/H signal (*steady-state mode*). The cancellation mechanism is based on the possibility to estimate the coupling channel impulse response and to locally reproduce it through a digital FIR filter. While operating in the *steady-state mode*, the OCR may keep tracking the possible channel variations by continuously transmitting the estimation signal superimposed to the useful signal. Moreover, in this phase, in order to both improve the estimation of

the coupling channel and continuously follow its variations, algorithms such as LMS can be usefully employed.

In the following we will focus on the initial *start-up* phase, describing the estimation techniques and providing some important performance figures [81].

The estimation of the coupling channel pulse response is performed opening the switch S, transmitting a pseudonoise signal (A) or a train of pulses (B), as described below, through the equivalent coupling channel and processing the signal samples re-entering the OCR. It has to be noticed that the disturbance affecting the estimation is due to both the thermal noise and the received DVB-T/H data signal.

Once the samples of the equivalent coupling channel have been estimated the echo canceller is initialized and the OCR switches to the steady-state operating mode, closing S and effectively repeating the received signal. The actual echo cancellation is performed through a digital FIR filter, realizing a negative feedback which cancels the positive coupling effects. Denoting with  $W(f)$  the transfer function of the cancelling filter, we have that the condition for a perfect echo cancellation would be

$$W(f) = H_{\text{eq}}(f) \quad (2.10)$$

for  $f \in \left[-\frac{1}{2T_s}, \frac{1}{2T_s}\right]$ . In practice, to realize the digital echo canceller we employ a shift register with  $D$  stages followed by a FIR filter with  $P$  taps, indicated with  $\{w_k\}_{k=0}^{P-1}$ . In fact the receiving and transmitting filters introduce a deterministic delay for the echo, which can be easily compensated through a shift register of proper length. The cancelling window covered by the FIR filter has a length of  $P \cdot T_s$  seconds, starting from instant  $D \cdot T_s$ . Thus, the transfer function  $W(f)$  of the overall echo canceller is:

$$W(f) = \sum_{k=0}^{P-1} w_k e^{-j2\pi f k T_s} e^{-j2\pi f D T_s}. \quad (2.11)$$

We set the filter taps to mimic the behaviour of the equivalent coupling channel. We notice that the ideal condition (2.10) is satisfied, for  $w_k = h_{\text{eq}}[k + D]$  (ideal estimation), only when  $h_{\text{eq}}[k] = 0, \forall k \in ]-\infty, 1] \cup [P + 1, \infty[$ . In this case the overall transferring function of the OCR is a constant in the frequency domain.

### 2.3.1 Pseudo-noise Method

Since the switch S is open, the transmitted signal (before the transmitting filter) is only constituted by the training signal

$$s_{\text{T}}^{(\text{pn})}[n] = \sqrt{\mathcal{P}}c[n] \quad (2.12)$$

where  $c[n]$  are the symbols composing the periodic training sequence of period  $M$ , with  $|c[n]|^2 = 1$  and  $c[n + M] = c[n] \quad \forall n$ , and  $\mathcal{P}$  is a constant determining the power of the training signal. In particular, the power spectral density of the transmitted training signal is approximately [84]

$$P_{s_T}^{(\text{pn})}(f) \approx \mathcal{P} T_s |H_T(f)|^2 \quad (2.13)$$

when  $\{c[n]\}$  has good autocorrelation properties (e.g. CAZAC or PN sequence).

After the equivalent coupling channel  $H_{\text{eq}}(f)$ , the signal  $r[k] = s_R^{\text{pn}}[k] + n[k] + d[k]$  is present, where the term

$$s_R^{(\text{pn})}[k] = \sum_{n=-\infty}^{+\infty} h_{\text{eq}}[n] s_T^{(\text{pn})}[k-n] = \sqrt{\mathcal{P}} \sum_{n=-\infty}^{+\infty} h_{\text{eq}}[n] c[k-n] \quad (2.14)$$

is due to the coupling channel,  $d[k]$  is the received DVB-T/H signal and  $n[k]$ 's are the noise samples, belonging to a WSS zero-mean gaussian random process. As shown in Appendix A, under the assumption  $0 \leq 1/(T_s B_{R,\text{eq}}) - 1 \ll 1$  (that is, the oversampling is not too high), we can neglect correlations between successive noise samples and consider the  $n[k]$ 's as statistically i.i.d. and distributed according to a Circular Symmetric Gaussian Distribution (CSGC) R.V., that is  $n[k] \sim \mathcal{CN}(0, 2N_0 B_{R,\text{eq}})$ . The goal of the channel estimator is to estimate the samples of the global channel impulse response  $h_{\text{eq}}(t)$ , i.e. the set  $\{h_{\text{eq}}(kT_s)\}$ . The estimation process simply consists of correlating the received samples  $s_R^{\text{pn}}[k]$  with local delayed replicas of the transmitted sequence  $\{c[n]\}$ , providing the set of estimated values  $\{\hat{h}_{\text{eq}}^{(\text{pn})}[k]\}$ :

$$\begin{aligned} \hat{h}_{\text{eq}}^{(\text{pn})}[k] &\triangleq \frac{1}{M\sqrt{\mathcal{P}}} \sum_{m=0}^{M-1} s_R^{\text{pn}}[m+k] \cdot c^*[m] \\ &= \sum_{n=-\infty}^{+\infty} h_{\text{eq}}[n] \frac{1}{M} \sum_{m=0}^{M-1} c[m+k-n] c^*[m] + \nu^{(\text{pn})}[k] \\ &= \frac{1}{M} \sum_{n=-\infty}^{+\infty} h_{\text{eq}}[n] R_c[k-n] + \nu^{(\text{pn})}[k], \end{aligned} \quad (2.15)$$

where we have incorporated all the disturbance components affecting the estimates in the term

$$\nu^{(\text{pn})}[k] = \frac{1}{M\sqrt{\mathcal{P}}} \sum_{m=0}^{M-1} (d[m+k] + n[m+k]) \cdot c^*[m] \quad (2.16)$$

and we have introduced the discrete autocorrelation function of the transmitted sequence:

$$R_c[i] \triangleq \sum_{m=0}^{M-1} c[i+m] c^*[m]. \quad (2.17)$$

Since  $d[k]$  is approximately Gaussian [85], for what shown in Appendix A we can assume the noise samples  $\nu^{(\text{pn})}[k]$  as statistically i.i.d. and distributed according to a CSGC R.V., i.e.

$$\nu^{(\text{pn})}[k] \sim \mathcal{CN}\left(0, \frac{2N_0 B_{\text{R,eq}}}{M\mathcal{P}} + \frac{P_{\text{DVB}}}{M\mathcal{P}}\right), \quad (2.18)$$

where  $N_0$  is the one-sided power spectral density of the thermal noise,  $P_{\text{DVB}}$  is the power of the signal  $d(t)$  and  $B_{\text{R,eq}}$  is the equivalent noise bandwidth of the receiving filter. We verified that this approximation well suits the case under study. As a training signal we will consider psuedo-noise (PN) sequences. Although other interesting possibilities exist (e.g. CAZAC sequences), PN sequences have the advantage of admitting a low-complex generation hardware and easily allow long sequence periods  $M$ . In this case we have  $c_m \in \{\pm 1\}$  and the autocorrelation function is:

$$R_c[r] = \begin{cases} M & \text{if } r = kM, k \in \mathbb{Z} \\ -1 & \text{otherwise.} \end{cases} \quad (2.19)$$

The channel estimates (2.15) then become

$$\hat{h}_{\text{eq}}^{(\text{pn})}[k] = h_{\text{eq}}[k] - \frac{1}{M} \sum_{n=-\infty, n \neq kM}^{+\infty} h_{\text{eq}}[n] + \nu^{(\text{pn})}[k], \quad (2.20)$$

where we have isolated the actual channel sample  $h_{\text{eq},k}$  from the disturbance components. By remembering (2.15) and (2.9):

$$\begin{aligned} w_k^{(\text{pn})} &= h_{\text{eq}}[k+D] \\ &= \sqrt{G} \sum_{l=0}^{L-1} h_l \sum_{i=-\infty}^{+\infty} h((k-i)T_s + DT_s - \tau_l) \frac{R_c[i]}{M} + \eta^{(\text{pn})}[k], \end{aligned} \quad (2.21)$$

where we have defined  $i \triangleq k + D - n$  and  $\eta^{(\text{pn})}[k] \triangleq \nu^{(\text{pn})}[k + D]$ . From (2.11) in the frequency domain it is:

$$\begin{aligned} W^{(\text{pn})}(f) &= \sum_{k=0}^{P-1} \left[ \sqrt{G} \sum_{l=0}^{L-1} h_l \sum_{i=-\infty}^{+\infty} \frac{R_c(i)}{M} h((k-i)T_s + DT_s - \tau_l) + \nu_k^{(\text{pn})'} \right] e^{-j2\pi f(k+D)T_s} \\ &= \sqrt{G} \sum_{l=0}^{L-1} h_l \sum_{k=0}^{P-1} \sum_{i=-\infty}^{+\infty} \frac{R_c(i)}{M} h[(k-i)T_s + DT_s + \tau_l] e^{-j2\pi f(k+D)T_s} + \sum_{k=0}^{P-1} \nu_k^{(\text{pn})'} e^{-j2\pi f(k+D)T_s} \end{aligned} \quad (2.22)$$

Defining

$$\Pi_{l,k} \triangleq \sum_{i=-\infty}^{+\infty} \frac{R_c(i)}{M} h[(k-i)T_s + DT_s + \tau_l] \quad (2.23)$$

for  $l = 0 \dots L - 1$  and  $k = 0 \dots P - 1$ , we have:

$$W^{(\text{pn})}(f) = \sqrt{G} \sum_{l=0}^{L-1} h_l \sum_{k=0}^{P-1} \Pi_{l,k}^{(\text{pn})} e^{-j2\pi f(k+D)T_s} + \sum_{k=0}^{P-1} \eta^{(\text{pn})}[k] e^{-j2\pi f(k+D)T_s}. \quad (2.24)$$

Exploiting the correlation properties of the PN sequences, we can write:

$$\begin{aligned} \Pi_{l,k} &= \frac{M+1}{M} h(kT_s - \tau_l + DT_s) - \frac{1}{M} \sum_{r=-\infty}^{+\infty} h[(k-r)T_s - \tau_l + DT_s] \\ &= \frac{M+1}{M} h(kT_s - \tau_l + DT_s) - \frac{H(0)}{MT_s} \end{aligned} \quad (2.25)$$

where, as usual, we have assumed  $f_s$  high enough to avoid any aliasing effects determined by the sampling of  $h(t)$ . According to our model, increasing the sample rate  $f_s$  implies an increment in the chip-rate of the PN sequence, spreading the spectrum of the training signal over a wider bandwidth. Since the power the training signal after the D/A conversion is fixed, the power effectively transmitted (i.e. after the filter and the amplifier stages) decreases. Moreover, introducing the functions

$$\Upsilon_l^{(\text{pn})}(f) \triangleq \sum_{k=0}^{P-1} \Pi_{l,k} e^{-j2\pi f(k+D)T_s} \quad (2.26)$$

and

$$\Omega^{(\text{pn})}(f) \triangleq \sum_{k=0}^{P-1} \eta^{(\text{pn})}[k] e^{-j2\pi f(k+D)T_s} \quad (2.27)$$

equation (2.24) becomes:

$$W^{(\text{pn})}(f) = \sqrt{G} \sum_{l=0}^{L-1} h_l \Upsilon_l^{(\text{pn})}(f) + \Omega^{(\text{pn})}(f). \quad (2.28)$$

### 2.3.2 Pulse Method

In the ‘‘pulse sounding’’ method, the actual shape of the transmitted pulse after the D/A conversion is  $h_T(t) = \mathcal{F}^{-1} \{T_s H_T(f) \text{rect}(fT_s)\}$ . In order to reduce the estimation errors, the pulses are repeated  $N$  times with interval  $T_p \triangleq K \cdot T_s$ , with  $K$  integer, and the samples of the corresponding responses are averaged.

The pulse train before the transmitting filter and the D/A converter is

$$s_T^{(\text{ps})}[n] = \sum_{m=0}^{N-1} p_m \delta_{mK-n} \quad (2.29)$$

with  $\delta_k$  representing the Kronecker delta at the  $k$ -th instant,  $p_m$  the complex amplitude of the  $m$ -th pulse and  $R$  the discrete-time interval between the pulses. The received signal is:

$$\begin{aligned} s_{\text{R}}^{(\text{ps})}[k] &= \sum_{n=-\infty}^{+\infty} s_{\text{T}}^{(\text{ps})}[n] h_{\text{eq}}[k-n] + d[k] + n[k] = \sum_{n=-\infty}^{+\infty} \sum_{m=0}^{N-1} p_m \delta_{mK-n} h_{\text{eq}}[k-n] + d[k] + n[k] \\ &= \sum_{m=0}^{N-1} p_m h_{\text{eq}}[k-mK] + d[k] + n[k], \end{aligned} \quad (2.30)$$

where  $d[k]$  and  $n[k]$  are the same as the pseudo-noise case.

Indicating the complex amplitude of the  $n$ -th pulse with  $p_n = Ae^{j\phi_n}$ , where  $A > 0$  is a fixed amplitude and  $\phi_n$  a proper phase shift, the samples of the equivalent coupling channel impulse response can be estimated by simply averaging the normalized received pulses, as shown below:

$$\begin{aligned} \hat{h}_{\text{eq}}^{(\text{ps})}[k] &= \frac{1}{N} \sum_{n=0}^{N-1} \frac{p_n^*}{A^2} s_{\text{R}}^{(\text{ps})}[nK+k] \\ &= \frac{1}{NA^2} \sum_{n=0}^{N-1} \sum_{m=0}^{N-1} p_n^* p_m h_{\text{eq}}[k+(n-m)K] + \frac{1}{NA^2} \sum_{n=0}^{N-1} p_n^* d[nK+k] + \frac{1}{NA^2} \sum_{n=0}^{N-1} p_n^* n[nK+k] \\ &= \frac{1}{N} \sum_{n=0}^{N-1} h_{\text{eq}}[k] + \frac{1}{NA} \sum_{n=0}^{N-1} e^{-j\phi_n} d[nK+k] + \frac{1}{NA} \sum_{n=0}^{N-1} e^{-j\phi_n} n[nK+k] \\ &= h_{\text{eq}}(kT_s) + \nu^{(\text{ps})}[k], \end{aligned} \quad (2.31)$$

where we have assumed that the interval  $K$  is long enough to have  $h_{\text{eq}}[n] \approx 0$ ,  $\forall n$  such that  $|n| \geq K$ , and where:

$$\nu^{(\text{ps})}[k] \triangleq \frac{1}{NA} \sum_{n=0}^{N-1} e^{-j\phi_n} d[nK+k] + \frac{1}{NA} \sum_{n=0}^{N-1} e^{-j\phi_n} n[nK+k]. \quad (2.32)$$

As in the pseudo-noise case, we can assume the noise samples  $\nu^{(\text{ps})}[k]$  as statistically i.i.d. (see Appendix A) and distributed according to a CSGC R.V., i.e.

$$\nu^{(\text{ps})}[k] \sim \mathcal{CN} \left( 0, \frac{2N_0 B_{\text{R,eq}}}{NA^2} + \frac{P_{\text{DVB}}}{NA^2} \right). \quad (2.33)$$

We verified that this Gaussian approximation well suits the case under study. From (2.31) and (2.9):

$$\begin{aligned}
w_k^{(\text{ps})} &= \hat{h}_{\text{eq}}^{(\text{ps})}[k + D] \\
&= h_{\text{eq}}^{(\text{ps})}[k + D] + \nu^{(\text{ps})}[k + D] \\
&= \sqrt{G} \sum_{l=0}^{L-1} h_l h((k + D)T_s - \tau_l) + \nu^{(\text{ps})}[k + D] \\
&= \sqrt{G} \sum_{l=0}^{L-1} h_l h(kT_s + DT_s - \tau_l) + \eta^{(\text{ps})}[k], \tag{2.34}
\end{aligned}$$

where  $\eta^{(\text{ps})}[k] \triangleq \nu^{(\text{ps})}[k + D]$ .

Inserting the expression of the  $w_k$ 's into (2.11) we obtain, for the pulse method:

$$\begin{aligned}
W^{(\text{ps})}(f) &= \sum_{k=0}^{P-1} \left[ \sqrt{G} \sum_{l=0}^{L-1} h_l h(kT_s + DT_s - \tau_l) + \nu^{(\text{ps})}[k + D] \right] e^{-j2\pi f k T_s} e^{-j2\pi f D T_s} \\
&= \sqrt{G} \sum_{l=0}^{L-1} \sum_{k=0}^{P-1} h_l h(kT_s + DT_s - \tau_l) e^{-j2\pi f (k+D)T_s} + \sum_{k=0}^{P-1} \eta^{(\text{ps})}[k] e^{-j2\pi f (k+D)T_s} \tag{2.35}
\end{aligned}$$

Moreover, introducing the functions

$$\Upsilon_l^{(\text{ps})}(f) \triangleq \sum_{k=0}^{P-1} h(kT_s + DT_s - \tau_l) e^{-j2\pi f (k+D)T_s} \tag{2.36}$$

and

$$\Omega^{(\text{ps})}(f) \triangleq \sum_{k=0}^{P-1} \eta^{(\text{ps})}[k] e^{-j2\pi f (k+D)T_s} \tag{2.37}$$

equation (2.35) becomes:

$$W^{(\text{ps})}(f) = \sqrt{G} \sum_{l=0}^{L-1} h_l \Upsilon_l^{(\text{ps})}(f) + \Omega^{(\text{ps})}(f). \tag{2.38}$$

## 2.4 Performance Evaluation

### 2.4.1 Rejection Ratio

After initializing the canceller filter, the switch S is closed and the OCR starts repeating the received signal. Denote  $P_s(f)$  the power spectrum of the signal the OCR is designed to repeat. From our previous assumptions, it turns out that  $P_s(f)$  is strictly zero for

frequencies above the Nyquist frequency, that is, more precisely,  $P_s(f) = 0 \quad \forall f$  such that  $|f| > \frac{1}{2T_s}$ . We define the Rejection Ratio for the considered signal as  $RR \doteq P_r/P_s$ , where  $P_s = \int_{-\infty}^{+\infty} P_s(f)df$  is the power of the transmitted signal and  $P_r$  is the residue of the transmitted power re-entering the OCR, after the echo cancellation and the D/A conversion. Basically, without any echo canceller, the RR represents the system loop-gain due to the amplifier and the echoes. According to the definition we can write<sup>3</sup>

$$RR = \int_{-\infty}^{+\infty} \text{rect}(fT_s) |H_{\text{eq}}(f) - W(f)|^2 \frac{P_s(f)}{P_s} df. \quad (2.39)$$

Since from (2.8) it is:

$$\begin{aligned} H_{\text{eq}}(f)\text{rect}(fT_s) &= \sqrt{G}H_R(f)H_T(f) \sum_{n=-\infty}^{+\infty} \sum_{l=0}^{L-1} h_l e^{-j2\pi(f-\frac{n}{T_s})\tau_l} \text{rect}(fT_s - n) \text{rect}(fT_s) \\ &= \frac{\sqrt{G}}{T_s} \overbrace{T_s H_R(f)H_T(f)\text{rect}(fT_s)}^{H(f)} \sum_{l=0}^{L-1} h_l e^{-j2\pi f\tau_l}, \end{aligned} \quad (2.40)$$

the expression (2.39) becomes

$$\begin{aligned} RR &= \int_{-\infty}^{\infty} \left| \sqrt{G} \frac{H(f)}{T_s} \sum_{l=0}^{L-1} h_l e^{-j2\pi f\tau_l} - \sum_{k=0}^{P-1} w_k e^{-j2\pi f(k+D)T_c} \right|^2 \frac{P_s(f)}{P_s} df \\ &= \int_{-\infty}^{\infty} \left| \sqrt{G} \sum_{l=0}^{L-1} h_l \frac{H(f)}{T_s} e^{-j2\pi f\tau_l} - \sqrt{G} \sum_{l=0}^{L-1} h_l \Upsilon_l(f) - \Omega(f) \right|^2 \frac{P_s(f)}{P_s} df \\ &= \int_{-\infty}^{\infty} \left| \sqrt{G} \sum_{l=0}^{L-1} h_l \left[ \frac{H(f)}{T_s} e^{-j2\pi f\tau_l} - \Upsilon_l(f) \right] - \Omega(f) \right|^2 \frac{P_s(f)}{P_s} df. \end{aligned} \quad (2.41)$$

We note here that the RR is a random variable, since, even fixing the coupling channel, it depends on the noise samples  $\nu'_k$  included in the definition of  $\Omega(f)$ .

#### 2.4.2 Mean Rejection Ratio

Let us introduce the normalized autocorrelation function for the transmitted signal

$$R_s(\tau) \triangleq \mathcal{F}^{-1} \left\{ \frac{P_s(f)}{P_s} \right\} \quad (2.42)$$

<sup>3</sup> Since the following equations are formally identical in the case of Pseudo-Noise method and in the case of Pulse method, we have neglected for simplicity the superscripts (pn) and (ps) over the functions that are defined differently in the two cases.

and, indicating with  $R_h(\tau)$  the autocorrelation function of  $h(t)$ , let us define

$$R_{h,s}(\tau) \triangleq R_h(\tau) \otimes R_s(\tau) \quad (2.43)$$

$$R_1(\tau) \triangleq h(\tau) \otimes R_s(\tau). \quad (2.44)$$

Given the coupling channel, the MRR is obtained by averaging the expression (2.41) over the random noise. After some tedious but straightforward analytical passages, we find that:

$$\begin{aligned} \text{MRR}^{(\text{pn})} &= \mathbb{E} \{ \text{RR} \} = \\ &= G \sum_{l=0}^{L-1} \sum_{l'=0}^{L-1} h_l h_{l'}^* \left[ \frac{R_{h,s}(\tau_l - \tau_{l'})}{T_s^2} - \sum_{k=0}^{P-1} \Pi_{l,k} \frac{R_1^*(kT_s - \tau_{l'} + DT_s)}{T_s} - \sum_{k=0}^{P-1} \Pi_{l',k}^* \frac{R_1(kT_s - \tau_l + DT_s)}{T_s} \right. \\ &\quad \left. + \sum_{k=0}^{P-1} \sum_{k'=0}^{P-1} \Pi_{l,k} \Pi_{l',k}^* R_s(kT_s - k'T_s) \right] + \frac{PN_{\text{eq}}}{M\mathcal{P}} \end{aligned} \quad (2.45)$$

$$\begin{aligned} \text{MRR}^{(\text{ps})} &= \mathbb{E} \{ \text{RR} \} \\ &= G \sum_{l=0}^{L-1} \sum_{l'=0}^{L-1} h_l h_{l'}^* \left[ \frac{R_{h,s}(\tau_l - \tau_{l'})}{T_s^2} - \sum_{k=0}^{P-1} h(kT_s + DT_s - \tau_l) \frac{R_1^*(kT_s - \tau_{l'} + DT_s)}{T_s} \right. \\ &\quad - \sum_{k=0}^{P-1} h^*(kT_s + DT_s - \tau_{l'}) \frac{R_1(kT_s - \tau_l + DT_s)}{T_s} \\ &\quad \left. + \sum_{k=0}^{P-1} \sum_{k'=0}^{P-1} h(kT_s + DT_s - \tau_l) h^*(k'T_s + DT_s - \tau_{l'}) R_s(kT_s - k'T_s) \right] + \frac{PN_{\text{eq}}}{NA^2} \end{aligned} \quad (2.46)$$

where we have defined the overall noise power

$$N_{\text{eq}} \triangleq 2N_0 B_{R,\text{eq}} + P_{\text{DVB}}. \quad (2.47)$$

The first term in (2.45) accounts for the distortion in the coupling channel impulse response, whereas the second term describes the estimation error due to noise. Increasing  $P$ , the first term of (2.45) decreases (assuming  $M$  sufficiently high), since the cancelling window length augments and the system tends to estimate and reproduce more precisely the

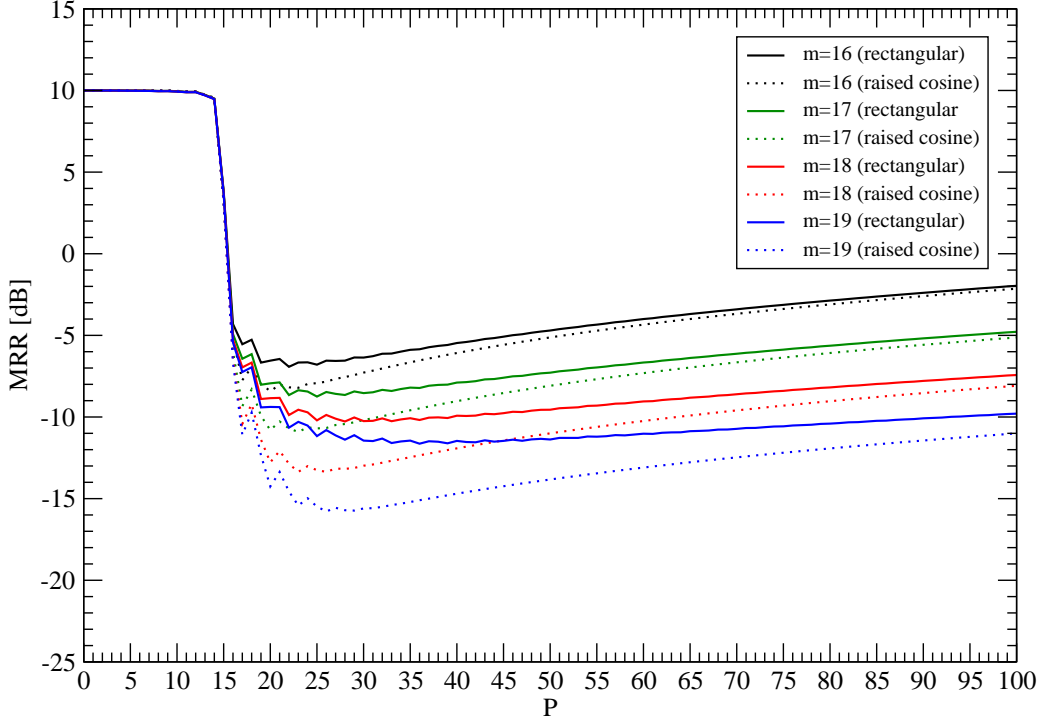


Fig. 2.2: Pseudonoise method. MRR as a function of the number of taps  $P$  when the coupling channel has only one tap: comparison between rectangular and raised cosine filtering for different values of the length of sequences  $M$ .

overall coupling channel impulse response. On the contrary, the noise component affecting the MRR increases with  $P$ , since each  $w_k$  in the cancelling filter includes an estimation error. An optimal tradeoff between these two contrasting effects exists and should be pursued. More precisely, the OCR design should jointly optimize the couple  $(P, D)$ , representing the length and the position of the cancelling window respectively, by solving the problem:

$$(P_{\text{opt}}, D_{\text{opt}}) = \arg \min_{(P, D)} \text{MRR}(P, D) \quad (2.48)$$

where we have explicitly indicated the dependence of the MRR from the parameters  $P$  and  $D$ .

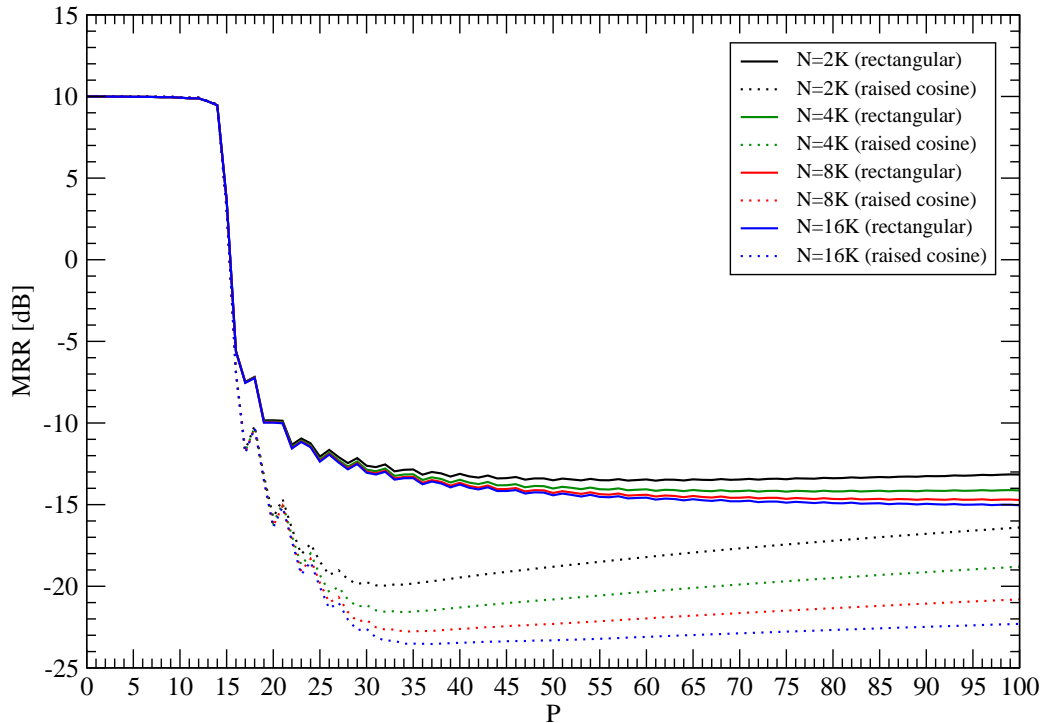


Fig. 2.3: Pulse method. MRR as a function of the number of taps P when the coupling channel has only one tap: comparison between rectangular and raised cosine filtering for different values of the number of accumulations  $N$ .

### 2.4.3 Echo Suppression

We point out that the MRR value quantifies the fraction of output power that re-enter the repeater due to the coupling effect between the transmitting and the receiving antennas, while the MRR variation due to the insertion of the echo canceler is directly related to the amount of echo suppression that has been achieved.

Thus, by denoting with  $\text{MRR}^{(0)}$  the MRR in the absence of canceler, we can define Echo Suppression ES as:

$$\text{ES}[dB] \triangleq -10 \log \left( \frac{\text{MRR}}{\text{MRR}^{(0)}} \right), \quad (2.49)$$

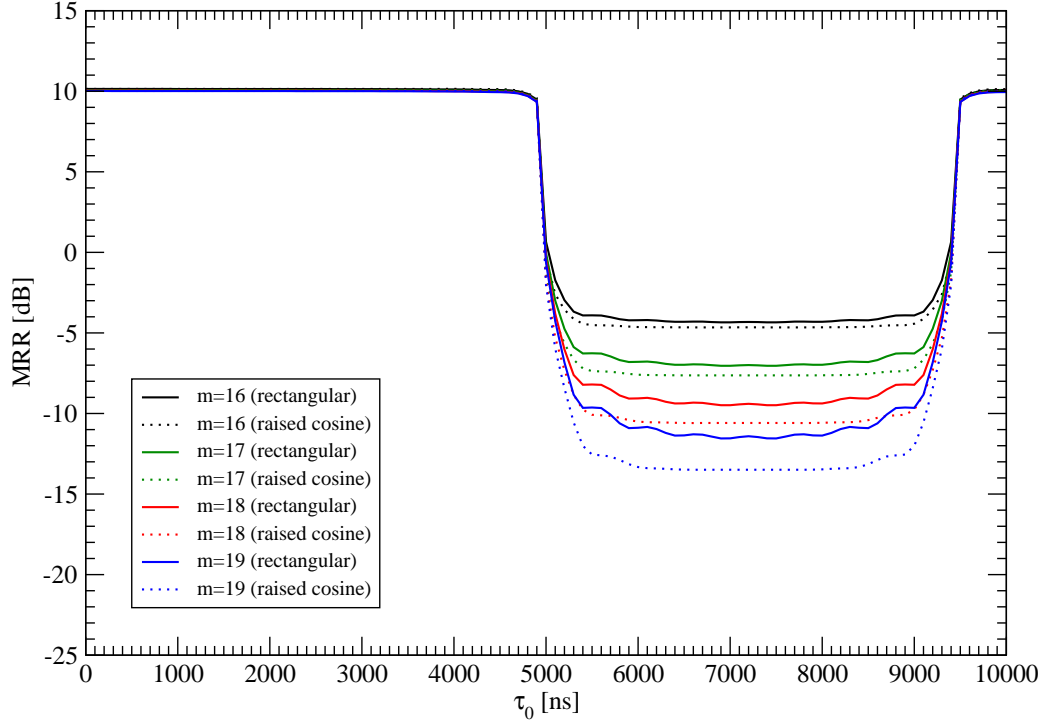


Fig. 2.4: Pseudonoise method. MRR as a function of the coupling channel delay  $\tau_0$  (only one tap channel is supposed): comparison between rectangular and raised cosine filtering for different values of the length of sequences  $M$ .

where from (2.41) (by setting  $w_k = 0$  for the absence of the echo canceler)  $\text{MRR}^{(0)}$  can be easily evaluated as:

$$\text{MRR}^{(0)} = G \sum_{l=0}^{L-1} \sum_{l'=0}^{L-1} h_l h_{l'}^* R_{h,s}(\tau_l - \tau_{l'}) . \quad (2.50)$$

In the case of Pulse Method, it is convenient for the following to define the Estimation Signal-to-Noise Ratio for Pulse as:

$$\gamma_p \triangleq \frac{E_p}{PT_s N_{\text{eq}}} \quad (2.51)$$

#### 2.4.4 Echo Suppression at Nominal Position

Although it is a significant metric and it is often used in the Literature to evaluate the quality of a repeater, the MRR is not the figure usually employed by the manufacturers

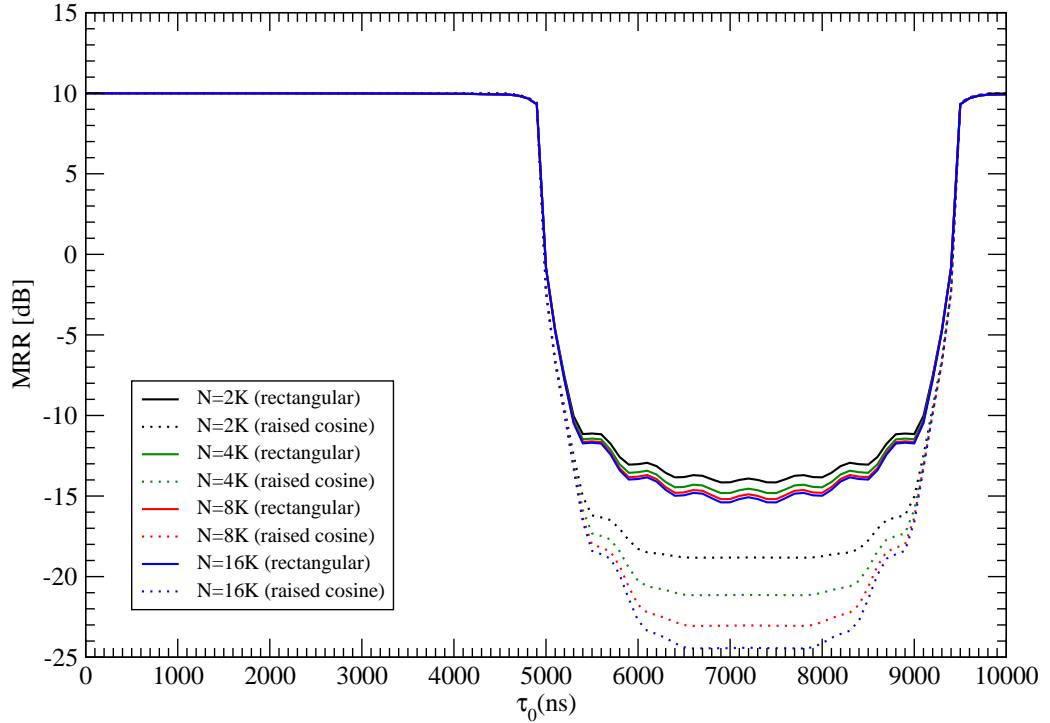


Fig. 2.5: Pulse method. MRR as a function of the coupling channel delay  $\tau_0$  (only one tap channel is supposed): comparison between rectangular and raised cosine filtering for different values of the number of accumulations  $N$ .

to describe the behavior of their equipment. The MRR value, in fact, cannot be directly measured from external devices. For this reason, another metric is often employed to quantify the level of echo suppression, namely the Echo Suppression at Nominal Position (ESNP). By indicating with  $\tau^*$  the instant in which the power of the echo pulse response is maximum in the absence of the canceller, with  $s_0(t)$  the signal returning in the repeater in the absence of the canceller, and with  $s_1(t)$  the returning signal in the presence of the canceller, the ESNP is defined as:

$$\text{ESNP} \triangleq \frac{\mathbb{E}\{|s_0(\tau^*)|^2\}}{\mathbb{E}\{|s_1(\tau^*)|^2\}} \quad (2.52)$$

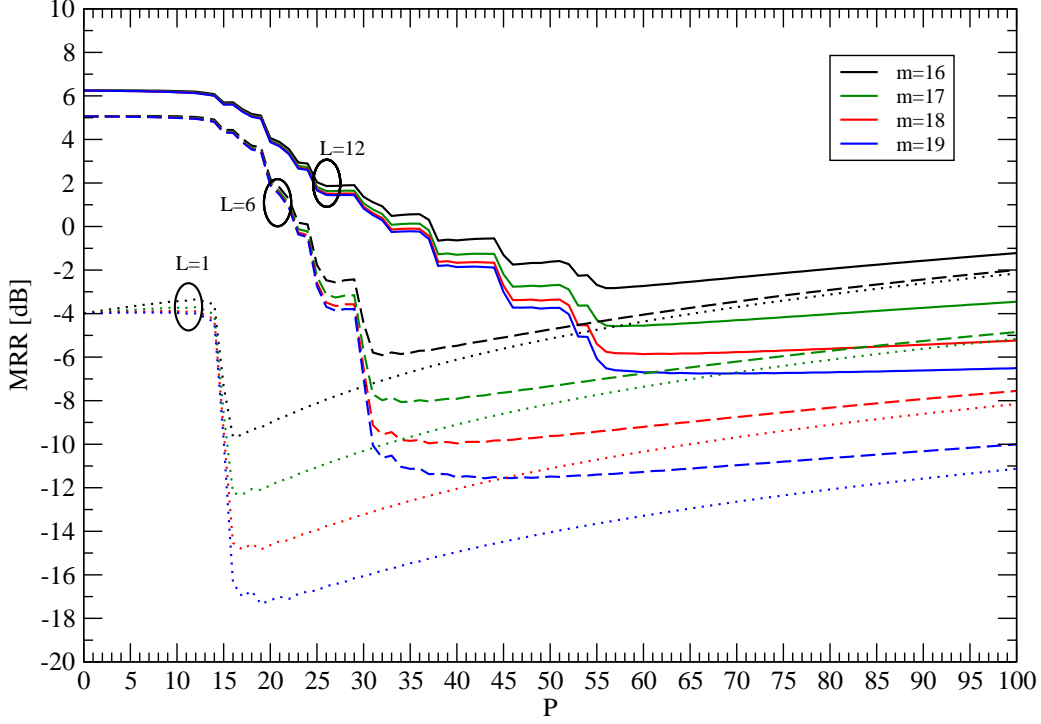


Fig. 2.6: Pseudonoise method. MRR as a function of the number of taps  $P$  when the coupling channel is modeled as TU12 and 1,6 and 12 echoes on 12 are considered respectively: comparison between different values of the length of sequences  $M$ .

By following the same method adopted for MRR derivation, its analytical expression can be derived as:

$$\text{ESNP}[dB] = -10 \log \left( \left| 1 - \sum_{k=0}^{P-1} \frac{\sum_{l=0}^{L-1} h_l h(DT_s + kT_s - \tau_l)}{\sum_{l=0}^{L-1} h_l h(\tau_l^* - \tau_l)} \text{sinc} \left( \frac{\tau_0}{T_s} - k \right) \right|^2 + \frac{\sum_{k=0}^{P-1} \text{sinc}^2 \left( \frac{\tau_l^*}{T_s} - D - k \right) B_{R,eq}^2}{G \left| \sum_{l=0}^{L-1} h_l h(\tau_l^* - \tau_l) \right|^2} \frac{1}{N\gamma_s} \right) \quad (2.53)$$

## 2.5 Upper bound on the Probability of Instability

### 2.5.1 Probability of Instability as a mark of real performance

The main problem caused by the presence of a coupling channel between the transmitting and receiving antennas is the possibility that the repeater becomes unstable due to

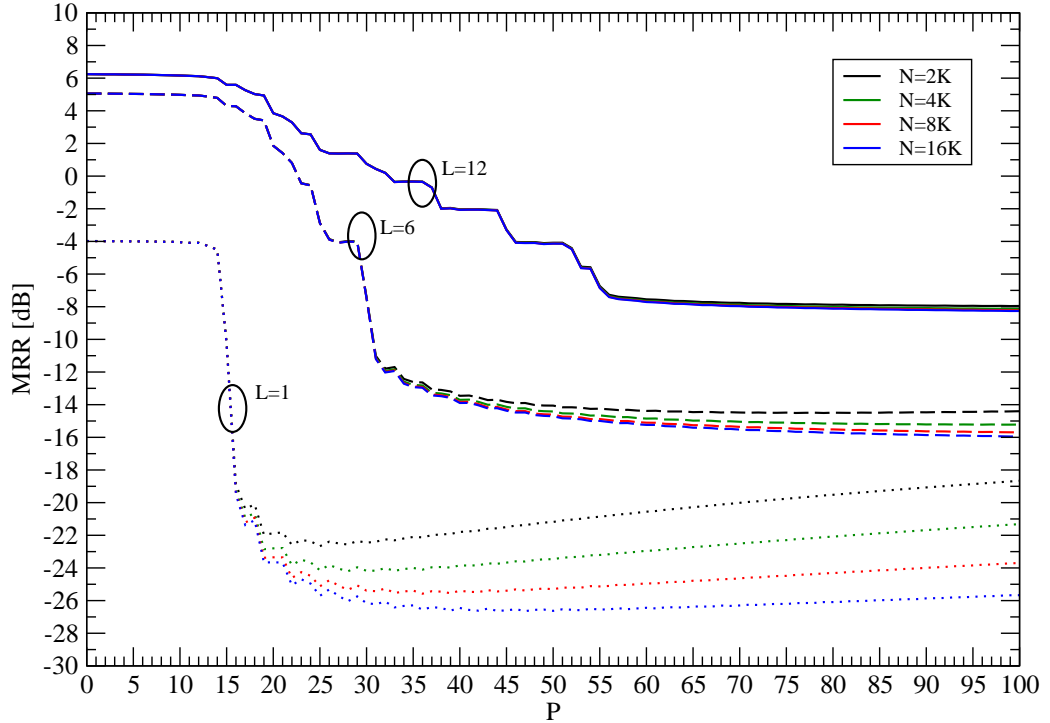


Fig. 2.7: Pulse method. MRR as a function of the number of taps  $P$  when the coupling channel is modeled as TU12 and 1,6 and 12 echoes on 12 are considered respectively: comparison between different values of the number of accumulations  $N$ .

non perfect channel estimation and noise. This condition occurrence has to be minimized as it puts the OCR in out of service for several seconds. At the best of our knowledge, no mathematical analysis has been developed to quantify the probability that a repeater becomes unstable due to the echo. Here we exploit the results of the pioneeristic work in [86], about the zeros distribution of a random polynomial, to develop an analytical framework to express an upper bound of the Probability of Instability as a function of the coupling channel echo. The goal is to predict how the insertion of an echo canceler improves the performance of a repeater in the terms of stability (a lower probability of instability means that it is possible to increase the gain of the HPA and so to cover a wider area and to reach more users).

## 2.5.2 Transfer Function of the OCR

According to the proposed model, the study of the stability of the repeater can be done studying the following transfer function in the  $Z$ -transform domain:

$$H_{\text{OCR}}(z) = \frac{1}{1 - [H_{\text{eq}}(z) - W(z)]} \quad (2.54)$$

where  $H_{\text{eq}}(z)$  and  $W(z)$  are the  $Z$ -transforms of the successions  $\{h_{\text{eq}}[k]\}$  and  $\{w[k - D]\}$  respectively, whose  $k$ -th components are given by (2.20) and (2.21), (2.34) for the pseudo-noise and pulse-sounding cases, respectively. Consequently we have:

$$H_{\text{eq}}(z) = \sum_{k=-\infty}^{+\infty} h_{\text{eq}}[k]z^{-k} = \sum_{k=-\infty}^{+\infty} \sqrt{G} \sum_{l=0}^{L-1} h_l h(kT_s - \tau_l) z^{-k} \quad (2.55)$$

and

$$W^{(\text{pn})}(z) = \sum_{k=D}^{D+P-1} w^{(\text{pn})}[k-D]z^{-k} = \sum_{k=D}^{D+P-1} \left( h_{\text{eq}}[k] + \frac{1}{M} \sum_{n=-\infty, n \neq k}^{+\infty} h_{\text{eq}}[n]R_c[k-n] + \nu^{(\text{pn})}[k] \right) z^{-k} \quad (2.56)$$

or

$$W^{(\text{ps})}(z) = \sum_{k=D}^{D+P-1} w^{(\text{ps})}[k-D]z^{-k} = \sum_{k=D}^{D+P-1} \left( h_{\text{eq}}[k] + \nu^{(\text{ps})}[k] \right) z^{-k}. \quad (2.57)$$

In general, the impulse response  $h_{\text{eq}}[k]$  is not time-limited. However, it can be found a couple of indices  $k_m$  and  $k_M$  so that  $h_{\text{eq}}[k] \approx 0, \forall k \notin [k_m, k_M]$ .

Therefore, the transfer function can be written as:

$$H_{\text{OCR}}^{(\text{pn})}(z) = \frac{1}{1 - [\sum_{k=k_{\min}}^{k_{\text{MAX}}} h_{\text{eq}}[k]z^{-k} - \sum_{k=D}^{D+P-1} \left( h_{\text{eq}}[k] + \frac{1}{M} \sum_{n=-\infty, n \neq k}^{+\infty} h_{\text{eq}}[n]R_c[k-n] + \nu^{(\text{pn})}[k] \right) z^{-k}]} \quad (2.58)$$

in the case of Pseudo Noise method, and

$$H_{\text{OCR}}^{(\text{ps})}(z) = \frac{1}{1 - [\sum_{k=k_{\min}}^{k_{\text{MAX}}} h_{\text{eq}}[k]z^{-k} - \sum_{k=D}^{D+P-1} \left( h_{\text{eq}}[k] + \nu^{(\text{ps})}[k] \right) z^{-k}]} \quad (2.59)$$

in the case of Pulse Method.

Let us consider for simplicity an ideal canceling windows, that is<sup>4</sup>:  $P = k_M - k_m + 1$  and  $D = k_m$ . In order to unify the analytical approach for the Pseudo-Noise case and for the

<sup>4</sup> It means that the canceling windows is large enough to fit completely the pulse response of the equivalent channel

Pulse Method one, we consider, in the case of Pseudo Noise Method, a sequence of length  $M$  sufficiently long to make the third term in (2.56) negligible, such that it becomes

$$W^{(\text{pn})}(z) = \sum_{k=D}^{D+P-1} \left( h_{\text{eq}}[k] + \nu^{(\text{pn})}[k] \right) z^{-k} \quad (2.60)$$

and we define the Estimation Signal-to-Noise-Ratio  $\gamma_e$  as

$$\gamma_e \triangleq \frac{1}{\mathbb{E} \{ |\nu^{(\text{pn})}[k]|^2 \}} = \frac{M\mathcal{P}}{2N_0 B_{\text{R,eq}} + P_{\text{DVB}}} \quad (2.61)$$

in the case of Pseudo Noise Method and

$$\gamma_e \triangleq \frac{1}{\mathbb{E} \{ |\nu^{(\text{ps})}[k]|^2 \}} = \frac{NA^2}{2N_0 B_{\text{R,eq}} + P_{\text{DVB}}} \quad (2.62)$$

in the case of Pulse Method.

Thanks to these definitions and assumptions, we can re-write (2.58) and (2.59) in an unified transfer function valid for both the cases<sup>5</sup>:

$$H_{\text{OCR}}(z) = \frac{1}{1 + \sum_{k=k_m}^{k_M} \nu[k] z^{-k}} = \frac{z^{k_M}}{z^{k_M} + \sum_{l=0}^{k_M-k_m} \nu[k_M-l] z^l} = \frac{z^{k_M}}{\sum_{l=0}^{k_M} p_l z^l}, \quad (2.63)$$

where

$$p_l \triangleq \begin{cases} \nu[k_M-l] & \text{for } l \in [0, k_M-k_m] \\ 0 & \text{for } l \in [k_M-k_m, k_M-1] \\ 1 & \text{for } l = k_M. \end{cases}, \quad (2.64)$$

and where, by exploiting (2.18) and (2.33) and by applying what supposed in section 2.3 about the i.i.d. noise components, we can write:

$$\nu[l] \sim \mathcal{CN} \left( 0, \frac{1}{\gamma_e} \right) \quad \forall l \quad (2.65)$$

and

$$\mathbb{E} \{ \nu[l] \nu[m] \} = \frac{1}{\gamma_e} \delta_{l,m} \quad (2.66)$$

being  $\delta_{i,j}$  the Kroenecker symbol

### 2.5.3 Random Polynomial

From (2.63), the stability of the repeater depends on the zeros distribution of the  $k_M$ -degree polynomial  $p(z)$  at the denominator of (2.63), i.e.,

$$p(z) \triangleq \sum_{l=0}^{k_M} p_l z^l \quad (2.67)$$

<sup>5</sup> For this reason in the following we will neglect the superscripts (P.N.) and (Pulse)

Thanks to this observation, we can apply the method presented in [86] to evaluate the probability density function  $f(z)$  of the zeros in the complex domain. To this aim, in the next section we will define and evaluate some stochastic parameters.

By defining the random vector  $\mathbf{p} \triangleq [p_0, p_1, \dots, p_{k_M}]^T$ , it is evident that the polynomial (2.67) can be written as:

$$p(z) = \sum_{l=0}^{k_M} p_l z^l = \mathbf{p}^T \mathbf{v}(z), \quad (2.68)$$

where  $\mathbf{v}(z) \triangleq [1, z, \dots, z^{k_M}]$ . The zeros of this polynomial are shown in [86] to be distributed in the complex domain according to the following probability density function:

$$f_z(z) = \frac{1}{\pi l_0(z)} \exp \left[ -\frac{|\mathbf{v}^T(z) \mathbf{u}_p|^2}{l_0(z)} \right] \left( \mathbf{v}'(z) - \frac{l_2(z)}{z l_0(z)} \mathbf{v}(z) \right)^T \Phi_{pp} \left( \mathbf{v}'(z^*) - \frac{l_2^*(z)}{z^* l_0^*(z)} \mathbf{v}(z^*) \right) \quad (2.69)$$

where  $\mathbf{v}'(z) \triangleq [0, 1, 2z, \dots, k_M z^{k_M-1}]^T$  and

$$\mathbf{u}_p \triangleq \mathbb{E} \{ \mathbf{p} \}, \quad (2.70)$$

$$\Phi_{pp} \triangleq \mathbb{E} \{ \mathbf{p} \mathbf{p}^H \}, \quad (2.71)$$

$$l_0(z) \triangleq \mathbf{v}^H(z) \mathbf{C}_{pp} \mathbf{v}(z), \quad (2.72)$$

$$l_1(z) \triangleq \mathbf{v}^H(z) \mathbf{C}'_{pp} \mathbf{v}(z), \quad (2.73)$$

$$l_2(z) \triangleq \mathbf{v}^H(z) \mathbf{C}''_{pp} \mathbf{v}(z), \quad (2.74)$$

being

$$\mathbf{C}_{pp} \triangleq \Phi_{pp} - \mathbf{u}_p \mathbf{u}_p^H, \quad (2.75)$$

and  $\mathbf{C}'_{pp}$  and  $\mathbf{C}''_{pp}$   $L \times L$  dimensional matrices whose generic element at the  $l$ -th line of the  $m$ -th column are respectively

$$\mathbf{C}'_{pp}[l, m] \triangleq l m \mathbf{C}_{pp}[l, m] \quad (2.76)$$

and

$$\mathbf{C}''_{pp}[l, m] \triangleq l \mathbf{C}_{pp}[l, m]. \quad (2.77)$$

In the appendix B we prove that:

$$f_z(z) = \frac{1}{\pi |z|^2} \frac{\exp \left[ -\gamma e^{\frac{|z|^{2k_M}}{\sum_{l=0}^{k_M-k_m} |z|^{2l}}} \right]}{\sum_{l=0}^{k_M-k_m} |z|^{2l}} [\Lambda(|z|) + \gamma_e \Psi(|z|)], \quad (2.78)$$

where we have defined the function in real domain:

$$\Lambda(x) \triangleq \sum_{l=0}^{k_M - k_m} \left( \left| l - \frac{\sum_{k=0}^{k_M - k_m} k x^{2k}}{\sum_{k=0}^{k_M - k_m} x^{2k}} \right|^2 x^{2l} \right) \quad (2.79)$$

and

$$\Psi(x) \triangleq \left| k_M - \frac{\sum_{k=0}^{k_M - k_m} k x^{2k}}{\sum_{k=0}^{k_M - k_m} x^{2k}} \right|^2 x^{2k_M} \quad (2.80)$$

Writing  $z = r e^{j\theta}$ , where  $r = |z|$  and  $\theta = \arg\{z\}$ , the p.d.f. and C.d.F. are respectively:

$$\begin{aligned} f_r(r) &\triangleq r \int_0^{2\pi} f_z(r \cos(\theta) + jr \sin(\theta)) d\theta = r \int_0^{2\pi} \frac{1}{\pi r^2} \frac{\exp\left[-\gamma e^{\frac{r^{2k_M}}{\sum_{l=0}^{k_M - k_m} r^{2l}}}\right]}{\sum_{l=0}^{k_M - k_m} r^{2l}} [\Lambda(r) + \gamma_e \Psi(r)] d\theta \\ &= \frac{2}{r} \frac{\exp\left[-\gamma e^{\frac{r^{2k_M}}{\sum_{l=0}^{k_M - k_m} r^{2l}}}\right]}{\sum_{l=0}^{k_M - k_m} r^{2l}} [\Lambda(r) + \gamma_e \Psi(r)] \end{aligned} \quad (2.81)$$

and

$$F_R(R) = \int_0^R f_r(r) dr. \quad (2.82)$$

Since its value for  $R = 1$  gives the mean number of zeros inside the unitary circle in the complex domain, it is clear that, for a  $k_M$  degree polynomial,  $k_M - F_R(1)$  gives the mean number  $\bar{n}$  of the zeros of  $p(z)$  outside the unitary circle:

$$\bar{n} \triangleq k_M - F_R(1) = k_M - \int_0^1 f_r(r) dr. \quad (2.83)$$

Since the number of zeroes have to be an integer it is also true that<sup>6</sup>:

$$\bar{n} = \sum_{i=1}^{k_M} i \text{Prob}\{p(z) \text{ has } i \text{ zeros outside the unitary circle}\}. \quad (2.84)$$

On the other side, the probability that the system is unstable is the probability that almost one zero is outside the unitary circle:

$$\begin{aligned} P_{oI} &\triangleq \text{Prob}\{p(z) \text{ has 1 zero outside the unitary circle}\} \cup \text{Prob}\{p(z) \text{ has 2 zeroes outside the unitary circle}\} \\ &\quad \cup \text{Prob}\{p(z) \text{ has } k_M \text{ zeroes outside the unitary circle}\} \\ &= \sum_{i=1}^{k_M} \text{Prob}\{p(z) \text{ has } i \text{ zeros outside the unitary circle}\} \\ &\leq \sum_{i=1}^{k_M} i \text{Prob}\{p(z) \text{ has } i \text{ zeros outside the unitary circle}\} = \bar{n}. \end{aligned}$$

<sup>6</sup>  $p(z)$  has always  $k_M$  zeroes, because, from (2.64), the  $k_M$ -th order coefficient is always 1

Thus we are interested in the evaluation of  $\bar{n} = k_M - F_R(1)$  because it is the upper bound of the instability probability. By substituting (2.81) in (2.82) we have:

$$\bar{n} = k_M - \int_0^1 \frac{2}{r} \frac{\exp\left[-\gamma_e \frac{r^{2k_M}}{\sum_{l=0}^{k_M-k_m} r^{2l}}\right]}{\sum_{l=0}^{k_M-k_m} r^{2l}} [\Lambda(r) + \gamma_e \Psi(r)] dr, \quad (2.86)$$

that can be easily evaluated numerically.

## 2.6 Numerical Results

### 2.6.1 MRR

In figure 2.2 we show the MRR of a canceller based on pseudonoise method as a function of the number of taps  $P$  for different values of the sequence length  $2^m$ , when the coupling channel has only one tap. The most relevant thing that can be noticed is that the minimum MRR is attained when the cancellation window (which begins at a given instant  $\tau_0$  and increase with  $P$ ) becomes long enough to include the echo delay. If the cancellation windows increases beyond this value, the MRR re-increases, because the higher number of (unnecessary) taps introduces only more noise. It can be observed an increasing of the performance every time the length of the pseudonoise sequence is doubled. We can also observe that, if a raised cosine filtering is employed, the performance improve of 1-2 dB with respect the case of rectangular filter.

In figure 2.3 the MRR of a canceller based on pulse method as a function of the number of taps  $P$  for different values of accumulation number  $N$ , when the coupling channel has only one tap is shown. Even in this case the MRR decreases of 20dB when the number of taps  $P$  attain a value such that the cancellation window includes the echo delay, but the minimum is attained for higher values of  $P$ . Moreover, the performance increasing given by the use of raised cosine filtering is greater (about 10dB) with respect the pseudonoise case. It is also interesting to note that, if rectangular filtering is employed, the performance increasing given by higher number of accumulation is negligible.

In figure 2.4 and 2.5 the MRR is depicted as a function of the time delay channel (only one tap is supposed as before) in the pseudonoise case and in the pulse method case, respectively, for different values of the sequence length and of the accumulation number. The number of taps is fixed ( $P = 56$ ) and the range of  $\tau_0$  values inside which the MMR is

decreased with respect its value without the canceller (10dB) represents (also graphically) the cancelling windows. It can be noticed that in the case of pseudonoise the value of MRR inside the cancelling windows are more regular, but their improvement thanks to the use of a raised cosine filtering is less relevant. Moreover, in the pulse method case, increasing the number of accumulation improves significantly the performance only when the raised cosine is employed instead of rectangular filtering.

In figure 2.6 we show the MRR of a canceller based on pseudonoise method as a function of the number of taps  $P$  for different values of the sequence length  $2^m$ , when 1, 6 and 12 of the 12 echoes of a TU12 channel model are considered arriving. The most evident thing is that, increasing the number of taps, the MRR decreases every time that one of the 1, 6 and 12 taps of the considered physical coupling channel becomes included in the cancelling windows. Moreover, it can be noticed that, while for low value of  $P$  (20-25) the MRR is much lower for lower number of echoes, for higher value of  $P$  the MRR has similar values for 1, 6, 12 arriving echoes. This means that, if the cancelling windows (and so the number of taps) is realized in order to cancel a certain number of echoes, the performance when few echoes arrive are much lower than what it could be with a lower number of taps  $P$ .

In figure 2.7 the MRR of a canceller based on pulse method as a function of the number of taps  $P$  for different values of accumulation number  $N$ , when as physical coupling channels we consider the same as before. Even in this case, increasing the number of taps, the MRR decreases every time that one of the 1, 6 and 12 taps of the considered physical coupling channel becomes included in the cancelling windows. Differently than the pseudonoise case, the MRR remain lower when less echoes arrive even for high value of  $P$ . This means that it can be possible to realize a large cancellation windows in order to cancel several echoes without reducing the performance in the case of few echoes with respect what it could be possible with a lower number of taps  $P$ .

### 2.6.2 ESNP vs ES

In Fig. 2.8 we reported, in the case of Pulse Method, the comparison between the values of Echo Suppression (ES) and ESNP for two different values of coupling channel attenuation, namely  $A_c = 0.2$  dB and  $A_c = 10$  dB, as a function of the estimation Signal-to-Noise Ratio ( $N\gamma_p$ ). It can be shown that ESNP is an overestimation of the ES level, because, while the latter consists in a ratio between average powers, the former takes into account only

the ratio between instantaneous powers, computed in correspondence of the main echo peak.

Moreover, it can be noticed that the higher is the coupling channel gain  $1/A_c$  (and so the strongest is the echo before the cancellation), the higher is the echo suppression, because a stronger echo permits a better estimation of the echo itself. However, while the ESNP always increases with  $N\gamma_p$  and with the coupling channel gain  $1/A_c$  (i.e. with the accuracy of the estimation), the ES is increasing with  $N\gamma_p$  only for the low values: for high values of  $N\gamma_p$ , it reaches a saturation level which is also independent of the coupling channel gain. In fact, according to (2.46), for high values of  $N\gamma_p$  the term related to the imperfect reconstruction of the coupling channel caused by the finite number of taps in the cancellation FIR becomes more relevant than the term related to the estimation errors caused by the noise. If this situation occurs, the high values of ESNP sometimes reported by manufacturers may be not really significant to describe the echo cancellation capability of the systems.

### 2.6.3 ESNP: comparison between theory and experimental results

In Figure 2.9 we show the ESNP, in the case of Pulse Method, as a function of the number of accumulations (for a fixed value of the Estimation Signal-to-Noise Ratio for Pulse). The values obtained through the presented theoretical analysis are compared to the values really measured through the TV-Analyzer applied to the FPGA evaluation board on which we have implemented the echo canceller as described in [81]. As it can be noticed from the reported curves, a good accordance has been achieved between the analytical model we developed and the implemented prototype, which validates the work so far realized.

### 2.6.4 Probability of instability

It is interesting to show the Upper Bound of the Probability of Instability as a function of the Estimation Signal-to-Noise Ratio  $\gamma_e$ . We can observe that, by increasing  $\gamma_e$ ,  $P_u$  tends to zero in a similar way to a classic Bit Error Probability versus SNR.

For too small values of  $\gamma_e$  the Upper bound is useless, since it is greater than 1 (or however much greater than the real unknown probability of instability), but for values of  $\gamma_e$  greater than 15dB it can provide an acceptable indication of how much the gain of the HPA can be increased without risking the instability.

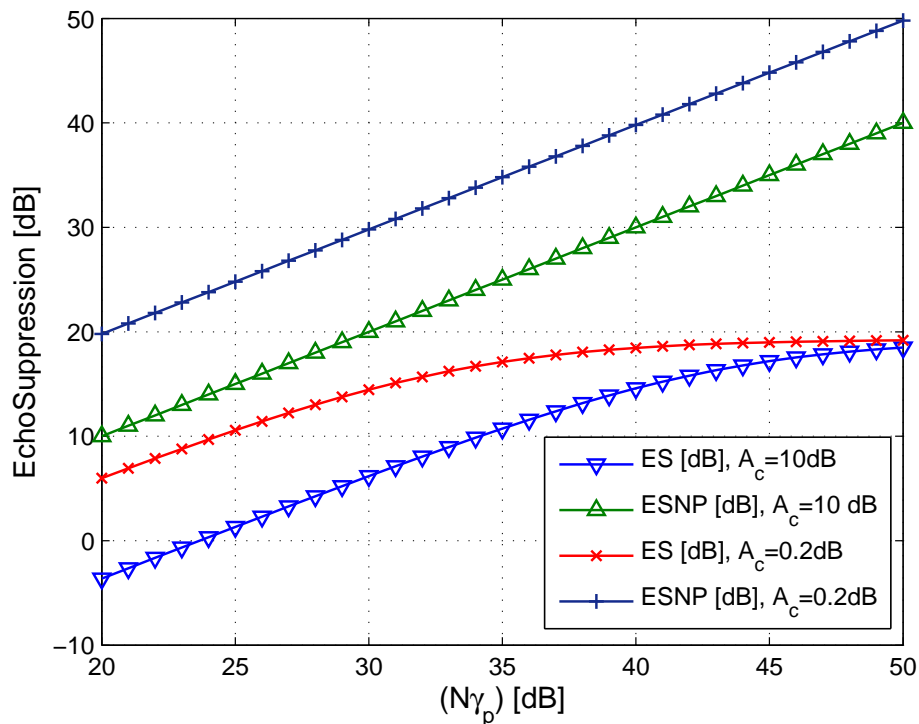


Fig. 2.8: Pulse Method. Echo suppression as a function of the estimation SNR. Theoretical comparison between ES and ESNP

## 2.7 Conclusions

In this chapter we have shown a low-complexity digital echo canceller based on the transmission of a locally generated signal (Pseudo-Noise sequences or opportune pulse trains). An analytical framework is developed to evaluate the performance in the term of MRR, ES and ESNP, providing important guidelines for the design process. The important question of the stability is discussed, and an analytical bound of the probability of instability is presented. The analytical results have been compared to the ones derived from measurement done on a practical implementation of the system on an FPGA board, in order to validate the theoretical model and the design strategies.

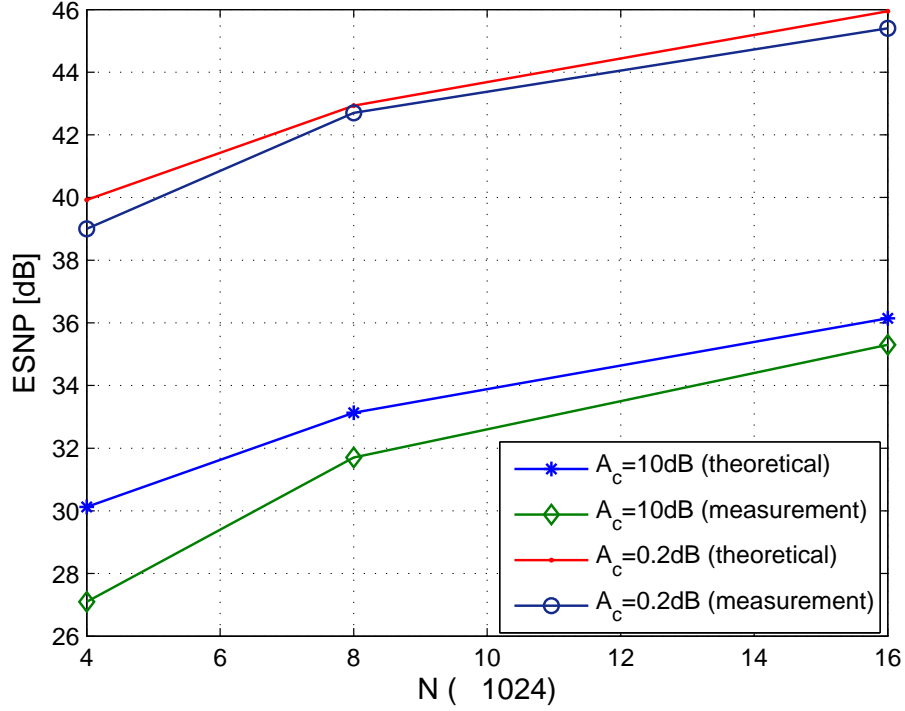


Fig. 2.9: Pulse Method. ESNP as a function of the number of accumulations: comparison between theoretical values and measurements.

## 2.8 Appendix A

Since  $d[k]$  and  $n[k]$  are the filtered components of the DVB-T signal and of the Gaussian noise, by supposing an ideal filtering with bandwidth  $B_{R,eq}$  we can consider:

$$R_d[k' - k] \triangleq \mathbb{E} \{d[k]d^*[k']\} = P_{DVB} \text{sinc}^2 [(k' - k)T_s B_{R,eq}] = P_{DVB} \text{sinc}^2 \left( \frac{k' - k}{1 + \alpha} \right) \quad (2.87)$$

and

$$R_n[k' - k] \triangleq \mathbb{E} \{n[k]n^*[k']\} = 2N_0 B_{R,eq} \text{sinc}^2 [(k' - k)T_s B_{R,eq}] = 2N_0 B_{R,eq} \text{sinc}^2 \left( \frac{k' - k}{1 + \alpha} \right), \quad (2.88)$$

where  $\alpha$  is the oversampling factor defined as:

$$\alpha \triangleq \frac{1}{T_s B_{R,eq}} - 1. \quad (2.89)$$

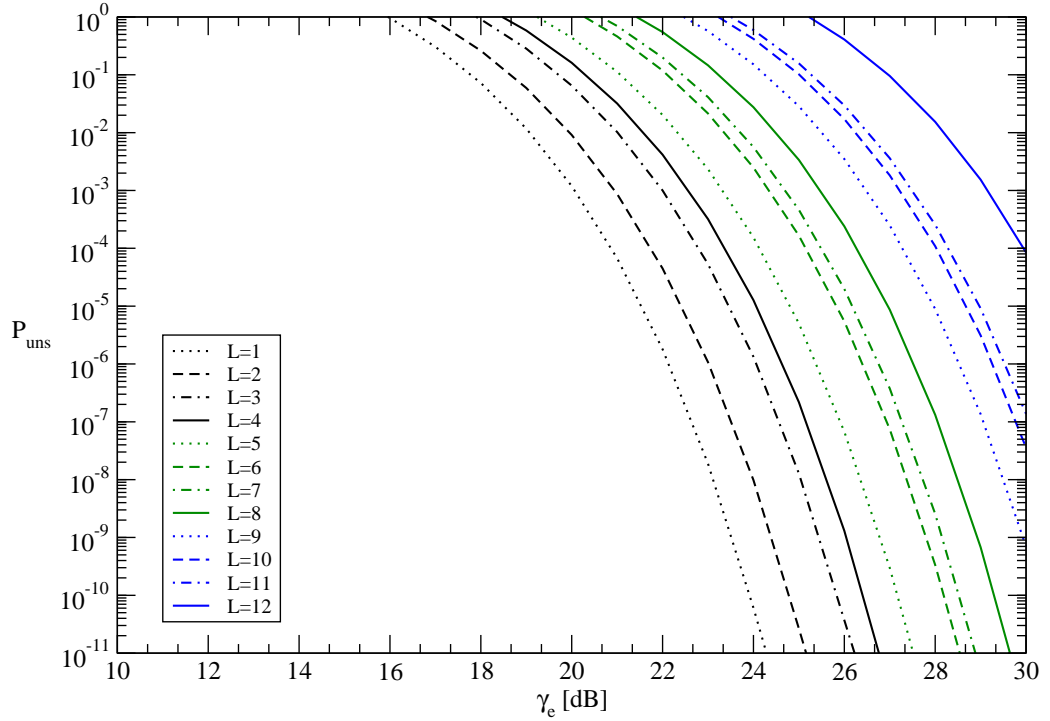


Fig. 2.10: The Upper Bound of the Probability of Instability as a function of the Estimation Signal-to-Noise Ratio for different number of considered echoes  $L$  (modeled according to TU12-channel)

If we suppose  $\alpha \ll 1$ , (2.87) and (2.88) can be approximated as follows:

$$R_d[k' - k] \approx P_{\text{DVB}} \delta_{k',k} \quad (2.90)$$

and

$$R_n[k' - k] \approx 2N_0 B_{\text{R,eq}} \delta_{k',k} . \quad (2.91)$$

In the case of pseudo-noise it is:

$$\nu^{(\text{pn})}[k] = \frac{1}{M\sqrt{\mathcal{P}}} \sum_{m=0}^{M-1} (d[m+k] + n[m+k]) \cdot c^*[m] \quad (2.92)$$

Therefore the term at the  $k$ -th line at the  $k'$ -th column of the correlation matrix is given by:

$$\begin{aligned}
\frac{1}{2}\mathbb{E}\left\{\nu^{(\text{pn})}[k]\nu^{(\text{pn})*}[k']\right\} &= \frac{1}{M^2\mathcal{P}}\sum_{m=0}^{M-1}\sum_{m'=0}^{M-1}\frac{1}{2}\mathbb{E}\left\{(d[m+k]+n[m+k])\cdot c^*[m](d^*[m'+k']+n^*[m'+k'])\cdot c[m']\right\}= \\
&= \frac{1}{M^2\mathcal{P}}\sum_{m=0}^{M-1}\sum_{m'=0}^{M-1}c^*[m]c[m']\frac{1}{2}(\mathbb{E}\{d[m+k]d^*[m'+k']\}+\mathbb{E}\{n[m+k]n^*[m'+k']\})= \\
&= \frac{1}{M^2\mathcal{P}}\sum_{m=0}^{M-1}\sum_{m'=0}^{M-1}c^*[m]c[m'](R_d[m-m'+k-k']+R_n[m-m'+k-k'])= \\
&\approx \frac{1}{M^2\mathcal{P}}\sum_{m=0}^{M-1}c^*[m]c[m+k-k'](P_{\text{DVB}}+2N_0B_{\text{R,eq}})= \\
&= \frac{(P_{\text{DVB}}+2N_0B_{\text{R,eq}})}{M^2\mathcal{P}}R_c[k'-k]= \\
&\approx \frac{(P_{\text{DVB}}+2N_0B_{\text{R,eq}})}{M\mathcal{P}}\delta_{k,k'}
\end{aligned} \tag{2.93}$$

where we have exploited the independance between the sequences  $d[m]$  and  $n[m]$  and we have considered  $M$  sufficiently large.

In the case of pulse-souding it is:

$$\nu^{(\text{ps})}[k]=\frac{1}{NA}\sum_{n=0}^{N-1}e^{-j\phi_n}d[nK+k]+\frac{1}{NA}\sum_{n=0}^{N-1}e^{-j\phi_n}n[nK+k]. \tag{2.94}$$

Therefore the term at the  $k$ -th line at the  $k'$ -th column of the correlation matrix is given by:

$$\begin{aligned}
\frac{1}{2}\mathbb{E}\left\{\nu^{(\text{ps})}[k]\nu^{(\text{ps})*}[k']\right\} &= \frac{1}{N^2A^2}\sum_{n=0}^{N-1}\sum_{n'=0}^{N-1}\left[e^{j(\phi_{n'}-\phi_n)}(R_d[(n'-n)K+k'-k]+R_n[(n'-n)K+k'-k])\right]= \\
&\approx \frac{1}{N^2A^2}\sum_{n=0}^{N-1}(P_{\text{DVB}}+2N_0B_{\text{R,eq}})= \\
&= \frac{(P_{\text{DVB}}+2N_0B_{\text{R,eq}})}{NA^2}\delta_{k',k}.
\end{aligned} \tag{2.95}$$

## 2.9 Appendix B

In this appendix, by exploiting the analysis and considerations done in the previous section, we evaluate the stochastic parameters defined there and the probability density function  $f_z(z)$ .

$$\mathbf{u}_p$$

By exploiting (2.65) in (2.64) it is immediate from definition (2.70) that:

$$\mathbf{u}_p = (0, 0, \dots, 1)^T . \quad (2.96)$$

$$\Phi_{pp}$$

From (2.64), (2.65) and (2.66), the generic element  $l$ -th row of the  $m$ -th column of the matrix defined by (2.71) is:

$$\Phi_{pp}[l, m] = \begin{cases} \frac{1}{\gamma_e} \delta_{l,m} & \text{for } l, m \in [0, k_M - k_m] \\ 1 & \text{for } l = m = k_M \\ 0 & \text{elsewhere .} \end{cases} \quad (2.97)$$

$$\mathbf{C}_{pp}$$

From (2.96), the generic element  $l$ -th row of the  $m$ -th column of the matrix  $\mathbf{u}_p \mathbf{u}_p^H$  is:

$$\mathbf{u}_p \mathbf{u}_p^H[l, m] = \begin{cases} 1 & \text{for } l = m = k_M \\ 0 & \text{elsewhere .} \end{cases} \quad (2.98)$$

Therefore, by substituting (2.97) in definition (2.75), it is possible to write the generic element  $l$ -th row of the  $m$ -th column of the matrix  $\mathbf{C}_{pp}$  as:

$$\mathbf{C}_{pp}[l, m] = \begin{cases} \frac{1}{\gamma_e} \delta_{l,m} & \text{for } l, m \in [0, k_M - k_m] \\ 0 & \text{elsewhere .} \end{cases} \quad (2.99)$$

$$\mathbf{C}'_{pp}$$

By substituting (2.99) in definition (2.76), it can be shown that the generic element  $l$ -th row of the  $m$ -th column of the matrix  $\mathbf{C}'_{pp}$  is:

$$\mathbf{C}'_{pp}[l, m] = \begin{cases} \frac{lm}{\gamma_e} \delta_{l,m} & \text{for } l, m \in [0, k_M - k_m] \\ 0 & \text{elsewhere .} \end{cases} \quad (2.100)$$

$$\mathbf{C}_{pp}''$$

By substituting (2.99) in definition (2.77), it is possible to show that the generic element  $l$ -th row of the  $m$ -th column of the matrix  $\mathbf{C}_{pp}''$  is:

$$\mathbf{C}_{pp}''[l, m] = \begin{cases} \frac{l}{\gamma_e} \delta_{l,m} & \text{for } l, m \in [0, k_M - k_m] \\ 0 & \text{elsewhere .} \end{cases} \quad (2.101)$$

$$l_0(z)$$

By substituting (2.99) in definition (2.72) we obtain:

$$l_0(z) = \sum_{l=0}^{k_M} \sum_{m=0}^{k_M} \mathbf{v}^*(z)[m] \mathbf{C}_{pp}''[l, m] \mathbf{v}(z)[l] = \sum_{l=0}^{k_M - k_m} \sum_{m=0}^{k_M - k_m} \frac{1}{\gamma_e} \delta_{l,m} z^l z^{*m} = \frac{1}{\gamma_e} \sum_{l=0}^{k_M - k_m} |z|^{2l} . \quad (2.102)$$

$$l_1(z)$$

By substituting (2.100) in definition (2.73) we obtain:

$$l_1(z) = \sum_{l=0}^{k_M} \sum_{m=0}^{k_M} \mathbf{v}^*(z)[m] \mathbf{C}_{pp}'[l, m] \mathbf{v}(z)[l] = \sum_{l=0}^{k_M - k_m} \sum_{m=0}^{k_M - k_m} \frac{lm}{\gamma_e} \delta_{l,m} z^l z^{*m} = \frac{1}{\gamma_e} \sum_{l=0}^{k_M - k_m} l^2 |z|^{2l} . \quad (2.103)$$

$$l_2(z)$$

By substituting (2.101) in definition (2.74) we obtain:

$$l_2(z) = \sum_{l=0}^{k_M} \sum_{m=0}^{k_M} \mathbf{v}^*(z)[m] \mathbf{C}_{pp}''[l, m] \mathbf{v}(z)[l] = \sum_{l=0}^{k_M - k_m} \sum_{m=0}^{k_M - k_m} \frac{l}{\gamma_e} \delta_{l,m} z^l z^{*m} = \frac{1}{\gamma_e} \sum_{l=0}^{k_M - k_m} l |z|^{2l} . \quad (2.104)$$

$$f(z)$$

By substituting (2.96), (2.102), (2.103) and (2.104) in (2.78) we finally obtain:

$$\begin{aligned}
f_z(z) &= \frac{1}{\pi \frac{1}{\gamma_e} \sum_{l=0}^{k_M-k_m} |z|^{2l}} \exp \left[ -\frac{\left| \sum_{l=0}^{k_M-k_m} z^l \mathbf{u}_p[l] \right|^2}{\frac{1}{\gamma_e} \sum_{l=0}^{k_M-k_m} |z|^{2l}} \right] \\
&\times \left[ \sum_{l=0}^{k_M-k_m} \sum_{m=0}^{k_M-k_m} \left( m z^{m-1} - \frac{\frac{1}{\gamma_e} \sum_{k=0}^{k_M-k_m} k |z|^{2k}}{z \frac{1}{\gamma_e} \sum_{k=0}^{k_M-k_m} |z|^{2k}} z^m \right) \mathbf{C}_{pp}[l, m] \left( l z^{*l-1} - \frac{\frac{1}{\gamma_e} \sum_{k=0}^{k_M-k_m} k |z|^{2k}}{z^* \frac{1}{\gamma_e} \sum_{k=0}^{k_M-k_m} |z|^{2k}} z^{*l} \right) \right] \\
&= \frac{\gamma_e}{\pi \sum_{l=0}^{k_M-k_m} |z|^{2l}} \exp \left[ -\gamma_e \frac{|z|^{2k_M}}{\sum_{l=0}^{k_M-k_m} |z|^{2l}} \right] \\
&\times \left[ \sum_{l=0}^{k_M-k_m} \sum_{m=0}^{k_M-k_m} \left( m z^{m-1} - \frac{\frac{1}{\gamma_e} \sum_{k=0}^{k_M-k_m} k |z|^{2k}}{z \frac{1}{\gamma_e} \sum_{k=0}^{k_M-k_m} |z|^{2k}} z^m \right) \delta_{l,m} \left( l z^{*l-1} - \frac{\frac{1}{\gamma_e} \sum_{k=0}^{k_M-k_m} k |z|^{2k}}{z^* \frac{1}{\gamma_e} \sum_{k=0}^{k_M-k_m} |z|^{2k}} z^{*l} \right) \right] \\
&+ \left( k_M z^{k_M-1} - \frac{\frac{1}{\gamma_e} \sum_{k=0}^{k_M-k_m} k |z|^{2k}}{z \frac{1}{\gamma_e} \sum_{k=0}^{k_M-k_m} |z|^{2k}} z^{k_M} \right) \left( k_M z^{*k_M-1} - \frac{\frac{1}{\gamma_e} \sum_{k=0}^{k_M-k_m} k |z|^{2k}}{z^* \frac{1}{\gamma_e} \sum_{k=0}^{k_M-k_m} |z|^{2k}} z^{*k_M} \right) \\
&= \frac{\gamma_e}{\pi \sum_{l=0}^{k_M-k_m} |z|^{2l}} \exp \left[ -\gamma_e \frac{|z|^{2k_M}}{\sum_{l=0}^{k_M-k_m} |z|^{2l}} \right] \\
&\times \left[ \sum_{l=0}^{k_M-k_m} \frac{1}{\gamma_e} \left| l z^{l-1} - \frac{\sum_{k=0}^{k_M-k_m} k |z|^{2k}}{z \sum_{k=0}^{k_M-k_m} |z|^{2k}} z^l \right|^2 + \left| k_M z^{k_M-1} - \frac{\sum_{k=0}^{k_M-k_m} k |z|^{2k}}{z \sum_{k=0}^{k_M-k_m} |z|^{2k}} z^{k_M} \right|^2 \right] \\
&= \frac{1}{\pi |z|^2} \frac{\exp \left[ -\gamma_e \frac{|z|^{2k_M}}{\sum_{l=0}^{k_M-k_m} |z|^{2l}} \right]}{\sum_{l=0}^{k_M-k_m} |z|^{2l}} \left[ \sum_{l=0}^{k_M-k_m} \left( \left| l - \frac{\sum_{k=0}^{k_M-k_m} k |z|^{2k}}{\sum_{k=0}^{k_M-k_m} |z|^{2k}} \right|^2 |z|^{2l} \right) + \gamma_e \left| k_M - \frac{\sum_{k=0}^{k_M-k_m} k |z|^{2k}}{\sum_{k=0}^{k_M-k_m} |z|^{2k}} \right|^2 \right] \\
&= \frac{1}{\pi |z|^2} \frac{\exp \left[ -\gamma_e \frac{|z|^{2k_M}}{\sum_{l=0}^{k_M-k_m} |z|^{2l}} \right]}{\sum_{l=0}^{k_M-k_m} |z|^{2l}} [\Lambda(|z|) + \gamma_e \Psi(|z|)] ,
\end{aligned}$$

where we have defined the function in real domain:

$$\Lambda(x) \triangleq \sum_{l=0}^{k_M-k_m} \left( \left| l - \frac{\sum_{k=0}^{k_M-k_m} k x^{2k}}{\sum_{k=0}^{k_M-k_m} x^{2k}} \right|^2 x^{2l} \right) \quad (2.106)$$

and

$$\Psi(x) \triangleq \left| k_M - \frac{\sum_{k=0}^{k_M-k_m} k x^{2k}}{\sum_{k=0}^{k_M-k_m} x^{2k}} \right|^2 x^{2k_M} \quad (2.107)$$



### 3. OUT OF BAND SPECTRUM REDUCTION THROUGH CANCELLATION CARRIERS FOR OFDM WITH NONLINEARITIES

#### 3.1 Introduction

Orthogonal frequency division multiplexing (OFDM) systems are known to achieve high data rate in band-limited channels. However, in real systems, the amount of power outside the assigned spectrum can cause interference on other systems working in the adjacent channels. There are two different causes of OOB (Out of Band) radiation in OFDM systems:

- a) the use of time-limited waveforms which implies a non-limited spectrum in the frequency domain;
- b) the presence of non-linearities (e.g. non linear amplifier) which leads to the rising of spectral components outside the bandwidth.

Till now, all the methods presented in the Literature [87–97] to reduce OOB radiation counteract or the cause a) or the cause b) separately. In both the cases, since the OFDM spectrum strictly depends on the input data, all the methods control the OOB modifying the transmitted symbols. In particular, in order to transmit symbols with the desired spectral characteristic, properly chosen cancellation symbols are added (or inserted to the data symbols) Since in both the cases the OFDM spectrum highly depends on the input data, all the methods are based on modifying the transmitted symbols, adding to the data symbols opportune "cancellation symbols" (in the frequency domain or in the time domain), which, together with data, produce an overall symbols sequence with the wanted spectral characteristics. The difference between methods is in which function related to OOB the methods actually minimize through cancellation symbols (i.e. OOB of the signal before the non-linear amplifier, Peak-to-Average Ratio, etc.).

The first kind of methods (see [94–97]) is characterized by the insertion of cancellation symbols that lead to the reduction of the OOB spectrum in the frequency domain, assuming the power amplifier in linear region, that is, counteract the cause a).

The second kind of methods (see [87–93]) are aimed to reduce Peak to Average Ratio (PAPR) in the transmitted signal, considering the power amplifier operating in saturation region. It is immediate to note that the more the High Power Amplifier (HPA) operates in the linear region, the more methods a) are effective, while the more the HPA operates in saturation region, the more methods b) are able to reduce OOB by reducing PAPR. To the best of our knowledge, the Literature does not provide a method which counteracts jointly the cause a) and the cause b). Such a method would be mostly effective in the most interesting case for practical application, i.e., in a middle situation between linear region and saturation region. The goal of this paper is to present a method which jointly minimize the OOB for both the saturation and linear regions able to achieve the best solution in the intermediate situation. In particular, the cancellation symbols inserted between the data symbols (in the frequency domain or in the time domain) are aimed to minimize the OOB of the signal after the HPA. This means that we extend the method of cancellation carriers (frequency domain) and the method of [Mohmoud] (time domain) by considering as cost function not the OOB of the signal before the HPA (typical of methods a), nor the PAPR (typical of methods b), but the actual OOB after the HPA. It is worthwhile noting that including a non-linear HPA highly increases the complexity of the optimization problem which is not anymore convex optimization. Solving this issue has been the main obstacle in the analytical work.

## 3.2 System Model

### 3.2.1 Key Idea

Typically, in a multi-carrier system the spectrum critically depends on the data input. As a very simple example, in 3.2.1 we consider a sequence of four binary symbols " $\pm 1$ " transmitted over four carriers. For sake of simplicity, we compare a sequence constituted by symbols with the same sign to another sequence constituted by symbols with alternate sign. We depicted on the left the carriers (modulated by the data symbols) in the time domain and on the right the resulting spectrum. It is evident how the symbol sequence "+1, +1, +1, +1" produces a spectrum with much less OOB than the sequence "+1, -1, +1, -1". Obviously, in a real system, when complex  $M-QAM$  symbols are employed instead of a simple BPSK, and when the number of subcarrier is much greater than four, the situation is much more complicated, but the key idea it remains the same: there are data sequence which produce higher OOB and data sequence which produce lower OOB. The original idea in the Literature consists in modifying the transmitted data in such a way that makes them similar to the sequences which produces lower OOB. This

can be done both in the frequency domain, by exploiting some of the unused carriers to transmit the so called "cancellation symbols" (3.2.2), and in the time domain, by adding opportune symbols between one OFDM-symbol and the other. By referring to a classical OFDM implementation via DFT, it means that in the first case the cancellation symbols are inserted before the IDFT block (they are carried by the so called cancellation carriers), in the second case the cancellation symbols are inserted after the IDFT block (after every time domain sequence corresponding to an OFDM-symbol). The Cancellation Carrier method, presented by [95] exploits some of the unused sub-carriers to transmit cancellation symbols, as shown in figure 3.2.2. The Adaptive Symbol Transition method, presented by [98] consists instead in adding cancellation symbols between one OFDM symbols and the other. Both the method are aimed to reduce the cost function defined as the OOB spectrum of the OFDM signal (thus, without considering any nonlinearities). Our goal is to extend both these two method in such a manner which considers as cost function the OOB spectrum of the OFDM signal after the HPA amplifier.

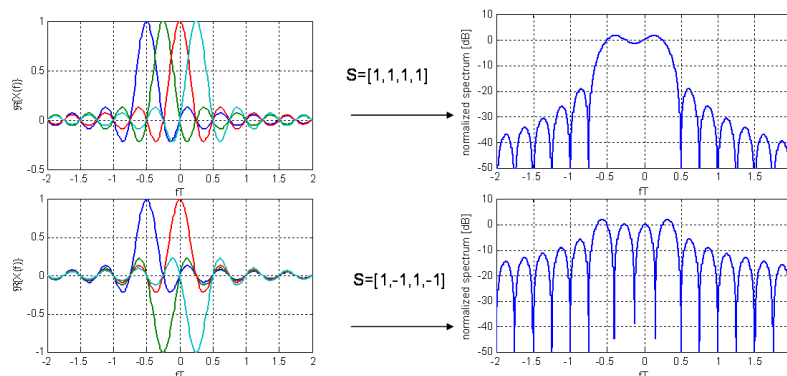


Fig. 3.1: OOB radiation as depending on the symbol sequence  $S$ . A very simple example ( $N = 4$ , BPSK modulation): on the left the contributions of each symbols in the frequency domain are depicted and on the right the related spectrum is shown. It is evident as the OOB of the sequence with alternate sign is much more higher with respect the sequence with the same sign

### 3.2.2 OFDM Transmitter with nonlinearities

In a classic OFDM transmitter (3.2.2), a sequence of  $N$  data symbols is serial-to-parallel converted, it is transformed through an IFFT, it is parallel-to-serial converted and it

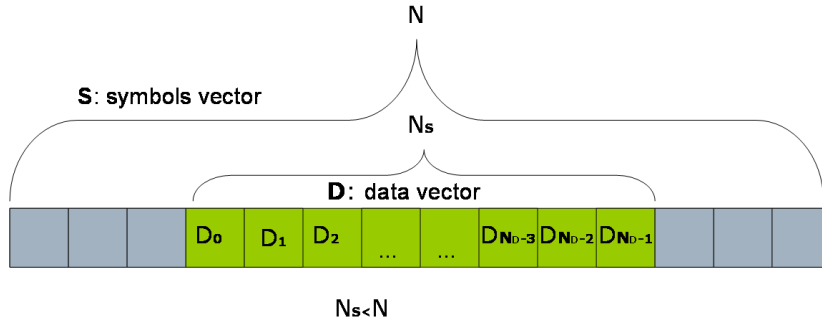


Fig. 3.2: Data symbols in the subcarrier vector in a classic OFDM scheme

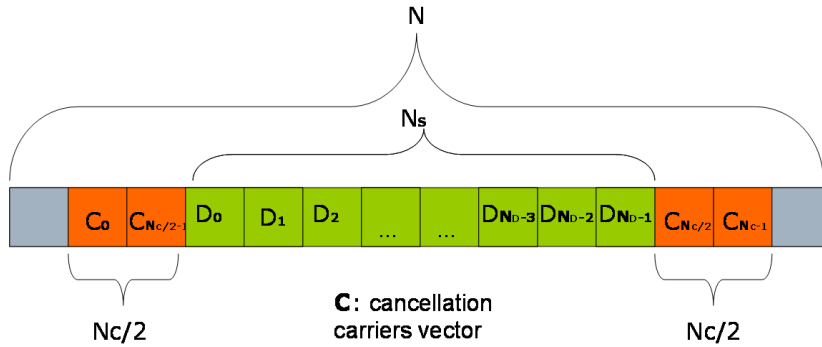


Fig. 3.3: Data symbols in the subcarrier vector in with Cancellation Carriers

generates a time-continuous signal  $x(t)$  through a waveform  $g(t)$ . Because of the nonlinearities of the HPA, the signal  $y(t)$  which is sent in air has an higher OOB with respect  $x(t)$ . The modified scheme is depicted in 3.2.2, where opportune cancellation carrier (CC) coefficients are introduced in order to minimize the OOB of  $y(t)$ . The adaptive methods previously presented in the Literature evaluate the CC in order to minimize the OOB of the signal  $x(t)$  before the HPA (that is, not considering the nonlinearities), or its PAPR (taking into account then nonlinearities, but not attaining the optimal solution whet the HPA does not operate in the saturation region). The adaptive methods presented here evaluate the CC in order to minimize instead directly the OOB of the signal  $y(t)$  after the HPA (attaining the optimal solution in all the HPA working condition).

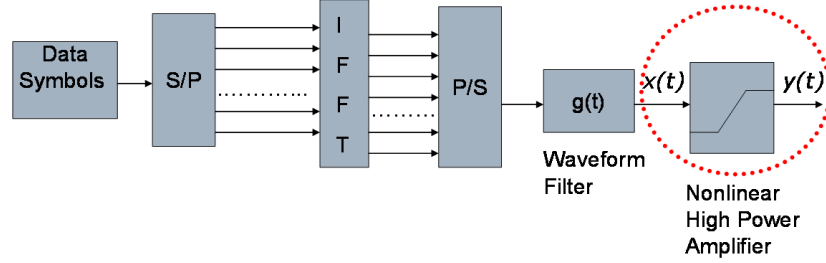


Fig. 3.4: Block Scheme of an OFDM transmitter with nonlinear HPA

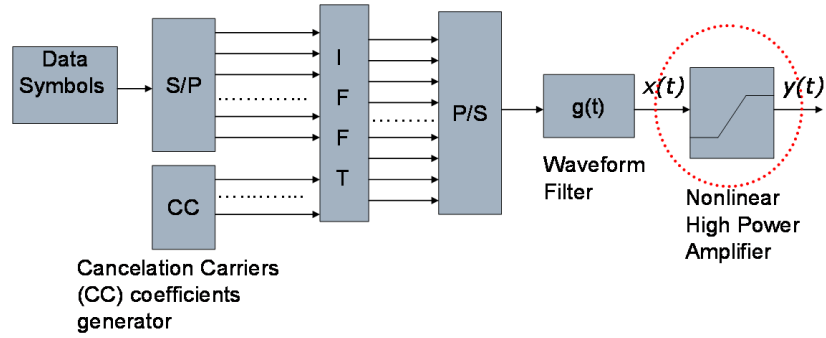


Fig. 3.5: Block Scheme of an OFDM transmitter with nonlinear HPA and Cancellation Carriers

### 3.2.3 Transmitted Signal

Let  $T_s$  be the time-domain sample duration,  $N$  the total number of sub-carriers,  $N_s$  the number of data and cancellation carriers,  $L$  the time-oversampling factor,  $NL$  the number of IDFT point,  $N_g$  the number of cyclic prefix symbols,  $g(t)$  the pulse waveform (practical duration  $T_s/L$ ),  $w(t)$  the time-domain windowing (of practical duration  $T_s$ ),  $s[k]$  and  $S[n]$  the time domain and frequency domain symbols, respectively. The complex envelope of the OFDM signal at the input of the HPA is, in a classical OFDM system without any algorithm (and in which we focus on one OFDM symbol):

$$x(t) = \sum_{k=-N_g L}^{NL-1} s[k] g\left(t - k \frac{T_s}{L}\right), \quad (3.1)$$

where

$$s[k] \triangleq \frac{w_R[k]}{\sqrt{N}} \sum_{n=-\frac{N_s}{2}}^{\frac{N_s}{2}-1} S[n] e^{j2\pi \frac{kn}{NL}}, \quad (3.2)$$

with

$$w_R[k] = w\left(k \frac{T_s}{L}\right) \quad (3.3)$$

and

$$S[n] = \begin{cases} D[n], & \text{for } n \in \mathcal{I}^{(d)}; \\ 0, & \text{for } n \in [0, \dots, N-1] - \mathcal{I}^{(d)}. \end{cases} \quad (3.4)$$

being  $D[n]$  the data symbol transmitted by the  $n$ -th carrier and  $\mathcal{I}^{(d)}$  the set of indices for the data carriers.

Now we examine how these expressions change both in the cases that a frequency-domain algorithm or a time-domain algorithm are applied to reduce OOB<sup>1</sup>.

In the Cancellation Carriers method some of the unused subcarriers are used to transmit the cancellation symbols  $C[n]$  and so the OFDM signal expression becomes:

$$x_{FD}(t) = \sum_{k=-N_g L}^{NL-1} s_{FD}[k] g\left(t - k \frac{T_s}{L}\right), \quad (3.5)$$

where

$$s_{FD}[k] \triangleq \frac{w_R[k]}{\sqrt{N}} \sum_{n=-\frac{N_s}{2}}^{\frac{N_s}{2}-1} S_{FD}[n] e^{j2\pi \frac{kn}{NL}}, \quad (3.6)$$

and

$$S_{FD}[n] = \begin{cases} D[n], & \text{for } n \in \mathcal{I}^{(d)}; \\ C[n], & \text{for } n \in \mathcal{I}^{(c)}. \end{cases} \quad (3.7)$$

being  $\mathcal{I}^{(c)}$  the set of indices for cancellation carriers.

In the case of Adaptive Symbols transition method, a  $N_a L$ -dimensional vector of cancellation symbols  $\mathbf{A} = (A[NL], \dots, A[NL + N_a L - 1])^T$  is inserted between two successive OFDM symbols  $\mathbf{s}_{pre} = (s_{pre}[0], \dots, s_{pre}[NL-1])^T$  and  $\mathbf{s}_{post} = (s_{post}[NL + N_a L], \dots, s_{post}[2NL + N_a L - 1])^T$  in the time domain. Thus, while in the cancellation carriers method we could consider only one generic OFDM symbol  $\mathbf{S} = (S[0], \dots, S[N-1])^T$ , two consecutive symbols  $\mathbf{S}_{pre} = (S_{pre}[0], \dots, S_{pre}[N-1])^T$  and  $\mathbf{S}_{post} = (S_{post}[0], \dots, S_{post}[N-1])^T$  have now to be

<sup>1</sup> we indicate with pedix *FD* the expressions referring to Frequency Domain method and with pedix *TD* the expressions referring to Time Domain method

considered, as done in ???. By defining:

$$N_d \doteq NL + N_gL + N_aL, \quad (3.8)$$

, with the same notation adopted before we can consider the complex equivalent of the transmitted OFDM signal as:

$$x_{\text{TD}}(t) = \sum_{k=-N_gL}^{NL+N_d-1} s_{\text{TD}}[k]g\left(t - k\frac{T_s}{L}\right), \quad (3.9)$$

being

$$s_{\text{TD}}[k] = \begin{cases} \frac{w_R[k]}{\sqrt{N}} \sum_{n=-\frac{N_s}{2}}^{\frac{N_s}{2}-1} S_{\text{pre}}[n]e^{j2\pi\frac{kn}{NL}}, & k \in K_1; \\ \frac{A[k]}{\sqrt{N}}, & k \in K_a; \\ \frac{w_R[k-N_d]}{\sqrt{N}} \sum_{n=-\frac{N_s}{2}}^{\frac{N_s}{2}-1} S_{\text{post}}(n)e^{j2\pi\frac{(k-N_d)n}{NL}}, & k \in K_2. \end{cases} \quad (3.10)$$

where  $K_1 \triangleq [-N_gL, NL-1]$ ,  $K_a \triangleq [NL-1, N_d-N_gL-1]$ ,  $K_2 \triangleq [N_d-N_gL, N_d+NL-1]$ .

### 3.2.4 Non-Linear Power Amplifier Model

The nonlinear HPA is modeled following the Rapp Model. The output  $y(t)$  of the HPA can be expressed as a function of the input  $x(t)$ :

$$y(t) = H_p[x(t)] = \frac{\sqrt{G}x(t)}{\left[1 + \left|\frac{x(t)}{x_{\text{sat}}}\right|^{2p}\right]^{\frac{1}{2p}}}, \quad (3.11)$$

where  $G$  is the power amplification gain,  $y_{\text{sat}}$  the output saturation value with corresponding saturation input  $x_{\text{sat}} \triangleq y_{\text{sat}}/\sqrt{G}$  and  $p$  is a parameter usually in the range  $[2-10]$ . The higher the parameter  $p$  is, the more similar the The relation between input and output according to this model is typically realistic in the case of solid state amplifiers.

### 3.2.5 Cost Function

In the methods proposed by the Literature the Cost Function is evaluated as the amount of power of the signal  $x(t)$  outside the band  $[f_1, f_u]$ . The novelty of the proposed algorithm consists in considering as the cost function the amount of power of the output signal  $y(t)$  outside the same band  $[f_1, f_u]$ :

$$\Upsilon = \int_{f_1-B_{\text{adj}}}^{f_1} |Y(f)|^2 df + \int_{f_u}^{f_u+B_{\text{adj}}} |Y(f)|^2 df, \quad (3.12)$$

being  $Y(f)$  the FT (Fourier Transform) of  $y(t)$  and  $B_{\text{adj}}$  the bandwidth of the adjacent channels. Rather than a continuous method, a discrete form based on the discrete values of frequency  $f_i$  can be considered:

$$\Upsilon_d = \sum_{i \in \mathcal{N}_{\text{adj}}} |Y(f_i)|^2 \Delta f, \quad (3.13)$$

where  $f_i = i/KNT_s$ ,  $K$  is the over-sampling factor in frequency,  $i \in \mathcal{N}_{\text{adj}}$  and  $\mathcal{N}_{\text{adj}}$  is the set of integer such that  $f_i \in (f_l - B_{\text{adj}}, f_l) \cup (f_u, f_u + B_{\text{adj}})$  and  $\Delta f = 1/KNT_s$ .

### 3.3 Frequency Domain Method: Cancellation Carriers

#### 3.3.1 Cost Function

In this section we specify the expression of cost function in the case of frequency domain method. After some algebra, taking also into account the Rapp Model, it can be written for the frequency domain case, that:

$$Y_{\text{FD}}(f_i) = \frac{T_s}{L} \sum_{k'=0}^{NL-1} \frac{\sqrt{G} g_0 s_{\text{FD}}[k'](\mathbf{C})}{\left(1 + \left|\frac{g_0 s_{\text{FD}}[k'](\mathbf{C})}{x_{\text{sat}}}\right|^{2p}\right)^{\frac{1}{2p}}} e^{-j2\pi \frac{ik'}{KNL}}, \quad (3.14)$$

for  $i \in [-KNL/2, KNL/2 - 1]$ , where, by putting in evidence how each symbol depends on the complex cancelation carriers vector  $\mathbf{C} = \{C(n)\}$ :

$$s_{\text{FD}}[k'](\mathbf{C}) = d[k'] + \frac{w_{\text{R}}[k']}{\sqrt{N}} \sum_{n \in \mathcal{I}^{(c)}} C(n) e^{j2\pi \frac{k'n}{NL}}, \quad (3.15)$$

being

$$d[k'] \triangleq \frac{w_{\text{R}}[k']}{\sqrt{N}} \sum_{n \in \mathcal{I}^{(s)}} D[n] e^{j2\pi \frac{k'n}{NL}}. \quad (3.16)$$

Denoting by  $N_{\text{ob}}$  the number of considered OOB side-lobes, the expression (3.14) is valid under the following conditions:

$$L > 1 + \frac{N_{\text{ob}}}{N} \quad (3.17)$$

and

$$K > 1 + \frac{N_{\text{g}}}{N}. \quad (3.18)$$

Since usually  $N_{\text{g}} < N$  and  $N_{\text{ob}} < 2N$  it is sufficient to have  $L \geq 3$  and  $K \geq 2$ .

We remember that  $\mathcal{N}_{\text{adj}} = [-KNL/2, -KN/2 + 1] \cup [KN/2, KNL/2 - 1]$ . Consequently,

for the frequency domain case, the (normalized) cost function becomes:

$$\tilde{\Upsilon}_{\text{FD}}(\mathbf{C}) = \sum_{i \in \mathcal{N}_{\text{adj}}} \left| \sum_{k'=0}^{NL-1} \frac{g_0 s_{\text{FD}}[k'](\mathbf{C})}{\left(1 + \left|\frac{g_0 s_{\text{FD}}[k'](\mathbf{C})}{x_{\text{sat}}}\right|^{2p}\right)^{\frac{1}{2p}}} e^{-j2\pi \frac{ik'}{KNL}} \right|^2. \quad (3.19)$$

### 3.3.2 Optimization

In this section we describe the optimization problem focused in minimizing the cost function  $\tilde{\Upsilon}_{\text{FD}}(\mathbf{C})$  with respect the values of the symbols in cancellation carriers  $\mathbf{C}$  through the so called gradient method, finding the optimal vector  $\hat{\mathbf{C}}$  such that:

$$\hat{\mathbf{C}} = \underset{\mathbf{C}}{\text{argmin}} \tilde{\Upsilon}_{\text{FD}}(\mathbf{C}). \quad (3.20)$$

#### Conversion to a problem in real variables

It can be easily verified that the derived cost function in (3.19) does not satisfy Cauchy-Riemann conditions and thus is not complex differentiable. It follow that the gradient method cannot be applied directly to the complex vector  $\mathbf{C}$  with complex-value elements  $C[n]$ .

In order to be able to employ the gradient method, we have to reduce the minimization of the cost function (a function from complex domain to real codomain) to a problem in real variables. Thus we define the  $2N_c$  real variables  $c_{n'}$  (with  $n' \in [0, 2N_c - 2]$ ) constituting the real vector  $\mathbf{c}$  and related to the  $N_c$  complex variables  $C[n]$  as<sup>2</sup>:

$$\begin{aligned} c_{n'} &= \Re\{C[n' - N_s/2]\} \\ c_{n'+N_c} &= \Im\{C[n' - N_s/2]\} \end{aligned} \quad (3.21)$$

for  $n' < N_c/2$ ,

$$\begin{aligned} c_{n'} &= \Re\{C[n' + N_s/2 - N_c]\} \\ c_{n'+N_c} &= \Im\{C[n' + N_s/2 - N_c]\}, \end{aligned} \quad (3.22)$$

for  $n' \geq N_c/2$ , and, on the other side,

$$C[n] = c_{n+N_s/2} + j c_{n+N_s/2+N_c} \quad (3.23)$$

<sup>2</sup> We assume that  $\mathcal{I}^c = [-N_s/2, -N_s/2 + N_c/2 - 1] \cup [N_s/2 - N_c/2, N_s/2 - 1]$

for  $-N_s/2 \leq n < -N_s/2 + N_c/2$ ,

$$C[n] = c_{n-N_s/2+N_c} + j c_{n-N_s/2+2N_c}, \quad (3.24)$$

for  $N_s - N_c/2 < n \leq N_s - 1$ . Now, the optimization problem (3.42) is re-stated as:

$$\hat{\mathbf{c}} = \operatorname{argmin}_{\mathbf{c}} \tilde{\Upsilon}_{\mathbf{d}}(\mathbf{c}). \quad (3.25)$$

Being  $\hat{\mathbf{c}} = (\hat{c}_1, \hat{c}_2, \dots, \hat{c}_{2N_c})^T$  the value of  $\mathbf{c} = (c_1, c_2, \dots, c_{2N_c})^T$  that minimizes the cost function, the elements of real vector  $\hat{\mathbf{c}}$  can be obtained in iterative fashion by applying the gradient method

$$\hat{c}_i^{(k+1)} = \hat{c}_i^{(k)} + \mu \frac{d\tilde{\Upsilon}_{\mathbf{d}}(\hat{\mathbf{c}})}{d\hat{c}_i^{(k)}}. \quad (3.26)$$

where  $\mu$  is the step-size of the gradient method. It is worthwhile to note that thanks to complex-real conversion, it is possible to employ the gradient method. Consequently also the cost function can be written as (3.27)(at the end), where (supposing real waveforms), it is (3.28), (3.29), being:

$$\begin{aligned} \tilde{\Upsilon}_{\text{FD}}(\mathbf{C}) = \sum_{i \in \mathcal{N}_{\text{adj}}} \left\{ \left( \sum_{k'=0}^{NL-1} \frac{p_{k'}(\mathbf{c}) \cos\left(\frac{2\pi k' i}{K N L}\right) + q_{k'}(\mathbf{c}) \sin\left(\frac{2\pi k' i}{K N L}\right)}{\alpha_{\text{FD}}[k](p, x_{\text{sat}}, \mathbf{c})} \right)^2 + \right. \\ \left. + \left( \sum_{k'=0}^{NL-1} \frac{-p_{k'}(\mathbf{c}) \sin\left[\frac{2\pi k' i}{K N L}\right] + q_{k'}(\mathbf{c}) \cos\left(\frac{2\pi k' i}{K N L}\right)}{\alpha_{\text{FD}}[k](p, x_{\text{sat}}, \mathbf{c})} \right)^2 \right\}. \end{aligned} \quad (3.27)$$

$$\begin{aligned} p_{k'}(\mathbf{c}) = \Re\{g_0 s_{\text{FD}}[k](\mathbf{C})\} = g_0 d_{k'}^{(R)} + g_0 \frac{w_{\text{R}}[k']}{\sqrt{N}} \sum_{n \in \mathcal{I}(\mathbf{c})} \Re\{C[n] e^{j 2\pi \frac{k' n}{N L}}\} = \\ = g_0 d_{k'}^{(R)} + g_0 \frac{w_{\text{R}}[k']}{\sqrt{N}} \sum_{n=-\frac{N_s}{2}}^{-\frac{N_s}{2} + \frac{N_c}{2} - 1} \left[ c_{n+N_s/2} \cos\left(2\pi \frac{k' n}{N L}\right) - c_{n+N_s/2+N_c} \sin\left(2\pi \frac{k' n}{N L}\right) \right] + \\ + g_0 \frac{w_{\text{R}}[k']}{\sqrt{N}} \sum_{n=\frac{N_s}{2} - \frac{N_c}{2}}^{\frac{N_s}{2} - 1} \left[ c_{n-N_s/2+N_c} \cos\left(2\pi \frac{k' n}{N L}\right) - c_{n-N_s/2+2N_c} \sin\left(2\pi \frac{k' n}{N L}\right) \right] \end{aligned} \quad (3.28)$$

$$\begin{aligned}
q_{k'}(\mathbf{c}) &= \Im\{g_0 s_{\text{FD}}[k](\mathbf{C})\} = g_0 d_{k'}^{(I)} + g_0 \frac{w_{\text{R}}(k')}{\sqrt{N}} \sum_{n \in \mathcal{I}(\mathbf{c})} \Im\{C[n] e^{j2\pi \frac{k'n}{NL}}\} = \\
&= g_0 d_{k'}^{(I)} + g_0 \frac{w_{\text{R}}[k']}{\sqrt{N}} \sum_{n=-\frac{N_s}{2}}^{-\frac{N_s}{2} + \frac{N_c}{2} - 1} \left[ c_{n+N_s/2} \sin\left(2\pi \frac{k'n}{NL}\right) + c_{n+N_s/2+N_c} \cos\left(2\pi \frac{k'n}{NL}\right) \right] + \\
&\quad + g_0 \frac{w_{\text{R}}[k']}{\sqrt{N}} \sum_{n=\frac{N_s}{2} - \frac{N_c}{2}}^{\frac{N_s}{2} - 1} \left[ c_{n-N_s/2+N_c} \sin\left(2\pi \frac{k'n}{NL}\right) + c_{n-N_s/2+2N_c} \cos\left(2\pi \frac{k'n}{NL}\right) \right] \quad (3.29)
\end{aligned}$$

$$d_k^{(R)} = \Re\{d[k]\}, \quad (3.30)$$

$$d_k^{(I)} = \Im\{d[k]\} \quad (3.31)$$

and

$$\begin{aligned}
\alpha_{\text{FD}}[k](p, x_{\text{sat}}, \mathbf{c}) &= \left(1 + \left| \frac{g_0 s_{\text{FD}}[k](\mathbf{C})}{x_{\text{sat}}} \right|^{2p} \right)^{\frac{1}{2p}} = \\
&= \left\{ 1 + \left[ \frac{p_{k'}^2(\mathbf{c}) + q_{k'}^2(\mathbf{c})}{x_{\text{sat}}^2} \right]^p \right\}^{\frac{1}{2p}}. \quad (3.32)
\end{aligned}$$

### Gradient

According to expression (3.27), the derivative with respect the generic term  $c_{n'}$  (where obviously  $n' \in [0, 2N_c - 1]$ ) is (3.33), where:

$$\begin{aligned}
\frac{\partial \tilde{\Upsilon}_{\text{FD}}}{\partial c_{n'}} &= \sum_{i \in \mathcal{N}_{\text{adj}}} \left\{ 2 \left[ \sum_{k'=0}^{NL-1} \frac{p_{k'}(\mathbf{c}) \cos\left(\frac{2\pi k' i}{K NL}\right) + q_{k'}(\mathbf{c}) \sin\left(\frac{2\pi k' i}{K NL}\right)}{\alpha_{\text{FD}}[k](p, x_{\text{sat}}, \mathbf{c})} \right] \left[ \sum_{k'=0}^{NL-1} \frac{\frac{\partial p_{k'}(\mathbf{c})}{\partial c_{n'}} \cos\left(\frac{2\pi k' i}{K NL}\right) + \frac{\partial q_{k'}(\mathbf{c})}{\partial c_{n'}} \sin\left(\frac{2\pi k' i}{K NL}\right)}{\alpha_{\text{FD}}[k](p, x_{\text{sat}}, \mathbf{c})} \right] \right. \\
&\quad - \frac{\partial \alpha_{k'}(p, \mathbf{c})}{\partial c_{n'}} \frac{p_{k'}(\mathbf{c}) \cos\left(\frac{2\pi k' i}{K NL}\right) + q_{k'}(\mathbf{c}) \sin\left(\frac{2\pi k' i}{K NL}\right)}{\alpha_{\text{FD}}^2[k](p, x_{\text{sat}}, \mathbf{c})} \left. + 2 \left[ \sum_{k'=0}^{NL-1} \frac{-p_{k'}(\mathbf{c}) \sin\left(\frac{2\pi k' i}{K NL}\right) + q_{k'}(\mathbf{c}) \cos\left(\frac{2\pi k' i}{K NL}\right)}{\alpha_{\text{FD}}[k](p, x_{\text{sat}}, \mathbf{c})} \right] \right. \\
&\quad \times \left[ \sum_{k'=0}^{NL-1} \frac{-\frac{\partial p_{k'}(\mathbf{c})}{\partial c_{n'}} \sin\left(\frac{2\pi k' i}{K NL}\right) + \frac{\partial q_{k'}(\mathbf{c})}{\partial c_{n'}} \cos\left(\frac{2\pi k' i}{K NL}\right)}{\alpha_{\text{FD}}[k](p, x_{\text{sat}}, \mathbf{c})} - \frac{\partial \alpha_{\text{FD}}[k](p, x_{\text{sat}}, \mathbf{c})}{\partial c_{n'}} \frac{-p_{k'}(\mathbf{c}) \sin\left(\frac{2\pi k' i}{K NL}\right) + q_{k'}(\mathbf{c}) \cos\left(\frac{2\pi k' i}{K NL}\right)}{\alpha_{\text{FD}}^2[k](p, x_{\text{sat}}, \mathbf{c})} \right]
\end{aligned}$$

$$\frac{\partial p_{k'}(\mathbf{c})}{\partial c_{n'}} = \begin{cases} g_0 \frac{w_R[k']}{\sqrt{N}} \cos \left[ 2\pi \frac{k'(n' - \frac{N_s}{2})}{NL} \right], & n' \in I_A; \\ g_0 \frac{w_R[k']}{\sqrt{N}} \cos \left[ 2\pi \frac{k'(n' + \frac{N_s}{2} - N_c)}{NL} \right], & n' \in I_B; \\ -g_0 \frac{w_R[k']}{\sqrt{N}} \sin \left[ 2\pi \frac{k'(n' - \frac{N_s}{2} - N_c)}{NL} \right], & n' \in I_C; \\ -g_0 \frac{w_R[k']}{\sqrt{N}} \sin \left[ 2\pi \frac{k'(n' + \frac{N_s}{2} - 2N_c)}{NL} \right], & n' \in I_D. \end{cases}$$

$$\frac{\partial q_{k'}(\mathbf{c})}{\partial c_{n'}} = \begin{cases} g_0 \frac{w_R[k']}{\sqrt{N}} \sin \left[ 2\pi \frac{k'(n' - \frac{N_s}{2})}{NL} \right], & n' \in I_A; \\ g_0 \frac{w_R[k']}{\sqrt{N}} \sin \left[ 2\pi \frac{k'(n' + \frac{N_s}{2} - N_c)}{NL} \right], & n' \in I_B; \\ g_0 \frac{w_R[k']}{\sqrt{N}} \cos \left[ 2\pi \frac{k'(n' - \frac{N_s}{2} - N_c)}{NL} \right], & n' \in I_C; \\ g_0 \frac{w_R[k']}{\sqrt{N}} \cos \left[ 2\pi \frac{k'(n' + \frac{N_s}{2} - 2N_c)}{NL} \right], & n' \in I_D. \end{cases}$$

being  $I_A \triangleq [0, 1, \dots, N_c/2 - 1]$ ,  $I_B \triangleq [N_c/2, N_c/2 + 1, \dots, N_c - 1]$ ,  $I_C \triangleq [N_c, N_c + 1, \dots, 3N_c/2 - 1]$ ,  $I_D \triangleq [3N_c/2, 3N_c/2 + 1, \dots, 2N_c - 1]$ , and:

$$\begin{aligned} \frac{\partial \alpha_{\text{FD}}[k](p, x_{\text{sat}}, \mathbf{c})}{\partial c_{n'}} &= \left\{ 1 + \left[ \frac{p_{k'}^2(\mathbf{c}) + q_{k'}^2(\mathbf{c})}{x_{\text{sat}}^2} \right]^p \right\}^{\frac{1}{2p} - 1} \times \\ &\times \left[ \frac{p_{k'}^2(\mathbf{c}) + q_{k'}^2(\mathbf{c})}{x_{\text{sat}}^2} \right]^{p-1} \frac{1}{x_{\text{sat}}^2} \\ &\times \left[ p_{k'}(\mathbf{c}) \frac{\partial p_{k'}(\mathbf{c})}{\partial c_{n'}} + q_{k'}(\mathbf{c}) \frac{\partial q_{k'}(\mathbf{c})}{\partial c_{n'}} \right]. \end{aligned} \quad (3.34)$$

By implementing (3.33) in the algorithm (3.26) it is possible to find, after several iterations, the optimized value of the cancellation carriers vector  $\hat{\mathbf{c}}$ .

### 3.4 Time Domain Method: Adaptive Symbol Transition

#### 3.4.1 Cost Function

In this section we develop the expression (3.13) in the case of time-domain method application it can be shown that, under the conditions:

$$L > 1 + \frac{N_{ob}}{N} \quad (3.35)$$

and

$$K > 2 \left( 1 + \frac{N_g + N_a}{N} \right). \quad (3.36)$$

(since usually  $N_g + N_a < N$ , and  $N_{ob} < 2N$  it is sufficient to have  $L \geq 4$  and  $K \geq 4$ ), the samples of the output signal in the spectrum can be written as:

$$Y(f_i) = \frac{T_s}{L} \sum_{k'=0}^{N_d+NL-1} \frac{\sqrt{G} g_{0s_{TD}}[k']}{\left( 1 + \left| \frac{g_{0s_{TD}}[k']}{x_{sat}} \right|^{2p} \right)^{\frac{1}{2p}}} e^{-j2\pi \frac{ik'}{KNL}}, \quad i \in [-KNL/2, KNL/2 - 1]. \quad (3.37)$$

Thus, the discrete cost function can be expressed as:

$$\begin{aligned} \tilde{\Upsilon}_{TD} &= \sum_{i \in \mathcal{N}} |Y(f_i)|^2 \Delta f = \\ &= \frac{GT_s}{KNL^2} \sum_{i \in \mathcal{N}} \left| \sum_{k'=0}^{N_d+NL-1} \frac{g_{0s_{TD}}[k'] e^{-j2\pi \frac{ik'}{KNL}}}{\left( 1 + \left| \frac{g_{0s_{TD}}[k']}{x_{sat}} \right|^{2p} \right)^{\frac{1}{2p}}} \right|^2, \end{aligned} \quad (3.38)$$

being  $\mathcal{N} = [-KNL/2, -KN/2 + 1] \cup [KN/2, KNL/2 - 1]$ .

The discrete and normalized cost function can be written, putting in evidence the dependence on the transition symbol vector  $\mathbf{A}$ , as:

$$\tilde{\Upsilon}_{TD}(\mathbf{A}) = \sum_{i \in \mathcal{N}} \left| \sum_{k'=0}^{NL+N_d-1} \frac{g_{0s_{TD}}[k'](\mathbf{A})}{\left( 1 + \left| \frac{g_{0s_{TD}}[k'](\mathbf{A})}{x_{sat}} \right|^{2p} \right)^{\frac{1}{2p}}} e^{-j2\pi \frac{ik'}{KNL}} \right|^2, \quad (3.39)$$

where we remember that  $\mathcal{N}_{adj} = [-KNL/2, -KN/2 + 1] \cup [KN/2, KNL/2 - 1]$ . By substituting (??) we can write

$$\tilde{\Upsilon}_{TD}(\mathbf{A}) = \sum_{i \in \mathcal{N}_{adj}} \left| d_i(x_{sat}, p) + \sum_{k'=NL}^{NL+N_aL-1} \frac{g_0 \frac{A[k']}{\sqrt{N}} e^{-j2\pi \frac{ik'}{KNL}}}{\left( 1 + \left| \frac{g_0 \frac{A[k']}{\sqrt{N}}}{x_{sat}} \right|^{2p} \right)^{\frac{1}{2p}}} \right|^2, \quad (3.40)$$

where we have defined:

$$\begin{aligned}
d_i(x_{sat}, p) \doteq & \sum_{k'=0}^{NL-1} \frac{\frac{g_0}{\sqrt{N}} \sum_{n=-\frac{N_s}{2}}^{\frac{N_s}{2}-1} S_{\text{pre}}[n] e^{j2\pi \frac{k'n}{NL}}}{\left(1 + \left| \frac{\frac{g_0}{\sqrt{N}} \sum_{n=-\frac{N_s}{2}}^{\frac{N_s}{2}-1} S_{\text{pre}}[n] e^{j2\pi \frac{k'n}{NL}}}{x_{sat}} \right|^{2p} \right)^{\frac{1}{2p}}} e^{-j2\pi \frac{ik'}{KNL}} + \\
& + \sum_{k'=N_d}^{N_d+NL-1} \frac{\frac{g_0}{\sqrt{N}} \sum_{n=-\frac{N_s}{2}}^{\frac{N_s}{2}-1} S_{\text{post}}[n] e^{j2\pi \frac{(k'-N_d)n}{NL}}}{\left(1 + \left| \frac{\frac{g_0}{\sqrt{N}} \sum_{n=-\frac{N_s}{2}}^{\frac{N_s}{2}-1} S_{\text{post}}[n] e^{j2\pi \frac{(k'-N_d)n}{NL}}}{x_{sat}} \right|^{2p} \right)^{\frac{1}{2p}}} e^{-j2\pi \frac{ik'}{KNL}} \quad (3.41)
\end{aligned}$$

### 3.4.2 Optimization

In this section we try to minimize the cost function through convex optimization methods. It consists in minimizing the cost function  $\tilde{\Upsilon}_{\text{TD}}(\mathbf{A})$  with respect the values of the transition symbols  $\mathbf{A}$  through the so called gradient method, finding the optimal vector  $\hat{\mathbf{A}}$  such that:

$$\hat{\mathbf{A}} = \underset{\mathbf{C}}{\text{argmin}} \tilde{\Upsilon}_{\text{TD}}(\mathbf{A}). \quad (3.42)$$

*conversion to a problem in real variables*

Note that crucial step to make problem solvable was to convert the problem to the real domain. In fact the cost function can be written as:

$$\begin{aligned}
\tilde{\Upsilon}_{\text{TD}}(\mathbf{A}) = & \sum_{i \in \mathcal{N}} \left\{ \left( d_i^{(R)}(x_{sat}, p) + \sum_{k'=NL}^{NL+N_aL-1} \frac{g_0 \frac{A_{k'}^{(R)}}{\sqrt{N}} \cos\left(\frac{2\pi k'i}{KNL}\right) + g_0 \frac{A_{k'}^{(I)}}{\sqrt{N}} \sin\left(\frac{2\pi k'i}{KNL}\right)}{\alpha_{k'}(x_{sat}, p, A)} \right)^2 + \right. \\
& \left. + \left( d_i^{(I)}(x_{sat}, p) + \sum_{k'=NL}^{NL+N_aL-1} \frac{-g_0 \frac{A_{k'}^{(R)}}{\sqrt{N}} \sin\left[\frac{2\pi k'i}{KNL}\right] + g_0 \frac{A_{k'}^{(I)}}{\sqrt{N}} \cos\left(\frac{2\pi k'i}{KNL}\right)}{\alpha_{k'}(x_{sat}, p, A)} \right)^2 \right\} \quad (3.43)
\end{aligned}$$

where

$$d_i^{(R)}(x_{sat}, p) = \Re\{d_i(x_{sat}, p)\}, \quad (3.44)$$

$$d_i^{(I)}(x_{sat}, p) = \Im\{d_i(x_{sat}, p)\}, \quad (3.45)$$

$$A_{k'}^{(R)} = \Re\{A[k']\}, \quad (3.46)$$

$$A_{k'}^{(I)} = \Im\{A[k']\} \quad (3.47)$$

and

$$\begin{aligned} \alpha_{k'}(x_{sat}, p, A) &= \left( 1 + \left| \frac{g_0 \frac{A_{k'}}{\sqrt{N}}}{x_{sat}} \right|^{2p} \right)^{\frac{1}{2p}} = \\ &= \left\{ 1 + \left[ \frac{A_{k'}^{(R)2} + A_{k'}^{(I)2}}{N x_{sat}^2} \right]^p \right\}^{\frac{1}{2p}}. \end{aligned} \quad (3.48)$$

It can be easily checked that the derived cost function does not satisfy Cauchy-Riemann conditions and thus is not complex differentiable. As a consequence, gradient method cannot be applied directly to the complex vector  $\mathbf{A}$  with complex-valued elements  $A_k$ .

In order to apply the gradient method, we have to reduce the minimization of our cost function (a function from complex domain to real codomain) to a problem in real variables. To this aim we define the  $2N_a$  real variables  $a_{k''}$  (with  $k'' \in [0, 2N_a - 1]$ ) related to the  $N_a$  complex variables  $A_{k'}$  as below<sup>3</sup>: for  $k'' < N_a L$ :

$$a_{k''} = \Re\{A(k'' + NL)\} \quad (3.49)$$

$$a_{k''+N_a L} = \Im\{A(k'' + NL)\}$$

and, on the other side, for  $-N_s/2 \leq n < -N_s/2 + N_c/2$ :

$$A(k') = a_{k'-NL} + j a_{k'-NL+N_a L}. \quad (3.50)$$

The optimization problem can be stated as

$$\Upsilon_{d,\min} = \min_{\mathbf{a}} \Upsilon_d(\mathbf{a}). \quad (3.51)$$

By calling  $\hat{\mathbf{a}}$  the value of  $\mathbf{a}$  that minimizes cost function, elements of real vector  $\hat{\mathbf{a}}$  can be obtained in iterative fashion applying gradient method

$$\hat{a}_k^{(n+1)} = \hat{a}_k^{(n)} + \mu \frac{d\Upsilon_d(\hat{\mathbf{a}})}{d\hat{a}_k^{(n)}}. \quad (3.52)$$

where  $\mu$  is the step-size of the gradient method.

<sup>3</sup> We suppose that  $k' \in [NL, NL + N_a L - 1]$ ,  $k'' \in [0, N_a L - 1]$

Consequently cost function can be written, by putting in evidence the dependance on the  $2N_a L$ -vector  $a$ , as:

$$\begin{aligned} \tilde{\Upsilon}_{\text{TD}}(\mathbf{A}) = \sum_{i \in \mathcal{N}} \left\{ \left( d_i^{(R)}(x_{\text{sat}}, p) + \sum_{k'=NL}^{NL+N_a L-1} \frac{g_0 \frac{a_{k'-NL}}{\sqrt{N}} \cos\left(\frac{2\pi k' i}{KNL}\right) + g_0 \frac{a_{k'-NL+N_a L}}{\sqrt{N}} \sin\left(\frac{2\pi k' i}{KNL}\right)}{\left\{ 1 + \left[ \frac{a_{k'-NL}^2 + a_{k'-NL+N_a L}^2}{Nx_{\text{sat}}^2} \right]^p \right\}^{\frac{1}{2p}}} \right)^2 + \right. \\ \left. + \left( d_i^{(I)}(x_{\text{sat}}, p) + \sum_{k'=NL}^{NL+N_a L-1} \frac{-g_0 \frac{a_{k'-NL}}{\sqrt{N}} \sin\left[\frac{2\pi k' i}{KNL}\right] + g_0 \frac{a_{k'-NL+N_a L}}{\sqrt{N}} \cos\left(\frac{2\pi k' i}{KNL}\right)}{\left\{ 1 + \left[ \frac{a_{k'-NL}^2 + a_{k'-NL+N_a L}^2}{Nx_{\text{sat}}^2} \right]^p \right\}^{\frac{1}{2p}}} \right)^2 \right\} \quad (3.53) \end{aligned}$$

### Gradient

According to expression (3.53), the derivative with respect the generic term  $a_{k''}$  (where obviously  $k'' \in [0, 2N_a L - 1]$ ) is:

$$\begin{aligned}
\frac{\partial \tilde{\Upsilon}_{\text{TD}}}{\partial a_{k''}} = & \sum_{i \in \mathcal{N}} \left\{ 2 \left( d_i^{(R)}(x_{\text{sat}}, p) + \frac{g_0}{\sqrt{N}} \sum_{k'=NL}^{NL+N_aL-1} \frac{a_{k'-NL} \cos\left(\frac{2\pi k' i}{KNL}\right) + a_{k'-NL+N_aL} \sin\left(\frac{2\pi k' i}{KNL}\right)}{\left\{ 1 + \left[ \frac{a_{k'-NL}^2 + a_{k'-NL+N_aL}^2}{Nx_{\text{sat}}^2} \right]^p \right\}^{\frac{1}{2p}}} \right) \times \right. \\
& \times \frac{g_0}{\sqrt{N}} \left[ \frac{\cos\left(\frac{2\pi(k''+NL)i}{KNL}\right)}{\left\{ 1 + \left[ \frac{a_{k''}^2 + a_{k''+N_aL}^2}{Nx_{\text{sat}}^2} \right]^p \right\}^{\frac{1}{2p}}} - \frac{a_{k''} \cos\left(\frac{2\pi(k''+NL)i}{KNL}\right) + a_{k''+N_aL} \sin\left(\frac{2\pi(k''+NL)i}{KNL}\right)}{\left\{ 1 + \left[ \frac{a_{k''}^2 + a_{k''+N_aL}^2}{Nx_{\text{sat}}^2} \right]^p \right\}^{\frac{1}{p}}} \right] \times \\
& \times \left\{ 1 + \left[ \frac{a_{k''}^2 + a_{k''+N_aL}^2}{Nx_{\text{sat}}^2} \right]^p \right\}^{\frac{1}{2p}-1} \left[ \frac{a_{k''}^2 + a_{k''+N_aL}^2}{Nx_{\text{sat}}^2} \right]^{p-1} \frac{a_{k''}}{Nx_{\text{sat}}^2} \Bigg] + \\
& + 2 \left( d_i^{(I)}(x_{\text{sat}}, p) + \frac{g_0}{\sqrt{N}} \sum_{k'=NL}^{NL+N_aL-1} \frac{-a_{k'-NL} \sin\left(\frac{2\pi k' i}{KNL}\right) + a_{k'-NL+N_aL} \cos\left(\frac{2\pi k' i}{KNL}\right)}{\left\{ 1 + \left[ \frac{a_{k'-NL}^2 + a_{k'-NL+N_aL}^2}{Nx_{\text{sat}}^2} \right]^p \right\}^{\frac{1}{2p}}} \right) \times \\
& \times \frac{g_0}{\sqrt{N}} \left[ \frac{\sin\left(\frac{2\pi(k''+NL)i}{KNL}\right)}{\left\{ 1 + \left[ \frac{a_{k''}^2 + a_{k''+N_aL}^2}{Nx_{\text{sat}}^2} \right]^p \right\}^{\frac{1}{2p}}} - \frac{-a_{k''} \sin\left(\frac{2\pi(k''+NL)i}{KNL}\right) + a_{k''+N_aL} \cos\left(\frac{2\pi(k''+NL)i}{KNL}\right)}{\left\{ 1 + \left[ \frac{a_{k''}^2 + a_{k''+N_aL}^2}{Nx_{\text{sat}}^2} \right]^p \right\}^{\frac{1}{p}}} \right] \times \\
& \times \left\{ 1 + \left[ \frac{a_{k''}^2 + a_{k''+N_aL}^2}{Nx_{\text{sat}}^2} \right]^p \right\}^{\frac{1}{2p}-1} \left[ \frac{a_{k''}^2 + a_{k''+N_aL}^2}{Nx_{\text{sat}}^2} \right]^{p-1} \frac{a_{k''}}{Nx_{\text{sat}}^2} \Bigg] \Bigg\}, \quad k'' \in [0, N_aL - 1] \quad (3.54)
\end{aligned}$$

and

$$\begin{aligned}
\frac{\partial \tilde{\Upsilon}_{\text{TD}}}{\partial a_{k''}} = & \sum_{i \in \mathcal{N}} \left\{ 2 \left( d_i^{(R)}(x_{\text{sat}}, p) + \frac{g_0}{\sqrt{N}} \sum_{k'=NL}^{NL+N_aL-1} \frac{a_{k'-NL} \cos\left(\frac{2\pi k' i}{KNL}\right) + a_{k'-NL+N_aL} \sin\left(\frac{2\pi k' i}{KNL}\right)}{\left\{ 1 + \left[ \frac{a_{k'-NL}^2 + a_{k'-NL+N_aL}^2}{Nx_{\text{sat}}^2} \right]^p \right\}^{\frac{1}{2p}}} \right) \times \right. \\
& \times \frac{g_0}{\sqrt{N}} \left[ \frac{\sin\left(\frac{2\pi(k''+NL-N_aL)i}{KNL}\right)}{\left\{ 1 + \left[ \frac{a_{k''-N_aL}^2 + a_{k''}^2}{Nx_{\text{sat}}^2} \right]^p \right\}^{\frac{1}{2p}}} + \right. \\
& \left. \left. \frac{a_{k''-N_aL} \cos\left(\frac{2\pi(k''+NL-N_aL)i}{KNL}\right) + a_{k''} \sin\left(\frac{2\pi(k''+NL-N_aL)i}{KNL}\right)}{\left\{ 1 + \left[ \frac{a_{k''-N_aL}^2 + a_{k''}^2}{Nx_{\text{sat}}^2} \right]^p \right\}^{\frac{1}{p}}} \right) \times \right. \\
& \left. \times \left\{ 1 + \left[ \frac{a_{k''-N_aL}^2 + a_{k''}^2}{Nx_{\text{sat}}^2} \right]^p \right\}^{\frac{1}{2p}-1} \left[ \frac{a_{k''-N_aL}^2 + a_{k''}^2}{Nx_{\text{sat}}^2} \right]^{p-1} \frac{a_{k''}}{Nx_{\text{sat}}^2} \right\} + \\
& + 2 \left( d_i^{(I)}(x_{\text{sat}}, p) + \frac{g_0}{\sqrt{N}} \sum_{k'=NL}^{NL+N_aL-1} \frac{-a_{k'-NL} \sin\left(\frac{2\pi k' i}{KNL}\right) + a_{k'-NL+N_aL} \cos\left(\frac{2\pi k' i}{KNL}\right)}{\left\{ 1 + \left[ \frac{a_{k'-NL}^2 + a_{k'-NL+N_aL}^2}{Nx_{\text{sat}}^2} \right]^p \right\}^{\frac{1}{2p}}} \right) \times \\
& \times \frac{g_0}{\sqrt{N}} \left[ \frac{\sin\left(\frac{2\pi(k''+NL-N_aL)i}{KNL}\right)}{\left\{ 1 + \left[ \frac{a_{k''-N_aL}^2 + a_{k''}^2}{Nx_{\text{sat}}^2} \right]^p \right\}^{\frac{1}{2p}}} + \right. \\
& \left. \left. \frac{-a_{k''-N_aL} \sin\left(\frac{2\pi(k''+NL-N_aL)i}{KNL}\right) + a_{k''} \cos\left(\frac{2\pi(k''+NL-N_aL)i}{KNL}\right)}{\left\{ 1 + \left[ \frac{a_{k''-N_aL}^2 + a_{k''}^2}{Nx_{\text{sat}}^2} \right]^p \right\}^{\frac{1}{p}}} \right) \times \right. \\
& \left. \times \left\{ 1 + \left[ \frac{a_{k''-N_aL}^2 + a_{k''}^2}{Nx_{\text{sat}}^2} \right]^p \right\}^{\frac{1}{2p}-1} \left[ \frac{a_{k''-N_aL}^2 + a_{k''}^2}{Nx_{\text{sat}}^2} \right]^{p-1} \frac{a_{k''}}{Nx_{\text{sat}}^2} \right\} \right\}, \tag{3.55}
\end{aligned}$$

for  $k'' \in [N_aL, 2N_aL - 1]$ .

### 3.5 Numerical Results

#### 3.5.1 Notation

A well known method to quantify the Out Of Band (OOB) radiation is the evaluation of Adjacent Channel Leak Ratio (ACLR) as a function of the Input Back Off (IBO). According to our notation, since we have defined the cost function  $\tilde{\Upsilon}_d$  as the power emitted in the adjacent channel, we can define:

$$ACLR \triangleq \frac{\sum_{i \in \mathcal{N}_{\text{adj}}} |Y(f_i)|^2}{\sum_{i=-KN/2}^{KN/2-1} |Y(f_i)|^2}. \quad (3.56)$$

and

$$IBO \triangleq \frac{\mathbb{E}\{||\mathbf{D}||^2\}}{x_{\text{sat}}^2}. \quad (3.57)$$

Since the value of  $\hat{\mathbf{c}}$  obtained (in both frequency-domain and time domain cases) through gradient method is dependent on the vector data  $\mathbf{D}$ , the saturation level  $x_{\text{sat}}$ , and  $Y(f_i)$  is a function of  $\mathbf{D}$  and  $\mathbf{C}$ , we have:

$$ACLR_{\text{opt}} = ACLR(\mathbf{D}, \hat{\mathbf{c}}(\mathbf{D}, x_{\text{sat}}, p), x_{\text{sat}}, p) = f(\mathbf{D}, p, IBO). \quad (3.58)$$

By fixing a particular realization of  $\mathbf{D}$  it is possible to evaluate the ACLR as a function of the IBO. and, by fixing also a value of IBO, it is possible (through (3.14) and (3.37)) to show the Power Spectral Density through the samples  $Y(f_i)$  as a function of the frequency index  $i$ .

#### 3.5.2 Methodology

Our aim consists in comparing the performance in the term of OOB suppression resulting from the analysis done above to what it can be measured by implementing the OFDM with the proposed algorithm on a DSP board and by realizing a non-linearity fitting the Rapp model.

In the following, we consider a system with only  $M = 64$  subcarrier in order to reduce the complexity. The evaluation board is done as following: the OFDM signal is realized on a DSP board (working at a certain symbol rate) followed by a DAC centered on the same frequency<sup>4</sup>. Then a physical nonlinearity fitting the Rapp model is realized by two diodes (3.5.2). Finally the time-continuous signal before and after the nonlinearity is measured

<sup>4</sup> In the practical realization, the time-discreet signal is opportunely up-sampled before the DAC

by a spectrum analyzer.

Since the proposed algorithm (which has to take into account the nonlinearities) requires a long time-evaluation it is not possible to evaluate in real time the values of  $\mathbf{C}$  corresponding to each data values  $\mathbf{D}$ , in order to verify the performance of the algorithm we has to do the following, for each value of  $IBO$ .

- We choose a fixed data symbol vector  $\mathbf{D}$ ;
- we evaluate off-line the corresponding values of  $\mathbf{C}$  through the gradient method;
- we analytically evaluate both the spectrum and the ACLR by substituting these just founded values of  $\mathbf{C}$  in (3.14), (3.37) and (3.56);
- we insert the value of  $\mathbf{C}$  evaluated offline in the OFDM transmitter implemented on the DSP board, and we measure the spectrum of the signal after the physical realized nonlinearity.

In this way we are able to evaluate the real performance of the proposed algorithm even without being able to implement it as a real time function. It is useful because it can predict if the algorithm will be suitable when the evaluation speed of the electronics will permit e real time implementation.

### 3.5.3 *Out of Band Spectrum*

In figure 3.5.3 and 3.5.3 we plot the spectrum of the OFDM signal at the input and at the output of the nonlinearity, respectively, when  $IBO = 5dB$ . We can appreciate the good agreement between the theory and the measurements.

### 3.5.4 *Frequency Domain*

In 3.5.4 we plot the ACLR as a function of the IBO, comparing the OOB with and without the proposed algorithm. We note that the proposed algorithm guarantees an echo suppression of several dB both in saturation region and in linear region of the HPA.

### 3.5.5 *Time Domain*

In Fig. 3.5.5 the ACLR as a function of the IBO is depicted. Three situation are compared: (i) without any algorithm, (ii) with an algorithm which does not take into account the nonlinearities (similar to the one presented by [98], (iii) with the proposed algorithm. It is

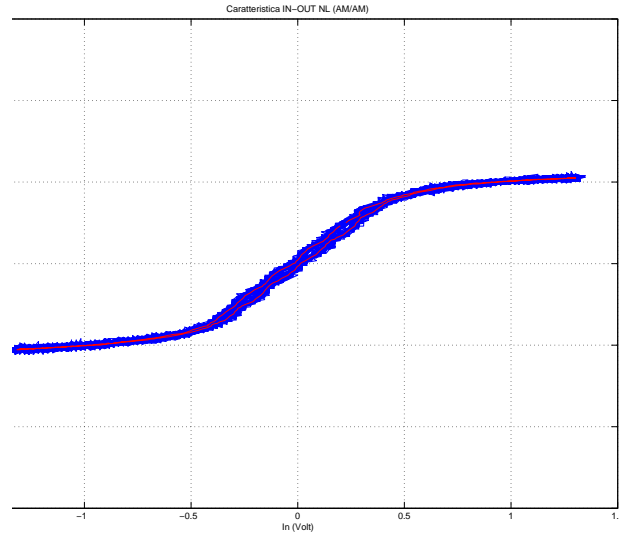


Fig. 3.6: Input-output characteristic of the non-linear element.  $I_{BO} = 15\text{dB}$ .  $\gamma = 0.001$ .

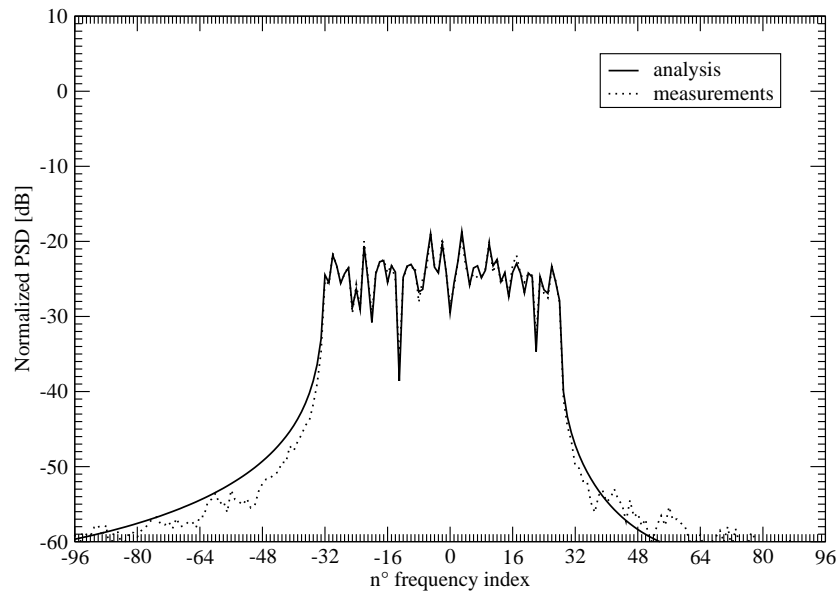


Fig. 3.7: OFDM Spectrum at the input of the nonlinearity ( $I_{BO} = 15\text{dB}$ . Comparison between theory and measurements)

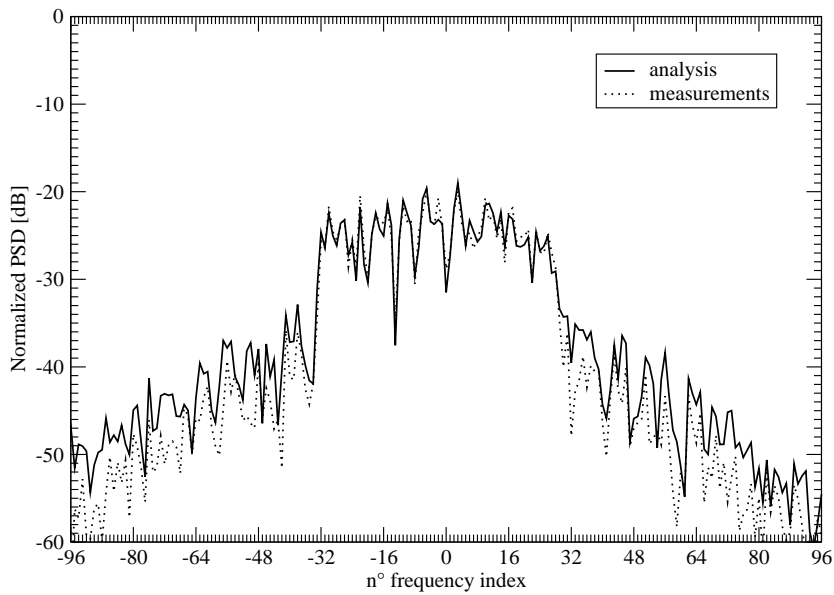


Fig. 3.8: OFDM Spectrum at the output of the nonlinearity ( $IBO = 15dB$ . Comparison between theory and measurements)

clear that the proposed algorithm performs as well as the linear algorithm when the HPA operates in

The proposed algorithm performs as well as the linear algorithm when the HPA operates in linear region (high values of IBO), and outperforms it when HPA operates near to the saturation region (low values of IBO).

### 3.6 Conclusions

In this chapter we have developed an analytical model to evaluate the Out of Band radiation in a OFDM system in the presence of nonlinearities. From the analytical model we have derived an algorithm in order to reduce the Out of Band radiation by inserting opportune symbols both in the frequency domain or in the time domain. To validate our model, we have implemented a nonlinearity on a DSP board and we have done the measurements.

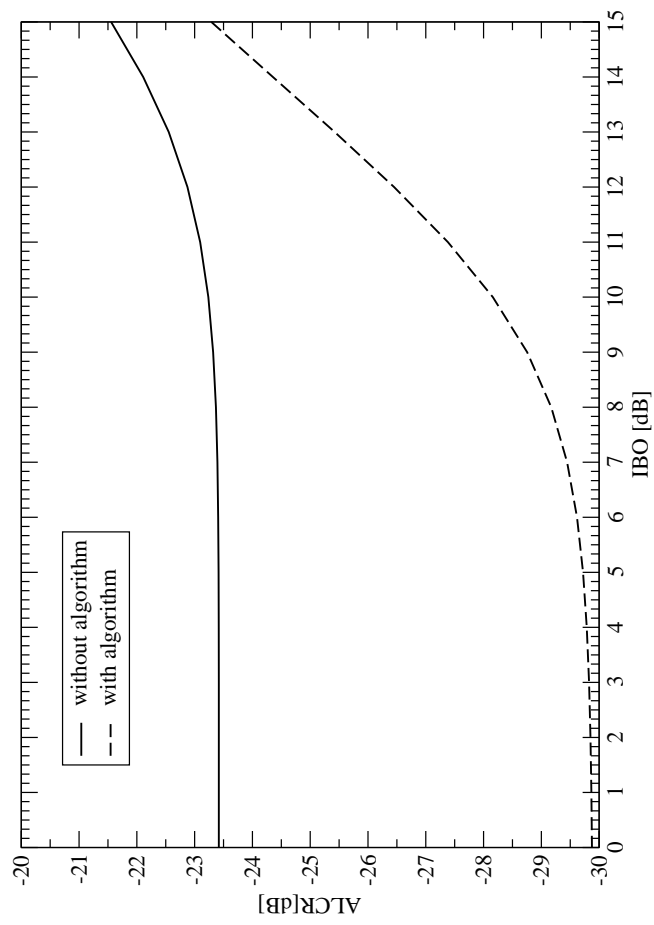


Fig. 3.9: ACLR vs IBO for Frequency Domain - 64 Subcarriers

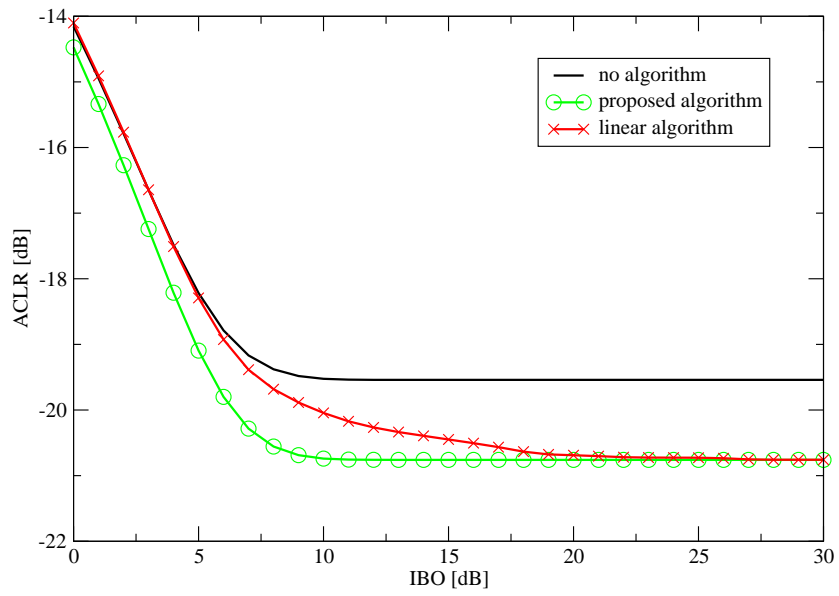


Fig. 3.10: ACLR vs IBO for Time Domain - 64 Subcarriers

## CONCLUSIONS

This thesis summarizes the work of three years of PhD. The first chapter has been dedicated to Multi-carrier code division multiple access (MC-CDMA), which is capable of supporting high data rates in next generation multiuser wireless communication systems. In particular, we have investigated the Partial equalization, and we have shown that it can be considered a low complexity receiver technique combining the signals of subcarriers for improving the achievable performance of MC-CDMA systems in terms of their bit error probability (BEP) and bit error outage (BEO) in comparison to maximal ratio combining, orthogonality restoring combining and equal gain combining techniques. We have analyzed the performance of the multiuser MC-CDMA downlink and derive the optimal PE parameter expression, which minimizes the BEP. Realistic imperfect channel estimation and frequency-domain (FD) block fading channels are considered. More explicitly, the analytical expression of the optimum PE parameter has been derived as a function of the number of subcarriers, the number of active users (i.e., the system load), the mean signal-to-noise ratio, the variance of the channel estimation errors for the above-mentioned FD block fading channel.

The second chapter investigate the problem of the coupling channel between the transmitting and the receiving antennas of a repeater in a SFN. Different design issues and performance aspects of a low-complexity echo canceller for digital on-channel repeaters have been described. Locally generated pulse trains are injected in the repeated signal to estimate the coupling channel between the transmitting and the receiving antennas. In particular, we have analyzed a low-complexity channel cancellation technique based on the reconstruction of the coupling channel pulse response via digital FIR filtering. After developing a proper theoretical model, the analytical expressions of some important performance figures have been determined, e.g. the Mean Rejection Ratio and the Echo Suppression at Nominal Position. Measurements done on echo canceller prototype implemented on FPGA board are reported as a validation of the analytical model. Then, an upper bound of the probability of instability is analytical derived.

The third chapter analyzes the problem of Out of Band radiation in OFDM systems in the

presence of nonlinearities. A cancellation carriers method to reduce the OOB radiation in OFDM systems with nonlinear power amplifier has been investigated. The proposed algorithm enables the reduction at the same time the amount of OOB radiation caused by both the side-lobes of the waveforms in the frequency domain and the nonlinear effects of the power amplifier. It has been shown that this method outperforms the known linear algorithms which reduce the OOB radiation in one between the linear region and the saturation region of the power amplifier.

Summarizing, the three chapters of this thesis have permitted me to study all the three main aspects of a wireless system: the transmission, the channel and the reception.

We have shown that the choice of the optimal PE technique significantly increases the achievable system load for given target BEP and BEO.

## BIBLIOGRAPHY

- [1] S. Hara and R. Prasad, "An Overview of multicarrier CDMA", IEEE 4th International Symposium on Spread Spectrum Techniques and Applications Proceedings, 22-25 Sept. 1996, Pages:107 - 114 vol.1.
- [2] N. Yee, J.-P. Linnartz and G. Fettweis, "Multi-Carrier-CDMA in indoor wireless networks", in Conference Proceedings PIMRC '93, Yokohama, Sept, 1993. p 109-113.
- [3] L. Hanzo, T. Keller, "OFDM and MC-CDMA - A Primer", J. Wiley and Sons, 2006.
- [4] L. Hanzo, Choi Byoung-Jo, "Near-Instantaneously Adaptive HSDPA-Style OFDM Versus MC-CDMA Transceivers for WIFI, WIMAX, and Next-Generation Cellular Systems", Proceedings of the IEEE Volume 95, Issue 12, Dec. 2007 Page(s):2368 - 2392
- [5] Hua Wei, L. Hanzo, "Semi-blind and group-blind multiuser detection for the MC-CDMA uplink", Vehicular Technology Conference, 2004. VTC 2004-Spring. 2004 IEEE 59th Volume 3, 17-19 May 2004 Page(s):1727 - 1731 Vol.3
- [6] I. Cosovic, S. Kaiser, "A unified analysis of diversity exploitation in multicarrier CDMA," *IEEE Trans. Veh. Technol.*, vol. 56, no. 4, pp. 2051-2062, July 2007.
- [7] S. Kaiser, "OFDM Code-Division Multiplexing in Fading Channels", IEEE Transactions on Communications, Vol. 50, No. 8, Aug. 2002, pp. 1266-1273.
- [8] K. Fazel and S. Kaiser, "Multi-Carrier and Spread Spectrum Systems". New York: Wiley, 2003.
- [9] M. K. Simon and M.-S. Alouini, *Digital Communication over Fading Channels: A Unified Approach to Performance Analysis*, New York, NY, 10158: John Wiley & Sons, Inc., first ed., 2000.
- [10] S. Chen, A. Livingstone, L. Hanzo, "Minimum bit-error rate design for space-time equalization-based multiuser detection", Communications, IEEE Transactions on Volume 54, Issue 5, May 2006 Page(s):824 - 832

- [11] M. Z. Win and J. H. Winters, "Virtual branch analysis of symbol error probability for hybrid selection/maximal-ratio combining in Rayleigh fading," *IEEE Trans. Commun.*, vol. 49, pp. 1926-1934, Nov. 2001.
- [12] S.B. Slimane, "Partial equalization of multi-carrier CDMA in frequency selective fading channels", *IEEE International Conference on Communications, 2000, Volume: 1, 18-22 June 2000 Pages:26 - 30 vol.1*
- [13] A. Conti, B. M. Masini, F. Zabini and O. Andrisano, "On the downlink Performance of Multi-Carrier CDMA Systems with Partial Equalization", *IEEE Transactions on Wireless Communications*, Volume 6, Issue 1, Jan. 2007, Page(s):230 - 239.
- [14] R. J. McEliece and W. E. Stark, "Channels with block interference", *IEEE Trans. Inform. Theory*, vol. IT-30, pp. 4453, Jan. 1984.
- [15] M. Chiani, A. Conti, O. Andrisano, "Outage evaluation for slow frequency-hopping mobile radio systems" *Communications*, *IEEE Transactions on* Volume 47, Issue 12, Dec. 1999 Page(s):1865 - 1874.
- [16] A.Conti, M.Z.Win, M.Chiani, and J.H.Winter, "Bit Error Outage for Diversity Reception in Shadowing Environment", *IEEE Communications Letters Theory*, vol.7, pp.15-17, Jan. 2003
- [17] P. Mary, M. Dohler, J. M. Gorce, G. Villemaud, M. Arndt, "BPSK Bit Error Outage over Nakagami-m Fading Channels in Lognormal Shadowing Environments", *Communications Letters*, *IEEE Volume* 11, Issue 7, July 2007 Page(s):565 - 567
- [18] M. Chiani, "Error probability for block codes over channels with block interference", *IEEE Trans. Inform. Theory*, vol. 44, pp. 29983008, Nov. 1998.
- [19] A. Lodhi, F. Said, M. Dohler, Hamid Aghvami, "Closed-Form Symbol Error Probabilities of STBC and CDD MC-CDMA With Frequency-Correlated Subcarriers Over Nakagami- $m$  Fading Channels", *Vehicular Technology*, *IEEE Transactions on* Volume 57, Issue 2, March 2008 Page(s):962 - 973
- [20] W.M. Gifford, M.Z. Win, M. Chiani, "Diversity with practical channel estimation", *Wireless Communications*, *IEEE Transactions on* Volume 4, Issue 4, July 2005 Page(s):1935 - 1947
- [21] W.M. Gifford, M. Win, M. Chiani, "Antenna subset diversity with non-ideal channel estimation" *Wireless Communications*, *IEEE Transactions on* Volume 7, Issue 5, Part 1, May 2008 Page(s):1527 - 1539

- 
- [22] Effect of Channel Estimation Error on Bit Error Probability in OFDM Systems over Rayleigh and Ricean Fading Channels Peng Tan; Beaulieu, N.C.; Communications, IEEE Transactions on Volume 56, Issue 4, April 2008 Page(s):675 - 685
- [23] Yunfei Chen, N.C. Beaulieu, "Optimum Pilot Symbol Assisted Modulation", Communications, IEEE Transactions on Volume 55, Issue 8, Aug. 2007 Page(s):1536 - 1546
- [24] IEEE Std 802.16-2004 IEEE Standard for Local and metropolitan area networks Part 16: Air Interface for Fixed Broadband Wireless Access Systems, October 2004
- [25] IEEE Std 802.16e-2005 and IEEE Std 802.16-2004/Cor1-2005 IEEE Standard for Local and metropolitan area networks Part 16: Air Interface for Fixed and Mobile Broadband Wireless Access Systems Amendment 2: Physical and Medium Access Control Layers for Combined Fixed and Mobile Operation in Licensed Bands and Corrigendum 1, February 2006
- [26] *Digital Video Broadcasting (DVB): Framing structure, channel coding and modulation for digital terrestrial television*, European Standard (Telecommunications series), European Telecommunications Standards Institute, Std. ETSI EN 300 744 v.1.4.1, Jan. 2001.
- [27] Athanasios Papoulis, S. Unnikrishna Pillai, *Probability, Random Variables and Stochastic Processes*, Fourth Edition, McGraw-Hill, New York Usa, 2002
- [28] I.S.Gradshteyn I.M. Ryzhik, *Table of Integrals, Series and Products*, 6th-edition, Alan Jeffrey, Editor; Daniel Zwillinger, Associate Editor, Translated from the Russian by Scripta Technica, Inc., Academic Press, San Diego, Usa, 2000
- [29] V. Erceg, L. J. Greenstein, S. Y. Tjandra, S. R. Parkoff, A. Gupta, B. Kulic, A. A. Julius, R. Bianchi, "An empirically based path loss model for wireless channels in suburban environments," *IEEE J. Select. Areas Commun.*, vol. 17, no. 7, July 1999, pp. 1205-1211.
- [30] A.Conti, M.Z.Win, and M.Chiani, "On the Inverse Symbol-Error Probability for Diversity Reception", IEEE Transaction on Communications, vol.7, pp.753-756, May. 2003
- [31] M. Chiani, A. Conti, R. Verdone, "Partial compensation signal-level-based up-link power control to extend terminal battery duration" Vehicular Technology, IEEE Transactions on Volume 50, Issue 4, July 2001 Page(s):1125 - 1131

- [32] European Telecommunications Standards Institute (ETSI). *Digital video Broadcasting (DVB); framing structure, channel coding and modulation for terrestrial television, ETSI EN 300 744 V.1.5.1*, November 2004.
- [33] European Telecommunications Standards Institute (ETSI). *Digital Video Broadcasting (DVB); Transmission System for Handheld Terminals (DVB-H), ETSI EN 302 304 V1.1.1*, November 2004.
- [34] W.K. Kim, Y.T. Lee, S.I. Park, H.M. Eum, J.H. Seo, and H.M. Kim. Equalization digital on-channel repeater in the single frequency networks. *IEEE Transactions on Broadcasting*, 52(2):137–146, June 2006.
- [35] H. Hamazumi, K. Imamura, K. Shibuya, and M. Sasaki. A study of a loop interference canceller for the relay stations in an sfn for digital terrestrial broadcasting. In *Proc. of IEEE Global Telecommunications Conference (GLOBECOM)*, volume 1, pages 167–171, San Francisco, November 2000.
- [36] Karim Medhat Nasr, John P. Cosmas, Maurice Bard, and Jeff Gledhill. Performance of an echo canceller and channel estimator for on-channel repeaters in dvb-t/h networks. *IEEE Transactions on Broadcasting*, 53(3):609–618, September 2007.
- [37] M. Mazzotti, F. Zabini, D. Dardari, O. Andrisano Performance of an Echo Canceller based on Pseudo-Noise Training Sequences IEEE Broadcast Symposium, Alexandria (VA), USA, Oct. 2008
- [38] F. Zabini, G. Chiurco, M. Mazzotti, R. Soloperto FPGA design and performance evaluation of a pulse-based echo canceller for DVB-T/H GTTI 2009, Parma, Jun. 2009
- [39] G. Pasolini, R. Soloperto, Multistage Decimators with Minimum Group Delay, IEEE International Conference on Communications 2009 (ICC 2009), Cape Town, South Africa, May 23-27 2010.
- [40] European Telecommunications Standards Institute (ETSI). *Electromagnetic compatibility and Radio spectrum Matters (ERM); Transmitting equipment for the digital television broadcast service, Terrestrial (DVB-T); Harmonized EN under article 3.2 of the RTTE Directive, ETSI EN 302 296 V1.1.1*, January 2005.
- [41] J. G. Proakis. *Digital communications*. McGraw Hill, 4th edition, 2001.

- 
- [42] D. Dardari, V. Tralli, and A. Vaccari. A theoretical characterization of nonlinear distortion effects in ofdm systems. *IEEE Transactions on Communications*, 48(10):1755–1754, October 2000.
- [43] R.Schober, W. H. Gerstacker, "The Zeros of Random Polynomials: Further Results and Applications", *IEEE TRANSACTIONS ON COMMUNICATIONS*, VOL. 50, NO. 6, JUNE 2002
- [44] S. Hara and R. Prasad, "An Overview of multicarrier CDMA", *IEEE 4th International Symposium on Spread Spectrum Techniques and Applications Proceedings*, 22-25 Sept. 1996, Pages:107 - 114 vol.1.
- [45] N. Yee, J.-P. Linnartz and G. Fettweis, "Multi-Carrier-CDMA in indoor wireless networks", in *Conference Proceedings PIMRC '93*, Yokohama, Sept, 1993. p 109-113.
- [46] L. Hanzo, T. Keller, "OFDM and MC-CDMA - A Primer", J. Wiley and Sons, 2006.
- [47] L. Hanzo, Choi Byoung-Jo, "Near-Instantaneously Adaptive HSDPA-Style OFDM Versus MC-CDMA Transceivers for WIFI, WIMAX, and Next-Generation Cellular Systems", *Proceedings of the IEEE* Volume 95, Issue 12, Dec. 2007 Page(s):2368 - 2392
- [48] Hua Wei, L. Hanzo, "Semi-blind and group-blind multiuser detection for the MC-CDMA uplink", *Vehicular Technology Conference, 2004. VTC 2004-Spring*. 2004 IEEE 59th Volume 3, 17-19 May 2004 Page(s):1727 - 1731 Vol.3
- [49] I. Cosovic, S. Kaiser, "A unified analysis of diversity exploitation in multicarrier CDMA," *IEEE Trans. Veh. Technol.*, vol. 56, no. 4, pp. 2051-2062, July 2007.
- [50] S. Kaiser, "OFDM Code-Division Multiplexing in Fading Channels", *IEEE Transactions on Communications*, Vol. 50, No. 8, Aug. 2002, pp. 1266-1273.
- [51] K. Fazel and S. Kaiser, "Multi-Carrier and Spread Spectrum Systems". New York: Wiley, 2003.
- [52] M. K. Simon and M.-S. Alouini, *Digital Communication over Fading Channels: A Unified Approach to Performance Analysis*, New York, NY, 10158: John Wiley & Sons, Inc., first ed., 2000.
- [53] S. Chen, A. Livingstone, L. Hanzo, "Minimum bit-error rate design for space-time equalization-based multiuser detection", *Communications, IEEE Transactions on* Volume 54, Issue 5, May 2006 Page(s):824 - 832

- [54] M. Z. Win and J. H. Winters, "Virtual branch analysis of symbol error probability for hybrid selection/maximal-ratio combining in Rayleigh fading," *IEEE Trans. Commun.*, vol. 49, pp. 1926-1934, Nov. 2001.
- [55] S.B. Slimane, "Partial equalization of multi-carrier CDMA in frequency selective fading channels", *IEEE International Conference on Communications, 2000, Volume: 1, 18-22 June 2000 Pages:26 - 30 vol.1*
- [56] A. Conti, B. M. Masini, F. Zabini and O. Andrisano, "On the downlink Performance of Multi-Carrier CDMA Systems with Partial Equalization", *IEEE Transactions on Wireless Communications*, Volume 6, Issue 1, Jan. 2007, Page(s):230 - 239.
- [57] R. J. McEliece and W. E. Stark, "Channels with block interference", *IEEE Trans. Inform. Theory*, vol. IT-30, pp. 4453, Jan. 1984.
- [58] M. Chiani, A. Conti, O. Andrisano, "Outage evaluation for slow frequency-hopping mobile radio systems" *Communications*, *IEEE Transactions on* Volume 47, Issue 12, Dec. 1999 Page(s):1865 - 1874.
- [59] A.Conti, M.Z.Win, M.Chiani, and J.H.Winter, "Bit Error Outage for Diversity Reception in Shadowing Environment", *IEEE Communications Letters Theory*, vol.7, pp.15-17, Jan. 2003
- [60] P. Mary, M. Dohler, J. M. Gorce, G. Villemaud, M. Arndt, "BPSK Bit Error Outage over Nakagami-m Fading Channels in Lognormal Shadowing Environments", *Communications Letters*, *IEEE* Volume 11, Issue 7, July 2007 Page(s):565 - 567
- [61] M. Chiani, "Error probability for block codes over channels with block interference", *IEEE Trans. Inform. Theory*, vol. 44, pp. 29983008, Nov. 1998.
- [62] A. Lodhi, F. Said, M. Dohler, Hamid Aghvami, "Closed-Form Symbol Error Probabilities of STBC and CDD MC-CDMA With Frequency-Correlated Subcarriers Over Nakagami- $m$  Fading Channels", *Vehicular Technology*, *IEEE Transactions on* Volume 57, Issue 2, March 2008 Page(s):962 - 973
- [63] W.M. Gifford, M.Z. Win, M. Chiani, "Diversity with practical channel estimation", *Wireless Communications*, *IEEE Transactions on* Volume 4, Issue 4, July 2005 Page(s):1935 - 1947
- [64] W.M. Gifford, M. Win, M. Chiani, "Antenna subset diversity with non-ideal channel estimation" *Wireless Communications*, *IEEE Transactions on* Volume 7, Issue 5, Part 1, May 2008 Page(s):1527 - 1539

- 
- [65] Effect of Channel Estimation Error on Bit Error Probability in OFDM Systems over Rayleigh and Ricean Fading Channels Peng Tan; Beaulieu, N.C.; Communications, IEEE Transactions on Volume 56, Issue 4, April 2008 Page(s):675 - 685
- [66] Yunfei Chen, N.C. Beaulieu, "Optimum Pilot Symbol Assisted Modulation", Communications, IEEE Transactions on Volume 55, Issue 8, Aug. 2007 Page(s):1536 - 1546
- [67] IEEE Std 802.16-2004 IEEE Standard for Local and metropolitan area networks Part 16: Air Interface for Fixed Broadband Wireless Access Systems, October 2004
- [68] IEEE Std 802.16e-2005 and IEEE Std 802.16-2004/Cor1-2005 IEEE Standard for Local and metropolitan area networks Part 16: Air Interface for Fixed and Mobile Broadband Wireless Access Systems Amendment 2: Physical and Medium Access Control Layers for Combined Fixed and Mobile Operation in Licensed Bands and Corrigendum 1, February 2006
- [69] *Digital Video Broadcasting (DVB): Framing structure, channel coding and modulation for digital terrestrial television*, European Standard (Telecommunications series), European Telecommunications Standards Institute, Std. ETSI EN 300 744 v.1.4.1, Jan. 2001.
- [70] Athanasios Papoulis, S. Unnikrishna Pillai, *Probability, Random Variables and Stochastic Processes*, Fourth Edition, McGraw-Hill, New York Usa, 2002
- [71] I.S.Gradshteyn I.M. Ryzhik, *Table of Integrals, Series and Products*, 6th-edition, Alan Jeffrey, Editor; Daniel Zwillinger, Associate Editor, Translated from the Russian by Scripta Technica, Inc., Academic Press, San Diego, Usa, 2000
- [72] V. Erceg, L. J. Greenstein, S. Y. Tjandra, S. R. Parkoff, A. Gupta, B. Kulic, A. A. Julius, R. Bianchi, "An empirically based path loss model for wireless channels in suburban environments," *IEEE J. Select. Areas Commun.*, vol. 17, no. 7, July 1999, pp. 1205-1211.
- [73] A.Conti, M.Z.Win, and M.Chiani, "On the Inverse Symbol-Error Probability for Diversity Reception", IEEE Transaction on Communications, vol.7, pp.753-756, May. 2003
- [74] M. Chiani, A. Conti, R. Verdone, "*Partial compensation signal-level-based up-link power control to extend terminal battery duration*" Vehicular Technology, IEEE Transactions on Volume 50, Issue 4, July 2001 Page(s):1125 - 1131

- [75] European Telecommunications Standards Institute (ETSI). *Digital video Broadcasting (DVB); framing structure, channel coding and modulation for terrestrial television, ETSI EN 300 744 V.1.5.1*, November 2004.
- [76] European Telecommunications Standards Institute (ETSI). *Digital Video Broadcasting (DVB); Transmission System for Handheld Terminals (DVB-H), ETSI EN 302 304 V1.1.1*, November 2004.
- [77] W.K. Kim, Y.T. Lee, S.I. Park, H.M. Eum, J.H. Seo, and H.M. Kim. Equalization digital on-channel repeater in the single frequency networks. *IEEE Transactions on Broadcasting*, 52(2):137–146, June 2006.
- [78] H. Hamazumi, K. Imamura, K. Shibuya, and M. Sasaki. A study of a loop interference canceller for the relay stations in an sfn for digital terrestrial broadcasting. In *Proc. of IEEE Global Telecommunications Conference (GLOBECOM)*, volume 1, pages 167–171, San Francisco, November 2000.
- [79] Karim Medhat Nasr, John P. Cosmas, Maurice Bard, and Jeff Gledhill. Performance of an echo canceller and channel estimator for on-channel repeaters in dvb-t/h networks. *IEEE Transactions on Broadcasting*, 53(3):609–618, September 2007.
- [80] M. Mazzotti, F. Zabini, D. Dardari, O. Andrisano Performance of an Echo Canceller based on Pseudo-Noise Training Sequences IEEE Broadcast Symposium, Alexandria (VA), USA, Oct. 2008
- [81] F. Zabini, G. Chiurco, M. Mazzotti, R. Soloperto FPGA design and performance evaluation of a pulse-based echo canceller for DVB-T/H GTTI 2009, Parma, Jun. 2009
- [82] G. Pasolini, R. Soloperto, Multistage Decimators with Minimum Group Delay, IEEE International Conference on Communications 2009 (ICC 2009), Cape Town, South Africa, May 23-27 2010.
- [83] European Telecommunications Standards Institute (ETSI). *Electromagnetic compatibility and Radio spectrum Matters (ERM); Transmitting equipment for the digital television broadcast service, Terrestrial (DVB-T); Harmonized EN under article 3.2 of the RTTE Directive, ETSI EN 302 296 V1.1.1*, January 2005.
- [84] J. G. Proakis. *Digital communications*. McGraw Hill, 4th edition, 2001.

- 
- [85] D. Dardari, V. Tralli, and A. Vaccari. A theoretical characterization of nonlinear distortion effects in ofdm systems. *IEEE Transactions on Communications*, 48(10):1755–1754, October 2000.
- [86] R.Schober, W. H. Gerstacker, "The Zeros of Random Polynomials: Further Results and Applications", *IEEE TRANSACTIONS ON COMMUNICATIONS*, VOL. 50, NO. 6, JUNE 2002
- [87] S. Hee Han, J. Hong Lee, "An Overview of Peak-to-Average Power Ratio Reduction Techniques for Multicarrier Transmission", *IEEE Wireless Communications*, April 2005
- [88] J. Tellado, L.M.C. Hoo, John M. Cioffi, "Maximum-Likelihood Detection of Nonlinearly Distorted Multicarrier Symbols by Iterative Decoding", *IEEE Transaction on Communication*, Vol.51, No.2, February 2003
- [89] F.Danilo-Lemoine, D.Falconer, C.-T.Lam, M. Sabbaghian, K. Wesolwski, "Power Backoff Reduction Techniques for Generalized multicarrier Waveforms", *Jourlan of Wireless Communication and Networking*, Vol.2008, Article ID 437801
- [90] A. Erdogan "A Subgradient Algorithm for Low Complexity DMT PAR Minimization", *ICASSP 09/2004*
- [91] A. Aggarwal, T. H. Meng "Minimizing the Peak-to-Average Power Ratio of OFDM Signals via Convex Optimization"
- [92] A. Aggarwal, T. Meng "Globally Optimal Tradeoff Curves for OFDM PAR Minimization", *SIPS 07/2004*
- [93] A. Aggarwal, E. R. Stauffer, and T. H. Meng "Optimal Peak-to-Average Power Ratio Reduction in MIMO-OFDM Systems"
- [94] L. Sanguinetti, A. A. D'Amico, I. Cosovic, "On the Performance of Cancellation Carrier-based schemes for Sidelobe Suppression in OFDM networks", *Vehicular Technology Conference, 2008. VTC Spring 2008. IEEE 11-14 May 2008* Page(s):1691 - 1696 Digital Object Identifier 10.1109/VETECS.2008.389
- [95] I. Cosovic, S. Brandes, M. Schnell, "Subcarrier weighting: a method for sidelobe suppression in OFDM systems", *Communications Letters, IEEE* Volume 10, Issue 6, June 2006 Page(s):444 - 446 Digital Object Identifier 10.1109/LCOMM.2006.1638610

- [96] S. Brandes, I. Cosovic, M. Schnell, "Reduction of Out-of-Band Radiation in OFDM Systems by Insertion of Cancellation Carriers" - Communications Letters, IEEE Volume 10, Issue 6, June 2006 Page(s):420 - 422 Digital Object Identifier 10.1109/LCOMM.2006.1638602
- [97] T. Magesacher, P. Odling, and P. Borjesson, Optimal intra-symbol spectral compensation for multicarrier modulation, in Proc. of the International Zurich Seminar on Communications, Zurich, February 22- 24, 2006, pp. 138 - 141.
- [98] H.A. Mahmoud, "Sidelobe suppression in OFDM-based spectrum sharing systems using adaptive symbol transition", in Communications Letters, IEEE, Volume 12, Issue 2, February 2008 Page(s):133 - 135
- [99] D. Dardari, V. Tralli, A. Vaccari, "A theoretical characterization of nonlinear distortion effects in OFDM systems ", Communications, IEEE Transactions on Volume 48, Issue 10, Oct. 2000 Page(s):1755 - 1764
- [100] D. Dardari, V. Tralli, A. Vaccari "A novel low complexity technique to reduce non-linear distortion effects in OFDM systems", Personal, Indoor and Mobile Radio Communications, 1998. The Ninth IEEE International Symposium on, Volume 2, 8-11 Sept. 1998 Page(s):795 - 800 vol.2,
- [101] A. Conti, D. Dardari, V. Tralli, "An analytical framework for CDMA systems with a nonlinear amplifier and AWGN", Communications, IEEE Transactions on, Volume 50, Issue7, July 2002 Page(s):1110 - 1120
- [102] A. Conti, D. Dardari, V. Tralli, "On the analysis of single and multiple carrier WCDMA systems with polynomial nonlinearities", Information, Communications and Signal Processing, 2003 and the Fourth Pacific Rim Conference on Multimedia. Proceedings of the 2003 Joint Conference of the Fourth International Conference on, Volume 1, 15-18 Dec. 2003 Page(s):369 - 375 Vol.1